AN INVESTIGATION OF THE CHARACTERISTICS OF PLASTIC HINGES IN REINFORCED CONCRETE.

by

W.W.L. Chan, B.Sc.(Eng.)

A Thesis submitted for the Degree of
Doctor of Philosophy
in the Faculty of Engineering
of the University of London.

Imperial College, London. February, 1954.

ACKNOWLEDGMENTS.

This thesis was prepared at the Imperial College of Science and Technology, London, under the supervision of Professor A.L.L. Baker, to whom the author is most grateful for encouragement and guidance.

The experimental research work was carried out in the Civil Engineering Laboratories of the College, where much willing cooperation was received from the Workshop and Laboratory technicians, in fabricating special equipment and test specimens.

The invaluable assistance given by members of the Concrete Technology research staff, colleagues and friends in recording test readings during the experimental work, is also gratefully acknowledged.

Finally, the author is indebted to the kind friends who have helped in the task of proof-reading, typing, stencilling, and photographic reproductions.

AN INVESTIGATION OF THE CHARACTERISTICS OF PLASTIC HINGES IN REINFORCED CONCRETE.

by W.W.L. Chan .

ABSTRACT.

This thesis presents analytical and experimental work on the strength and deformation of plastic hinges in reinforced concrete, in the light of application to the ultimate load method of design of structures by the Plastic Hinge Theory.

The concept of plastic hinges in statically indeterminate structures is first explained with a review of the Plastic Hinge Theory. A further comparison of this theory with exact analysis of the plastic behaviour of structures enables the validity and accuracy of the Plastic Hinge Theory to be examined, and the definition of plastic hinge rotations to be established from first principles.

A proposed stress-strain relationship, valid for both plain and laterally bound concrete, is used as a basis for developing the strength and deformation equations for reinforced concrete members.

The behaviour of plastic hinges is then discussed with reference to the main governing factors such as reinforcement, axial load, and lateral binding, and a procedure for the rapid design of plastic hinges is also outlined.

Experimental work is described of tests of 23 reinforced concrete specimens. Tests of 9 laterally bound prisms and 7 spirally bound cylinders loaded by eccentric compression enabled the behaviour of bound concrete to be studied, and its application to bound plastic hinges considered. The formation of plastic hinges in columns was examined by further tests of 7 struts loaded axially and laterally, from which the curvature distribution and influence of axial load could be studied. The experimental results are then correlated and discussed.

Finally, the conclusions which appear warranted are presented, and with the limitations of the scope of this work in mind, recommendations are given for future work in this field.

CONTENTS

Introduction. 1

Part I : The Plastic Hinge Concept in Statically Indeterminate Structures. 6

Part II: The Stress-Strain Relationship of Plain and Bound Concrete 33

Part III: The Strength and Deformation of Plain and Bound Reinforced Concrete 48

Part IV : The Behaviour of Plastic Hinges 67

Part V : Experimental Work 89

Part VI: Conclusion 125

Bibliography 134

INTRODUCTION

The plastic theory of frameworks has been recognised recently as a more realistic and rational approach to the economic design of statically indeterminate structures than the elastic theory. It examines the conditions prior to failure of a structure, taking into account its ability to redistribute the share of load amongst its various members in the most economic manner possible. Thus a truer measure of the ultimate strength of the structure as a whole is obtained. Furthermore, the plastic theory is simpler to apply since each member is known to be capable of contributing its ultimate strength and deformation, and hence the work of solving tedious elastic equations is greatly reduced.

Plastic hinges, forming at critical sections of members under progressive loading, successively reduce the degree of indeterminacy of the structure since the plastic moments of resistance of the hinges are known. These moments remain approximately constant with further load and deformation, and failure is finally brought about when the structure or part of it forms sufficient hinges to become a mechanism, or when one or more of its plastic

hinges fail through excessive deformation.

Successful application of the plastic theory to structural steel frames was achieved through the extensive research work of J.F. Baker and others.[1,2] The problem mainly lies in finding rapid methods of correct plastic hinge location, and of assessing collapse loads and forms of mechanisms.

Due to the different properties of reinforced concrete, hinge positions may be prescribed at will since the strength and deformation at any section along a member may be locally adjusted by detailing. On the other hand, the capacity of flexural deformations is considerably limited by brittleness. The problem is thus resolved into finding methods of assessing appropriate values of plastic moments within safe limits of deformation at pre-selected hinge positions to give the most economic distribution of bending moments throughout the structure. Such methods were proposed by Professor A.L.L. Baker [3,4,5,6].

Compressive plastic hinges, occurring at over-reinforced concrete sections and at sections subjected to high axial load, contribute plastic deformations mainly by the initial yield of concrete, and because the strain capacity of concrete

is small, such plastic deformations are rather small. It was anticipated, however, that the use of close spaced lateral binding could be relied upon to provide lateral compression on the bound concrete and delay failure by concrete crushing, so that sufficiently large deformations required for the most economic ultimate load designs can be safely accommodated.

This thesis presents the methods and results of an experimental and analytical investigation undertaken in an attempt to contribute new information on the strength and deformation of plastic hinges, and in particular, the critical cases of compressive hinges, so that safer and more economic design rules may be used with advantage in the Plastic Hinge Theory of design.

The theoretical work covers a review of the Plastic Hinge Theory and a comparison of this with the actual plastic behaviour of structures, in order to examine the validity and accuracy of the Plastic Hinge Theory.

A generalized stress-strain relationship for plain and bound concrete is proposed which is shown by tests to be sufficiently accurate, and which forms the basis on which the strength and deformation of

plastic hinges throughout the elastic, unbound plastic, and bound plastic ranges of strain are explained.

An analysis is presented of the strength and deformation equations of plain and bound reinforced concrete sections, subjected to pure bending, axial load or both, at all stages of loading, which is essential to the study of plastic hinge behaviour.

The influence of bending moment distribution, axial load, depth of concrete cover and spalling, percentage of longitudinal steel and of lateral binding on the propagation of the plastic zone, and on the final plastic hinge rotation is discussed. A rapid method of determining the available rotation at a given hinge is also given.

The experimental work consisted of the preparation and testing of 9 laterally bound reinforced concrete prisms and seven spirally bound reinforced concrete cylinders subjected to eccentric compression, so that the behaviour of bound plastic members in the light of its application to bound compressive hinges could be studied. In addition, seven struts tested by loading axially and bending laterally, provided information on the influence of axial load on the plastic zone and the curvature distribution and its

relation to plastic hinge rotations.

Experimental results are presented, in which the relationship between lateral binding and the ultimate strength and deformation of bound concrete is established. Curvature distribution factors are also obtained from the strut tests. The general behaviour of test specimens is compared with that predicted by analysis.

The correlation of all analytical and experimental results enables the ultimate plastic hinge rotations to be calculated in terms of lateral binding ratios, and to be compared with some hinge rotation values required in typical structures for complete redistribution of moments.

The work presented in this thesis is finally summarised and the conclusions which appear warranted are given, together with recommendations for further research work in this field.

PART I

THE PLASTIC HINGE CONCEPT IN STATICALLY INDETERMINATE STRUCTURES

The basic principles of the plastic theory of structures are generally well known, and need not be repeated here. The ability of statically indeterminate structures of ductile material to yield at critically stressed sections while maintaining approximately constant moments of resistance at these sections, causes further load increments to be redistributed onto other stronger parts of the structure so that the structure will bear as much load as it possibly can before failure occurs. This forms the basic concept, whether the theory is applied to reinforced concrete or structural steelwork.

The two main advantages claimed by the plastic theory over elastic methods are that realistic designs with rational factors of safety are achieved, generally resulting in more economical structures, and that the mathematical work involved is far simpler. Some knowledge of the elastic theory is, however, required in order to appreciate and apply

the plastic method of analysis.

The transition from elastic to plastic or non-linear behaviour of a structure subjected to predominately bending stresses, obviously commences at the peak points of the moment line under progressive loading. Plastic behaviour characterized by large plastic rotations without appreciable change in moments of resistance at these points under further loading causes the extra loads to be borne by other critical sections which still remain elastic. Such regions behave like hinges rotating under constant plastic moments and are termed plastic hinges.

Failure of the structure is brought about when the number of plastic hinges is sufficient for the structure, or part of it, to become a mechanism, or when one or more of its hinges fail through excessive deformation.

In structural steelwork, failure of plastic hinges by excessive deformation can be conveniently ignored, since its ductility is sufficiently high to accommodate plastic hinge deformations required in almost all practical cases. On the other hand, due to the material being made in standard sections of uniform strength, it is necessary to devise methods of locating correct

plastic hinge positions and various cases of collapse mechanisms in order to determine the collapse load. Tests of steel frames [1] show that the plastic theory is a simple and rational basis of design.

Reinforced concrete can only accommodate small plastic rotations, these being limited by the small ultimate strain capacity of concrete. As concrete is less ductile than steel, it is evident that plastic rotations mainly contributed by steel yield would be higher than that contributed mainly by concrete plasticity. However, because reinforced concrete can be detailed locally to suit strength and deformation requirements, plastic hinge positions may be readily located. The application of the plastic theory to reinforced concrete, therefore, requires that both the ultimate strength and deformations have to be considered.

Tests by various investigators [7,8,9] on reinforced concrete frames and continuous beams have shown beyond doubt that economic moment redistribution takes place after the structure has commenced to yield, and that the assumption of trapezoidal moment-load relationship at critically stressed regions gives an approximately true design solution.

It is found that complete moment redistribution can take place prior to failure in normal structures and loadings, but in cases where high ratio of support to mid-span moments, heavy reinforcement, and high axial loads occur, plastic rotations may not be sufficiently high for complete redistribution. In such cases, close lateral binding at critical hinge sections may be effectively employed to delay failure and allow higher plastic rotations to be accommodated. Numerous tests by the author on the behaviour of such bound members is described later.

The positions of the peaks of the bending moment diagram in statically indeterminate structures generally occur, with some exceptions, near the supports or intersections of continuous members, and thus determine the positions of the assumed plastic hinges.

Full moment redistribution is realized when the mid-span moments and support moments are finally equalized in the ultimate plastic condition for beams, and when the support moments are equalized at both ends for columns.

Full moment redistribution may not always be advantageous, due to one or more of the plastic hinges being incapable of developing the required rotations,

or due to the unfavourable form of loading or structure, or to premature yielding of mid-span sections. This results in a structure which is, in the ultimate load condition, either partially redistributed in moments, or without redistribution at all, that is, elastic. Although this condition does not produce the most even distribution of moments, it may in certain cases be the most economic design, since the cost of structural materials required to achieve full redistributidn may be more expensive.

A Review of the Plastic Hinge Theory.

The application of the plastic theory of structures to reinforced concrete frameworks has been the subject of recent papers [3,4,5] by Professor A.L.L. Baker, in which a comprehensive method is presented suitable for the analysis of complex structures many hundreds of times statically indeterminate.

In Professor Baker's Plastic Hinge Theory, both the ultimate strength and allowable deformations are calculated. It consists essentially of first assigning to a structure which is n times statically indeterminate, n plastic hinges at suitable positions, these being determined from a preliminary analysis of the probable stress distribution in the structure. Knowledge of the nature of the applied loads enables good guess values of plastic moments to be given to the n hinges which would result in the most economic distribution of bending moments in the structure. Moment-deformation equations are then systematically applied to the plastic hinges to find the values of plastic rotations required for the desired condition of moment distribution.

If rotations so found are of the wrong sense, then such hinge positions may have been wrongly selected, or

some intermediate sections between assumed hinge positions will yield before the hinges. Required rotations must also be within the safe allowable strains which can be accommodated at the hinge sections.

Adjustments such as reinforcement, binding, positions of hinges and plastic moment values may then have to be made until the two conditions of plastic rotations are satisfactory.

This trial and error adjustment process may also be used to determine the moment distribution under elastic working load conditions, to ensure that no excessive deflections or cracks occur in the structure.

It is assumed that the moment-load characteristics of the hinges follow a trapezoidal relationship, the extent of the horizontal moment line being governed by the strain capacity of the hinges.

Plastic hinges are assumed to be concentrated at points, and although this is not exactly true for any structure, it nevertheless affords a convenient idealized conception of what are in fact short plastic lengths of members giving rotations equivalent to those of hinges. Frame members spanning between the hinges

are assumed to be elastic throughout.

In certain complex frameworks, "blocks" and critical hinges can be selected so that rotation checking equations need only be applied to a few hinges in certain blocks. This greatly simplifies the work of solving complex structures.

The governing equations in the Plastic Hinge Theory express the relation between the deformation caused by the applied load and internal restraints, and the plastic rotations or "angles of discontinuity" at the n hinges. Expressed in Influence Coefficients, the n equations are of the form

$$d_{0k} + \bar{X}_1 . d_{1k} + \bar{X}_2 . d_{2k} + \text{---} + \bar{X}_n . d_{nk} = - \theta_k \qquad \text{--------(I.1)}$$

where k may be any number from 1 to n, and where

$\bar{X}_1, \bar{X}_2, \text{---} \bar{X}_n$ denote plastic moment values at hinges 1, 2, --- n;

$d_{ik} = \int \frac{M_i \ M_k}{EI_\theta} ds$ denotes the relative rotation in direction X_i of ends of members at the hinge point of X_i, caused by the action of $X_k = 1$;

and d_{Oi} denotes the rotation in the same direction caused by the action of all external loads.

From these general equations may be developed plastic rotation or θ equations for the different types of beam and column hinges for the general case of frameworks having $\underline{n}$ bays and $\underline{m}$ storeys. From these, the selection of blocks and critical hinges as mentioned earlier may be made. These details are fully given in Professor Baker's papers, and is also being studied by Yu [10].

After the plastic moment values have been finally determined by the trial and adjustment method, the hinge sections may then be designed accordingly by the Plastic Theory [3] for ultimate strength. The remaining parts of the frame members are then designed to remain elastic at ultimate load.

The required plastic rotation at each hinge as determined by equation (I.1) is safe if it does not exceed the available plastic rotation that is possible to be developed by the hinge. This is given by the Plastic Hinge Theory as

$$\theta = \frac{s_p \, l_p}{n l d} \qquad \text{---------- (I.2)}$$

where l_p denotes length of member over which yield occurs;

s_p denotes concrete strain at compression edge; and n_1 " ultimate neutral axis depth factor.

The value of l_p is simply assumed to be equal to the effective depth of the beam for the case of hinges with initial steel yield, and d/2 - (half beam depth) or not greater than d or 1/10 of the length of the column or beam in other cases.

The value of n_1 may be obtained from the ultimate strength equations in the Plastic Theory.

The concrete strain s_p is assumed to have a safe limiting value of 0.002 for plain hinges, while much higher values are expected to be possible with laterally bound hinges.

It must be mentioned here that the value of θ given by equation (I.2) represents the total rotation at a hinge, that is, both elastic and plastic rotations are included. To obtain the net plastic rotation which effects moment redistribution therefore, the elastic rotations over the same length l_p, calculated by the same equation with appropriate elastic values of s_p and n_1, should be deducted from the total rotation. This will be proved from first principles later. This does not mean that equation (I.2) cannot be used, but the safe limiting values of s_p, n_1

and l_p must be suitably chosen so that the resulting value of θ calculated from equation (I.1) represents the true net plastic rotation, excluding elastic rotations.

Although excessive rotations can generally be avoided, critical hinges may occur in internal columns where the required rotations are relatively large accompanied by very high axial load. In certain cases where the effects of settlement have to be allowed for [4], required θ values may also be quite excessive, especially for plasticity at hinges depending mainly on concrete. In such cases it is anticipated that the use of laterally bound compressive plastic hinges, which are capable of accommodating much higher concrete strains, may provide sufficiently large available rotations.

The behaviour of laterally bound concrete is described in a later part of this thesis.

Relation between Plastic Hinge Concept and Actual Behaviour of Structures.

It was stated earlier that plastic hinges are assumed for convenience to be concentrated at points, an idealized conception of what is in reality short plastic lengths of members over which develop plastic rotations or "angles of discontinuity" when moment redistribution takes place.

The available rotation of a plastic hinge, given as

$$\theta = \frac{l_p \, s_p}{n_1 d} \qquad \text{-----} \quad (I.1)$$

describes in mathematical terms, the influence of the main factors governing the hinge rotation, although it does not necessarily represent the exact plastic behaviour within the hinge zone. This however, is justified if the factors in the equation are chosen by studying actual behaviour.

Again, the Plastic Hinge Theory may in fact be shown to be a powerful approximate method of analysing statically indeterminate structures subject to yield and moment redistribution, based on certain idealized assumptions, and therefore some degree of error or departure from actual behaviour would be involved in the approximation. This degree of error

can only be determined if the actual behaviour is studied.

With the foregoing considerations in mind, the following analysis aims at correlating the Plastic Hinge Theory and the exact or actual behaviour of structures, so that the degree and nature of approximation resulting from the idealized assumptions made in the Plastic Hinge Theory and the significance of θ values can be assessed, and the validity of the Plastic Hinge Theory examined from first principles.

Consider a structure which is n times statically indeterminate, in stable equilibrium under ultimate load where moment redistribution has taken place:

Case (a) : Plastic Hinge Theory. The assumption of n point hinges with wholly elastic members in between, of trapezoidal moment-load characteristic for the plastic hinges, and of abrupt "angles of discontinuity" at hinges, gives equation (I.1), which reads, as before,

$$d_{0k} + \bar{X}_1 . d_{1k} + \bar{X}_2 . d_{2k} + \text{---} + \bar{X}_n . d_{nk} = -\theta_k$$

in which all EI values are elastic.

Case (b) : Actual Behaviour. If the assumed positions of the plastic hinges were correctly assumed in case (a), they would of course coincide with the

actual moment peak points. However, with reference to Fig. I.1, the departure of the actual moment-load characteristics from the idealized case, postulates that:

i. Plastic rotation at a hinge does not actually occur at a point, and therefore

ii. Framework members consist of partly elastic and partly plastic lengths at ultimate load;

iii. No actual "angle of discontinuity" can take place at a point between ends of members; if it were possible, it would imply that the member would be totally severed at that point. Although effective

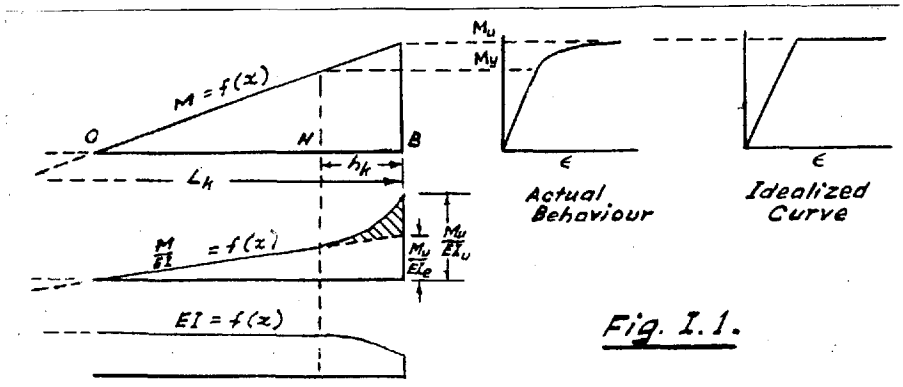


Fig. I.1.

plastic rotations do occur over the length of the plastic zone, there is in fact no Θ rotations at the assumed hinge points for the structure to be stable. This may perhaps be more readily visualised by substituting for the partly plastic structure, an imaginary equivalent structure of identical shape and centre-

line dimensions which is wholly elastic, and where the stiffnesses along or between members may be ... altered at will, until a final distribution of moments identical to the actual partly plastic structure is obtained. For this equivalent structure, it can be seen that moment redistribution can occur by elastic adjustments, with $\theta_k = 0$.

From these arguments, the actual behaviour of the structure under ultimate load and with redistributed moments, may be expressed by similar Influence Coefficients as

$$d'_{0k} + \bar{X}_1 . d'_{1k} + \bar{X}_2 . d'_{2k} + \text{---} + \bar{X}_n . d'_{nk} = 0. \qquad \text{-------(I.3)}$$

where $d'_{ik} = \int \frac{M_i \, M_k}{EI_s} . ds$, the value of EI_s being the actual EI value along the length of a given member, and referring to Fig.I.1, for a member of constant section and reinforcement, OH is elastic and HB plastic.

If d'_{ik} is separated into the elastic and plastic parts so that

$$d'_{ik} = {}_{el}d'_{ik} + {}_{p2}d'_{ik}$$

$$= \int_0^{(L_k - h_k)} \frac{Mi\ Mk}{EI_e}\, ds + \int_{(L_k-h_k)}^{L_k} \frac{Mi\ Mk}{EI_s}\, ds\ ,$$

equation (I.3) then becomes

$$({}_{e1}d'_{0k} + {}_{p2}d'_{0k}) + \bar{X}_1({}_{e1}d'_{1k} + {}_{p2}d'_{1k}) + \bar{X}_2({}_{e1}d'_{2k} + {}_{p2}d'_{2k}) + \text{---} + \bar{X}_n({}_{e1}d_{nk} + {}_{p2}d_{nk}) = 0 \qquad \text{----------(I.3a)}$$

Equation (I.1) given by the Plastic Hinge Theory can also be expressed by splitting each d_{ik} term into two parts, both having elastic EI terms as assumed, so that

$$({}_{e1}d_{0k} + {}_{e2}d_{0k}) + \bar{X}_1({}_{e1}d_{1k} + {}_{e2}d_{1k}) + \bar{X}_2({}_{e1}d_{2k} + {}_{e2}d_{2k}) + \text{---} + \bar{X}_n({}_{e1}d_{nk} + {}_{e2}d_{nk}) = -\theta_k \qquad \text{----------(I.1a)}$$

where $${}_{e1}d_{ik} = \int_0^{(L_k - h_k)} \frac{Mi\ Mk}{EI_e}\, ds$$

and $${}_{e2}d_{ik} = \int_{(L_k-h_k)}^{L_k} \frac{Mi\ Mk}{EI_e}\, ds$$

noting that both terms have elastic EI values.

Since both equations refer to the same structure under the same applied loads and the same plastic moment values, (I.3a) and (I.1a) may be superimposed. Subtracting equation (I.1a) from (I.3a) gives

$$\theta_k = ({}_{p2}d'_{0k} - {}_{e2}d_{0k}) + \bar{X}_1({}_{p2}d'_{1k} - {}_{e2}d_{1k}) + \text{---} + \bar{X}_n({}_{p2}d'_{nk} - {}_{e2}d_{nk}) \qquad \text{-----(I.4)}$$

Working out the ${}_{p2}d'_{ik}$ and ${}_{e2}d_{ik}$ terms in full and re-grouping, it can be shown that

$$\theta_k = \sum_{k=1}^{k=n} \left[\int_0^{h_k} M_k \, (M_0 + M_1\bar{X}_1 + M_2\bar{X}_2 + \text{---} + M_n\bar{X}_n) \left(\frac{1}{EI_s} - \frac{1}{EI_e} \right) ds \right]$$

Now $(M_0 + M_1\bar{X}_1 + M_2\bar{X}_2 + \text{---} + M_n\bar{X}_n) = M$, the resultant bending moment at any section, and hence

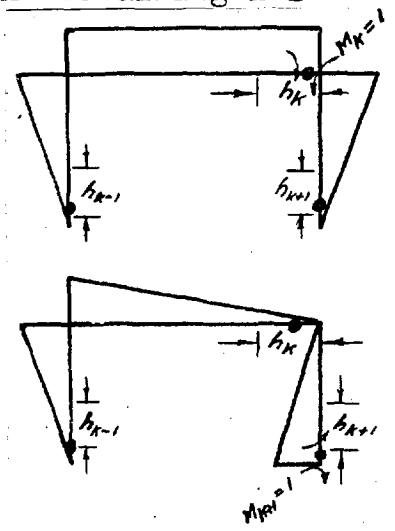
$$\theta_k = \sum_{k=1}^{k=n} \left[\int_0^{h_k} M_k . M \left(\frac{1}{EI_s} - \frac{1}{EI_e} \right) ds \right] \qquad \text{------(I.5)}$$

This equation expresses the exact relationship between the plastic rotation θ as defined by the Plastic Hinge Theory and the actual plastic behaviour, and shows that in fact, the available hinge rotation θ_k for the k^{th} hinge is determined not only by its

own plasticity, but is also influenced to some extent by the plasticity of every other of the remaining n-1 hinges as well.

However, in the n terms of the summation in equation (I.5), all terms with the exception of the k^{th} term

$$\int_0^{h_k} M_k \cdot M \left(\frac{1}{EI_s} - \frac{1}{EI_e} \right) ds$$



Typical $M_k = 1$ Diagrams

Fig. I.2.

are very negligibly small, since the $M_k = 1$ diagram gives maximum values within the plastic zone of the k^{th} hinge only. Referring to the examples given in Fig. I.2, it can be seen that other than the k^{th} hinge, the $M_k = 1$ diagram is very small for the remaining hinges, and tails off to zero at the assumed positions of the hinges. Also, the plastic zones h_k are generally very short compared with the lengths of the framework members. From these considerations, little error is incurred by neglecting the n-1 secondary terms. This is further justified by the fact that both positive and negative terms are generally included, thus further diminishing the magnitude of the sum of the secondary terms. Yu has

shown [10] that there are generally more positive than negative secondary terms, so that any slight error due to neglecting these terms will be on the safe side, since the approximate available rotation will then be less than the actual value.

Thus equation (I.5) reads, after simplification,

$$\theta_k = \int_0^{h_k} M_k \cdot M \left(\frac{1}{EI_s} - \frac{1}{EI_e} \right) ds$$

or

$$= \int_0^{h_k} \frac{M_k \cdot M}{EI_s} ds - \int_0^{h_k} \frac{M_k \cdot M}{EI_e} ds \qquad \text{-----(I.5a)}$$

Now $\int \frac{M_k \cdot M}{EI} ds$ is, by Mohr's rule, the expression for the slope at the support caused by the elastic weight M/EI. Referring to Fig.I.3, the reaction at A due to the M/EI diagram is

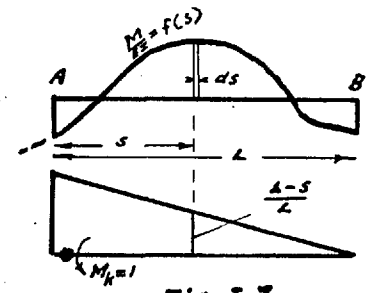


Fig. I. 3.

$$R_A = \int \frac{M}{EI} \cdot \frac{L - s}{L} ds$$

$$= \int M_k \cdot M / EI \; ds$$

since (L-s)/L is the value of M_k=1 at distance s from A.

Hence the plastic hinge rotation given by equation (I.5a) represents the total change in slope due

to plasticity over the plastic zone h_k less the elastic change of slope over the same length and under the same load.

Now a study of Influence Coefficients and typical framework examples [3,4,5,10] shows that the form of $M_k = 1$ diagrams for straight members is either a rectangle, a trapezium, or a triangle (Fig. I.4). Equation (I.5a) would be greatly simplified if the term M_k could be eliminated by assuming a constant value of $M_k = 1$ in all cases, i.e., Fig. I.4a, so that equation (I.5a) would then read

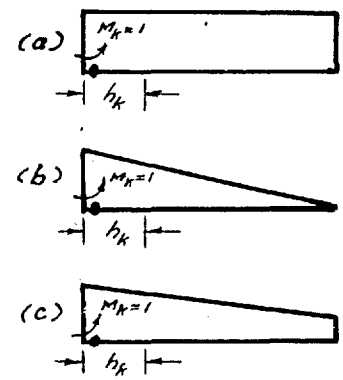


Fig. I.4.

$$\theta_k = \int_0^{h_k} \frac{M}{EI_s} ds - \int_0^{h_k} \frac{M}{EI_e} ds$$

The error introduced for the cases (a), (b) & (c) in Fig.I.4 due to assuming the value of $M_k = 1$ to be constant will now be considered.

Case (a). For a rectangular $M_k = 1$ diagram, no error is introduced since M_k is of constant value throughout the length of the member.

Case (b). For a triangular $M_k = 1$ diagram, the greatest error is introduced, since the rate of change of

M_k is greater than that of the two other possible cases. Taking the most ill-conditioned arrangement, assume that due to high axial load, the whole column has yielded, that is, $h_k = H/2$. Assume also that the plastic M/EI_s diagram is a parabola, and that the ultimate EI_u at B (Fig. I.5) is 0.4 EI_e; these assumed values represent worst values as observed from tests.

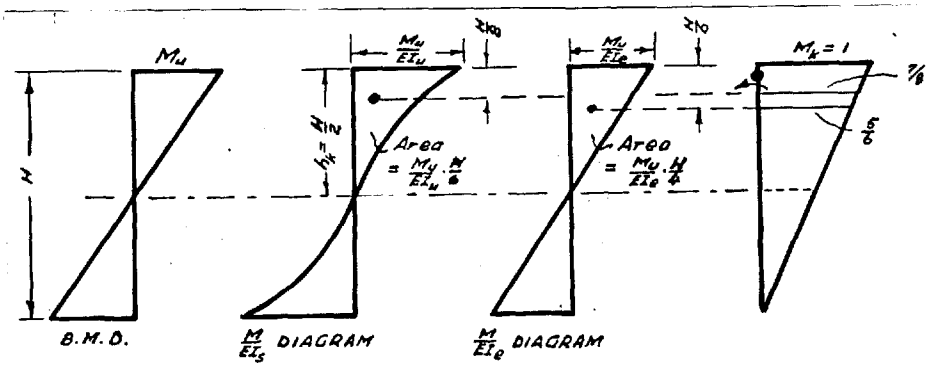


Fig. I.5.

Referring to Fig.I.5, and applying equation (I.5a) in full, we have

$$\theta_k = \int_0^{h_k} \frac{M_k \cdot M}{EI_s}\, ds \quad - \int_0^{h_k} \frac{M_k \cdot M}{EI_e}\, ds$$

$$= \frac{M_u}{EI_s} \cdot \frac{H}{6} \cdot \frac{7}{8} - \frac{M_u}{EI_e} \cdot \frac{H}{4} \cdot \frac{5}{6} \quad \text{by the rules}$$

of integration,

$$= 0.156\, \frac{M_u H}{EI_e} .$$

Now applying equation (I.5a) in the proposed

simplified form by omitting $M_k = 1$ = constant, we have,

$$\theta_k = \int_0^{h_k} \frac{M}{EI_s} ds - \int_0^{h_k} \frac{M}{EI_e} ds$$

$$= \frac{M_u}{EI_u} \cdot \frac{H}{6} - \frac{M_u}{EI_e} \cdot \frac{H}{4}$$

$$= 0.1665 \frac{M_u H}{EI_e} .$$

The discrepancy between the two θ_k values is thus $(0.1665 - 0.156)\ M_u/EI_e$

$$= 0.0105\ M_u/EI_e ,$$

and the percentage error is $0.0105/0.156$

$$= 6.7\ \%$$ (on the unsafe side).

This degree of error, based on the worst conditions that could occur in reinforced concrete structures, represents a very negligible figure considering that much higher variations are obtained from the erratic nature of concrete alone.

Case (c). For a trapezoidal $M_k = 1$ diagram, the error incurred is evidently intermediate between Case (a) and Case (b), and is therefore negligible.

The above evidence shows that it is sufficiently accurate to determine the available effective plastic hinge rotation of the k^{th} hinge of a structure n times

statically indeterminate from the simplified equation

$$\theta_k = \int_0^{h_k} \frac{M}{EI_s}\,ds - \int_0^{h_k} \frac{M}{EI_e}\,ds \qquad \text{----(I.6)}$$

incurring only very small errors in the worst cases. ~~and generally on the safe side~~. The value of θ_k is thus given by the hatched area in Fig. I.1.

Here proof is also given that the elastic deformations should be subtracted from the total rotation in order to obtain the effective rotation or θ value as defined by the Plastic Hinge Theory.

This deduction of elastic rotations is an important factor, since to ignore subtracting the elastic term gives available θ values which are too high, that is, erring on the unsafe side. This error is most serious in ordinary unbound hinges, where the concrete elastic strain is at least 30% of the ultimate strain.

In laterally bound hinges where high strain capacities may be developed by induced tri-axial compression, in hinges heavily reinforced in compression, and in structural steel hinges, the elastic strain is but a very small fraction of the ultimate strain, so that ignoring elastic rotations may not incur serious error.

For this reason, the plastic theory of steel

frames tacitly assumes that the moment-plastic rotation curve is as depicted in Fig.I.6a, rather than the actual complete curve as in Fig.I.6b. It follows that in calculating the collapse load by the Virtual Work approach, the work done by plastic deformations only (d, θ_i) excluding elastic work, appears in the general equation

$$\sum P.d = \sum M_i \theta_i$$

This was recently pointed out by English [11].

Although elastic deformations can be safely ignored in steel structures, it certainly cannot be overlooked in reinforced concrete.

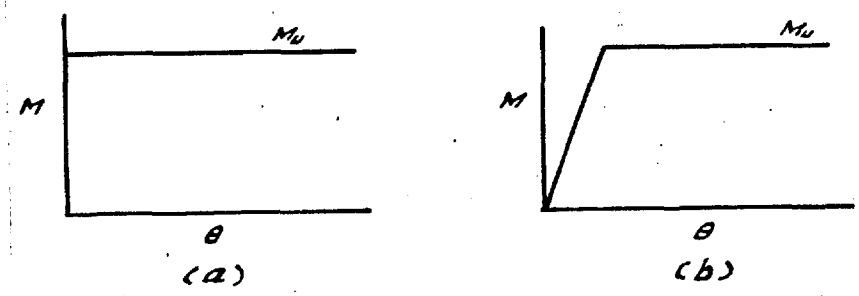


Fig. I.6.

Interpretation and Application of the Plastic Hinge Theory.

A study of the Plastic Hinge Theory and a comparison with actual behaviour of structures under ultimate load, indicates that:

i. The Plastic Hinge Theory is a powerful approximation technique by which very complex statically indeterminate structures of ductile material can be rapidly designed, with full advantage taken of the economic redistribution of bending moments at ultimate load, and where both the strength and deformation of the structure are taken into account.

ii. The assumption of concentrated point hinges and abrupt "angles of discontinuity" or plastic rotations at these hinge points, and of wholly elastic members spanning between hinges, represent convenient idealized conceptions which depart slightly from actual behaviour. For the purpose of determining the best distribution of bending moments by the trial and adjustment method, the error involved in the idealized assumptions is shown to be negligibly small.

iii. The "angles of discontinuity" or θ values given by the assumed plastic hinge behaviour, may be regarded as a correction factor which reconciles plastic hinge

behaviour with actual behaviour. For a 100 % correction, the value of θ for a particular hinge is shown to be dependent on the deformations of each of the n hinges of an n times statically indeterminate structure. However, a sufficiently accurate correction involving only a few percent maximum error ~~on the safe side~~ is obtained by considering the deformation in the plastic zone of the particular hinge only.

iv. The effective hinge rotation θ as defined in iii., ia approximately the total change in slope over the plastic zone, less the corresponding elastic change of slope with reference to the ultimate load.

v. The actual length of the plastic hinge zone is generally very short in flexural members, but may be considerably lengthened by the presence of high axial load. While it has been shown that the assumption of elastic members spanning between point hinges is an accurate approximation for the analysis of the state of moment distribution in the structure, it is evident that due regard must be given to the actual plastic length when detailing critical sections to develop the required strength and rotation.

vi. It follows from iv. and v. that in order to calculate the available θ values of plastic hinges,

the following properties of reinforced concrete have to be known:

(a). The stress-strain relationship of the materials; these include the steel reinforcement and both plain and laterally bound concrete.

(b), The strength and deformation of reinforced concrete members under various forms of loading and at all stages of their loading history.

(c). The length of the plastic zone in the vicinity of the assumed hinge positions.

(d). The distribution of unit rotation or the M/EI curve in the plastic zone length.

These items are discussed in detail in the following chapters.

PART II

THE STRESS-STRAIN RELATIONSHIP OF PLAIN AND BOUND CONCRETE.

The theory of plasticity shows that any brittle material can be transformed into a more ductile material by the application of lateral pressure. This has been proved by tests, and amongst these the most classical experiments were performed by von Karman [12] on marble.

The ability of lateral reinforcement to bind the enclosed concrete effectively and increase the load-bearing capacity of concrete compression members was probably first recognized and investigated by Considere [13] in 1903.

F.E. Richart and co-workers [14,15] conducted experiments on concrete prisms by applying axial, biaxial and triaxial compression, and observed that the strength of the prisms increased many times with the presence of lateral pressures, accompanied by large deformations ranging from 0.5% to more than 7%.

Further tests by the same workers on spirally reinforced concrete prisms in compression showed that triaxial compression took place after the

prisms had reached their ordinary crushing strength, when large lateral deformations stretched the spirals and induced lateral pressure which supported the otherwise crushed concrete. The results of this series were found to agree with the previous set of experiments.

The most important result of the findings of the various investigators can be expressed by the equation:

$$f = f_c + Kf_2.$$

where f = longitudinal concrete stress.

f_c = compressive strength of plain concrete.

f_2 = unit lateral stress.

and K is a constant varying from 2.8 to 4.2 for various concrete mixes.

Prior to failure in a laterally bound member, considering that certain elements of the material have begun to deform plastically, these elements must be supported laterally if they are to carry further load. This lateral support must be afforded by the tensile strength of the surrounding elastic elements and by the lateral pressure developed by the binders. In plain concrete members no lateral support is available, and the concrete completely collapses when

this tensile strength is exceeded. In laterally bound concrete, the formation of arches of concrete within the clearances of adjacent binders enables the intermittent bands of binders to act as a continuous surface of lateral restraint.

As strains progress into the bound range, the large lateral deformations accompanying high tensile stresses in the concrete develop further pressure against the binders, and as the support of surrounding elastic elements is lost through a splitting action, so requisite support is gained from the binders.

As this action progresses, the concrete becomes more of a plastic mass, carrying further load only as fast as the lateral supporting force of the binders can be built up. When loading is applied more rapidly than the lateral support can be furnished, failure commences.

While the general observations on numerous experiments on laterally bound concrete specimens by the author (see Part V) showed fair agreement with the behaviour of similar tests by previous investigators, it was felt that a satisfactory relationship between stress and strain at all stages of loading

was lacking for an analysis of bound concrete behaviour.

Thus the equation $f = f_c + Kf_2$ relates internal stresses, and does not relate stress with strain. For plain concrete, most of the well known plastic theories only give the stress-strain relationship for the ultimate strength condition. Hognestad [16] recently proposed a satisfactory form of curve for the entire range of stress-strain, but, notwithstanding the fact that most of the specimens in his tests had appreciable amounts of lateral binding, the influence of this variable was not identified.

The following generalized stress-strain relationship proposed by the author, and verified by test results, aims at providing a simple basis for the analysis of bound compressive concrete members, applicable to the elastic, plastic and bound plastic ranges of strength and deformation.

Generalized Stress Strain Curve.

So many complicated factors govern the behaviour of laterally bound concrete, such as the stability of arches spanning between binders, depression of binding into the concrete, progressive internal splitting,

that the exact analysis of its stress-strain relationship would be hopelessly involved and inconvenient to apply in practical design.

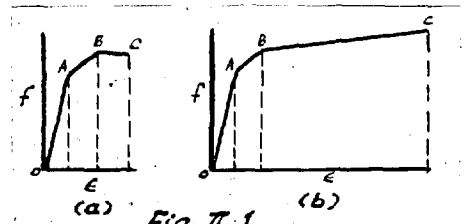


Fig. II.1

Test results show that the compressive stress-strain curve of laterally bound concrete may be closely approximated by the three stages OA, AB, and BC as shown in Fig.II.1. OA represents the elastic stage, and AB represents the greater portion of the unbound plastic range. OA and AB are defined by the physical constants E_e, ϵ_e, λ_1, (Fig.II, 2) and their values may be obtained from bending tests as will be shown later. For unbound concrete the last line BC is short and drops slightly, but for bound concrete this line may extend to a considerable length with a rising gradient, as shown in Fig. II.1a and Fig. II.1b. It will be realized that the portion of the curve OAB is independent of the influence of lateral binding, since the latter has been found to have no effect before the stress approaches that of the normal crushing value.

Line BC is expressed by the constants γ_2 and λ_2 which are a function of the amount and type of lateral

binding. The author's tests show that within the useful range of strength, this straight line satisfactorily represents its actual behaviour. Since there is no abrupt failure in bound concrete, a section is considered to have failed when it can no longer sustain a steady load.

It is also assumed that in flexure, a given stress may be identified with a specific strain, irrespective of the position of the element considered.

Finally, it is assumed for simplicity that the stress-strain relationship is identical for flexure as for axial compression. This appears to incur some error, since it is well known that concrete in flexure is capable of stress relief at the extreme fibres and thereby accommodate higher strains than when axially loaded. However, considering that the initial parts of the stress-strain curves in flexure and in axial compression are almost identical [17], it is felt that this is a reasonable simplifying assumption.

Referring to Fig. II.2:

In the elastic range OA,

$\epsilon \leq \epsilon_e$, $\quad f = \epsilon E_e \quad$ ---(II.1a)

or expressing in terms of f_p,

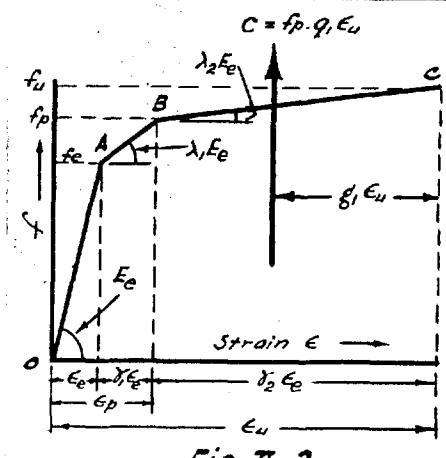


Fig. II. 2

$$f = \frac{f_p}{(1+\gamma_1\lambda_1)}\frac{\epsilon}{\epsilon_e} \qquad \text{----------(II.1b)}$$

and when $\epsilon = \epsilon_e$,

$$f_e = f_p \,/\, (1+\gamma_1\lambda_1) \qquad \text{-------(II.1c)}$$

In the plastic range AB, $\epsilon_e < \epsilon < \epsilon_p$,

$$f = \frac{f_p}{(1+\gamma_1\lambda_1)} \cdot \left[1 + (\frac{\epsilon}{\epsilon_c} - 1)\lambda_1\right] \qquad \text{----(II.2a)}$$

and when $\epsilon = \epsilon_p$,

$$f_p = f_e \cdot (1+\gamma_1\lambda_1) \qquad \text{----------(II.2b)}$$

In the plastic range BC, $\epsilon_p < \epsilon < \epsilon_u$,

$$f = \frac{f_p}{(1+\gamma_1\lambda_1)} \cdot \left[1 + \gamma_1\lambda_1 + \lambda_2 \left(\frac{\epsilon}{\epsilon_e} - \frac{\epsilon_p}{\epsilon_e}\right)\right] \qquad \text{----------(II.3a)}$$

and when $\epsilon = \epsilon_u$,

$$f_u = \frac{f_p}{(1+\gamma_1\lambda_1)} \cdot \left[1 + \gamma_1\lambda_1 + \gamma_2\lambda_2\right] \qquad \text{---(II.3b)}$$

In equilibrium equations for the strength of reinforced concrete sections in bending, knowledge of the concrete resultant force $C = f_p q_1 n_1 bd$ and its line of action $g_1 n_1 d$ at a particular load stage, enables these equations to be conveniently solved. It is therefore useful to derive the values of q_1 and g_1 in terms of concrete strain.

Concrete Compression Factor q_1.

Referring again to Fig. II.2, the resultant concrete force may be expressed as

$$C = f_p . q_1 . \epsilon \ ,$$

and equating this to the summation of areas under the stress strain curve up to the value of strain ϵ, gives:

In the elastic stage OA, $\epsilon \leq \epsilon_e$,

$$q_1 = \frac{1}{2} \frac{\epsilon}{\epsilon_e} \frac{1}{(1+\gamma_1\lambda_1)} \qquad \text{--------(II.4a)}$$

and when $\epsilon = \epsilon_e$,

$$q_1 = \frac{1}{2(1+\gamma_1\lambda_1)} \qquad \text{--------(II.4b)}$$

In the plastic stage AB, $\epsilon_e < \epsilon < \epsilon_p$,

$$q_1 = \frac{\epsilon_e \left[2\frac{\epsilon}{\epsilon_e} - 1 - \lambda_1 \left(\frac{\epsilon}{\epsilon_e} - 1\right)^2\right]}{2\epsilon\,(1+\gamma_1\lambda_1)} \qquad \text{----(II.5a)}$$

and when $\epsilon = \epsilon_p$,

$$q_1 = \frac{1+2\gamma_1+\lambda_1\gamma_1^2}{2(1+\gamma_1)(1+\gamma_1\lambda_1)} \qquad \text{---------(II.5b)}$$

In the plastic range BC, $\epsilon_p < \epsilon < \epsilon_u$,

$$q_1 = \frac{\epsilon_e \left\{(2\gamma_1+1)+\lambda_1\gamma_1^2+\left(\frac{\epsilon-\epsilon_p}{\epsilon_e}\right)\left[2(1+\gamma_1\lambda_1)+\lambda_2\left(\frac{\epsilon-\epsilon_p}{\epsilon_e}\right)\right]\right\}}{\epsilon \quad 2\,(1+\gamma_1\lambda_1)}$$

$$\text{----------(II.6a)}$$

and when $\epsilon = \epsilon_u$,

$$q_1 = \frac{(2\gamma_1+1)+\lambda_1\gamma_1^2+\gamma_2\left[2(1+\lambda_1\gamma_1)+\lambda_2\gamma_2\right]}{2(1+\gamma_1+\gamma_2)(1+\gamma_1\lambda_1)} \qquad \text{---(II.6b)}$$

Compression Centroid Factor g_1.

Taking moments, it may be shown that from geometric considerations (Fig.II.2):

In the elastic stage, $\epsilon \leq \epsilon_e$,

$$g_1 = 1/3 \qquad \text{----------(II.7)}$$

In the plastic stage AB, $\epsilon_e < \epsilon \leq \epsilon_p$,

$$g_1 = \frac{(\epsilon - \frac{2}{3}\epsilon_e) + \frac{1}{3}(\frac{\epsilon}{\epsilon_e} - 1)^2 \left[3\epsilon_e + (\epsilon - \epsilon_e)\lambda_1\right]}{\epsilon\left[(2\frac{\epsilon}{\epsilon_e} - 1) + \lambda_1(\frac{\epsilon}{\epsilon_e} - 1)^2\right]} \qquad \text{----------(II.8a)}$$

and when $\epsilon = \epsilon_p$,

$$g_1 = \frac{(\frac{1}{3} + \gamma_1) + \frac{1}{3}\gamma_1^2(3 + \gamma_1\lambda_1)}{(1+\gamma_1)(1+2\gamma_1 - \lambda_1\gamma_1^2)} \qquad \text{--------(II.8b)}$$

In the Plastic range BC, $\epsilon_p < \epsilon < \epsilon_u$,

$$g_1 = \frac{(\epsilon - \frac{2}{3}\epsilon_e) + \gamma_1(2+\gamma_1\lambda_1)\left[(\epsilon - \epsilon_p) + \frac{1}{3}\gamma_1\epsilon_e\frac{3+\lambda_1\gamma_1}{2+\lambda_1\gamma_1}\right] + \frac{1}{3}(\frac{\epsilon - \epsilon_p}{\epsilon_e})^2\left[3\epsilon_e(1+\gamma_1\lambda_1) + \lambda_2(\epsilon - \epsilon_p)\right]}{\epsilon\left\{1 + \gamma_1(2+\gamma_1\lambda_1) + (\frac{\epsilon - \epsilon_p}{\epsilon_e})\left[2(1+\gamma_1\lambda_1) + \lambda_2(\frac{\epsilon - \epsilon_p}{\epsilon_e})\right]\right\}} \qquad \text{--------(II.9a)}$$

and when $\epsilon = \epsilon_u$,

$$g_1 = \frac{(\frac{1}{3} + \gamma_1 + \gamma_2) + \gamma_1(2+\gamma_1\lambda_1)\left[\gamma_2 + \frac{1}{3}\gamma_1\frac{3+\lambda_1\gamma_1}{2+\lambda_1\gamma_1}\right] + \frac{1}{3}\gamma_2^2\left[3(1+\gamma_1\lambda_1) + \lambda_2\gamma_2\right]}{(1+\gamma_1+\gamma_2)\left\{1 + \gamma_1(2+\gamma_1\lambda_1) + \gamma_2\left[2(1+\gamma_1\lambda_1) + \lambda_2\gamma_2\right]\right\}} \qquad \text{--------(II.9b)}$$

For a given concrete, sets of values of q_1 and g_1 may be plotted as curves against values of ϵ since all the constants are known. Such typical curves are given in Figs. 1 and 2.

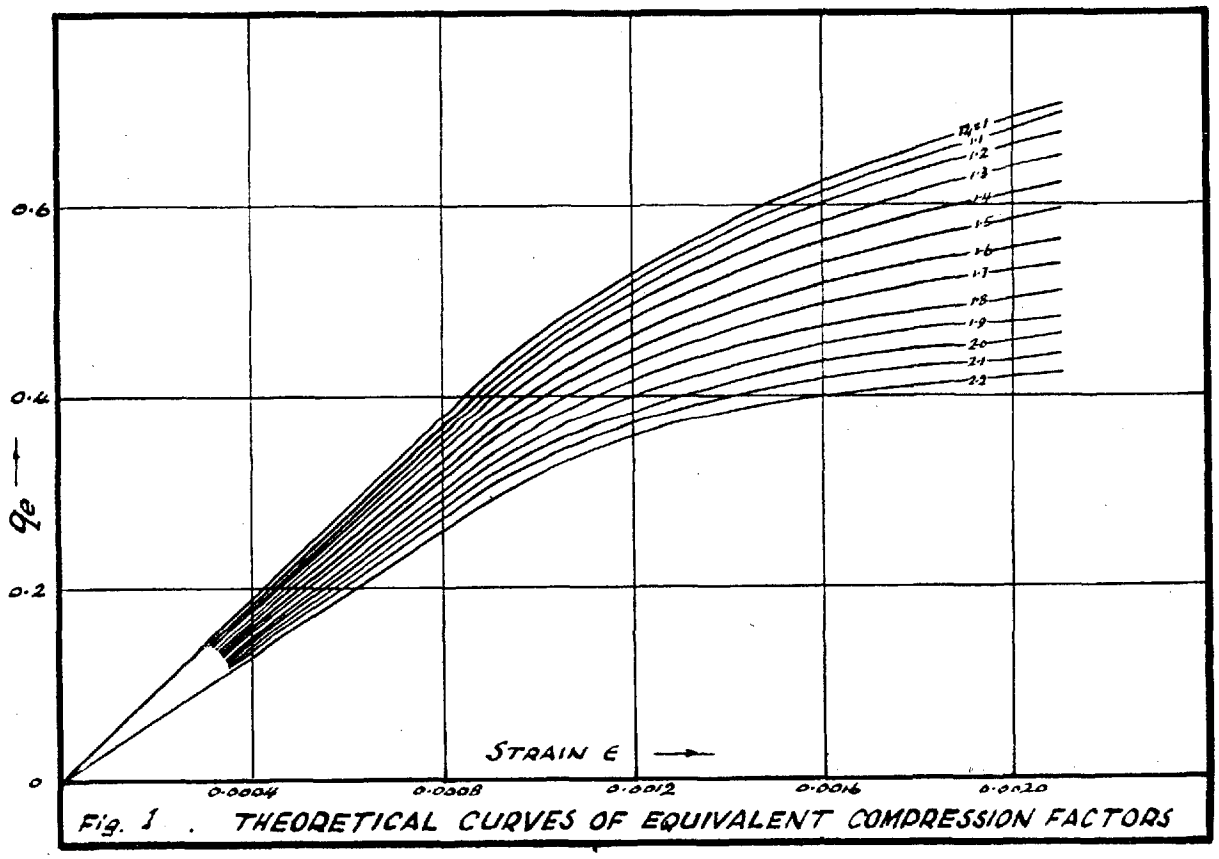


Fig. 1 . THEORETICAL CURVES OF EQUIVALENT COMPRESSION FACTORS

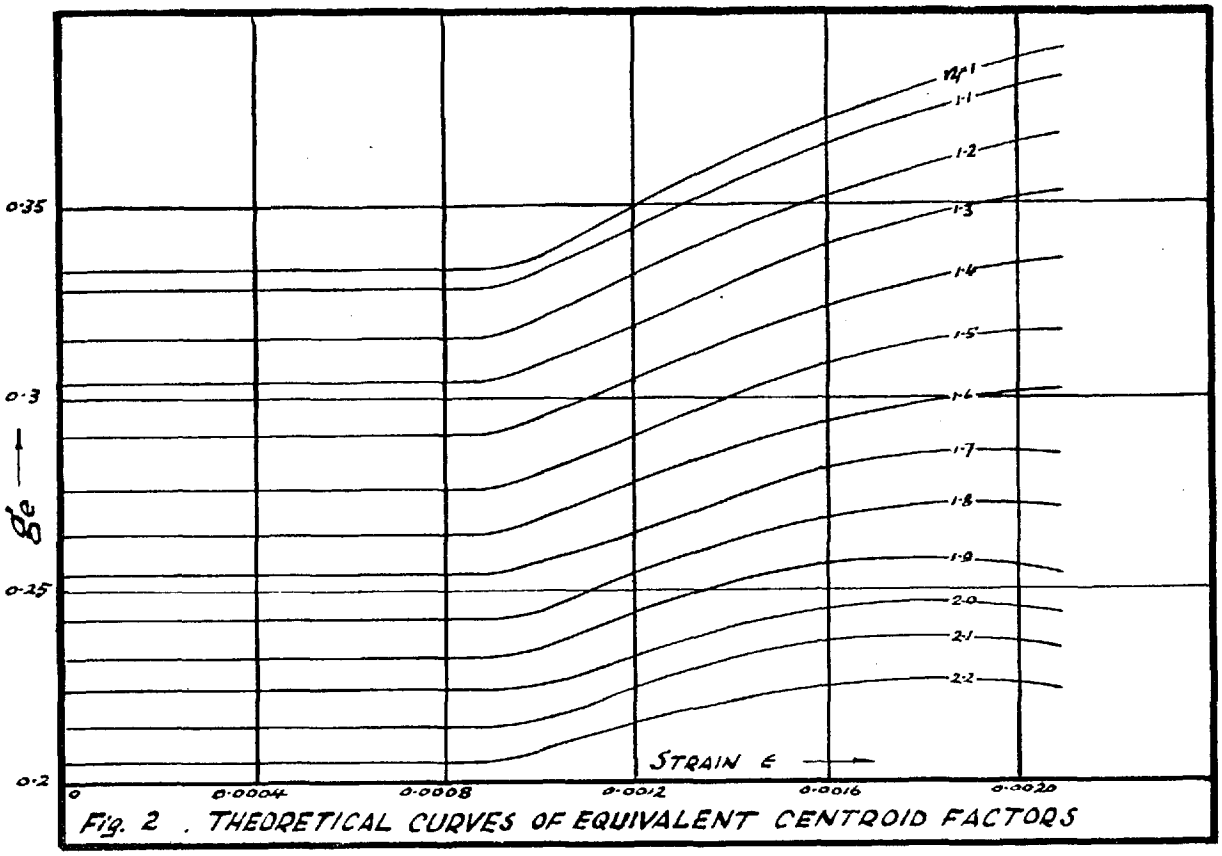


Fig. 2 . THEORETICAL CURVES OF EQUIVALENT CENTROID FACTORS

The Determination of Stress-Strain Curve Constants.

Elastic and Unbound Plastic Range.

The stress-strain curve of an elasto-plastic material in flexure may be determined by considering small increments of load and strain in a short-time bending test. Nadai [18] has given such equations for a homogeneous material, and Prentis [19] has derived suitable equations for reinforced and prestressed concrete.

Since the experiments conducted by the author were all of specimens subjected to combined bending and axial loading, these equations had to be modified to allow for axial load as well as compression reinforcement.

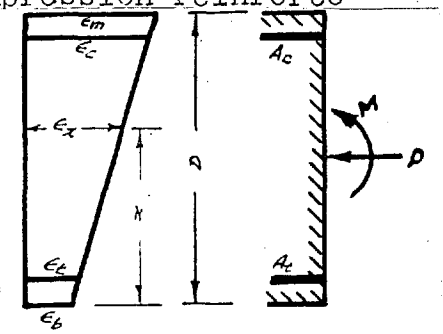


Fig. II.3.

Referring to Fig.II.3, if the stress-strain relationship is given by $f = \varphi(\epsilon)$, then equating forces,

$$P - A_c f_c - A_t f_t = b\int_0^D \varphi(\epsilon)\,dx \qquad \text{----------(II.10)}$$

If plane sections remain plane,

$$\epsilon_x = \epsilon_b + \frac{x}{D}(\epsilon_m - \epsilon_b) \qquad \text{----------(II.11)}$$

or

$$d\epsilon = \frac{(\epsilon_m - \epsilon_b)}{D}\,dx.$$

Substituting into (II.10),

$$P - (A_c f_c + A_t f_t) = \frac{bD}{(\epsilon_m - \epsilon_b)} \int_{\epsilon_b}^{\epsilon} \varphi(\epsilon)\, d\epsilon \,. \quad \text{---(II.12)}$$

Taking moments about O,

$$M + P\frac{D}{2} - \left[A_t f_t . t_1 d - A_c f_c (D - t_1 d)\right] = b \int_0^D x . f . dx$$

$$= \frac{bD^2}{(\epsilon_m - \epsilon_b)^2} \int_{\epsilon_b}^{\epsilon_m} (\epsilon_x - \epsilon_b)\varphi(\epsilon) d\epsilon \,.$$

Re-arranging and differentiating, it can be shown that,

$$f_m bD^2 = (\epsilon_m - \epsilon_b) . \frac{d}{d\epsilon_m} \left\{ M + P\frac{D}{2} - \left[A_t f_t . t_1 d - A_c f_c (D - t_1 d)\right] \right\}$$

$$+ 2 \left[M + P\frac{D}{2} - \left\{ A_t f_t . t_1 d + A_c f_c (D - t_1 d) \right\} \right] \left(1 - \frac{d\epsilon_b}{d\epsilon_m} \right)$$

$$+ \left[P - (A_c f_c + A_t f_t) \right] D \, . \frac{d\epsilon_b}{d\epsilon_m} \quad \text{------(II.13)}$$

Similarly, it can be shown that,

$$f_b bD^2 = (\epsilon_m - \epsilon_b) . \frac{d}{d\epsilon_b} \left[M - P\frac{D}{2} + \left\{ A_c f_c . t_1 d + A_t f_t (D - t_1 d) \right\} \right]$$

$$- 2 \left[M - P\frac{D}{2} + \left\{ A_c f_c . t_1 d + A_t f_t (D - t_1 d) \right\} \right] \left(1 - \frac{d\epsilon_m}{d\epsilon_b} \right)$$

$$+ \left[P - (A_c f_c + A_t f_t) \right] D . \frac{d\epsilon_m}{d\epsilon_b} \quad \text{-------(II.14)}$$

After cracking, $f_b = 0$, and (II.13) becomes

$$f_m . bD = \frac{d}{d\epsilon_m} \left\{ \left[P - (A_c f_c + A_t f_t) \right] . (\epsilon_m - \epsilon_b) \right\} \quad \text{----(II.15)}$$

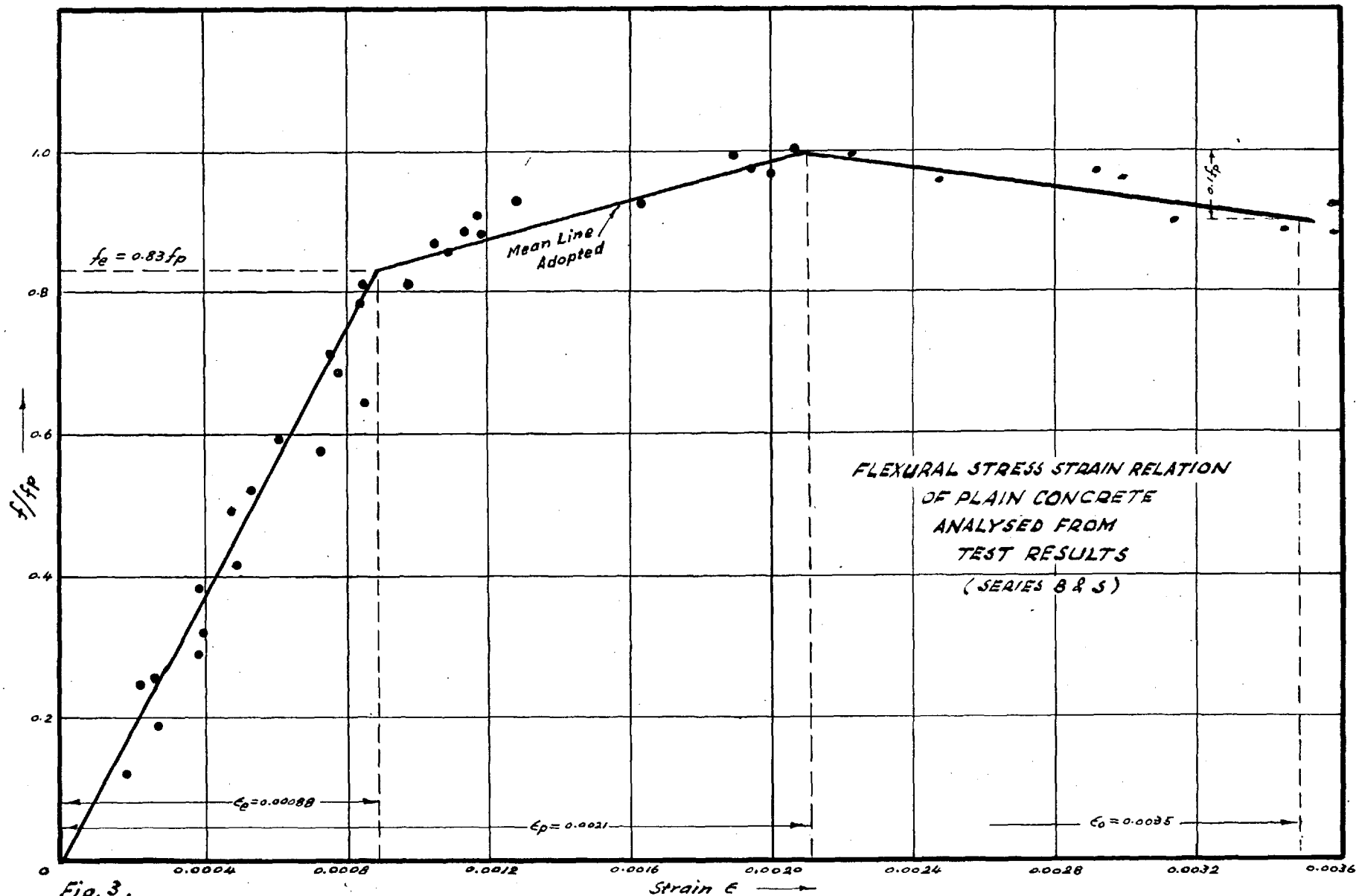

FLEXURAL STRESS STRAIN RELATION
OF PLAIN CONCRETE
ANALYSED FROM
TEST RESULTS
(SERIES B & S)
Mean Line
Adopted
$f_e = 0.83 f_p$
$\epsilon_e = 0.00088$
$\epsilon_p = 0.0021$
$\epsilon_0 = 0.0035$
f/f_p
Strain ϵ
0
0.2
0.4
0.6
0.8
1.0
0.0004
0.0008
0.0012
0.0016
0.0020
0.0024
0.0028
0.0032
0.0036

Fig. 3.

The concrete stress strain curve from bending test data may thus be obtained by applying equations II.13,14,&15. This method is applicable up to the ordinary crushing strain; after this range,i.e., in the binder range, due to the very high strains and creep with very small increments in stress, the graphical differentiation becomes very inaccurate.

Fig. 3 shows stress-strain curve points plotted for the author's tests of 16 rectangular specimens subjected to combined bending and axial loading, in terms of the concrete stress f_p. Two mean lines OA and AB drawn through these experimental points can be seen from Fig. 3 to represent sufficiently accurately the actual stress-strain relationship of the given concrete.

These two mean lines adopted, in accordance with the stress-strain curve proposed earlier, give values of the constants for the concrete used, as follows:

Concrete strength at 28 days = 3500 psi.

Maximum elastic strain ϵ_e = 0.00088.

Strain at max. stress f_p, ϵ_p = 0.0021.

Unbound concrete max. strain ϵ_o = 0.0035.

Maxumum elastic stress f_e = 0.83 f_p.

Unbound concrete ult. stress f_o = 0.90 f_p.

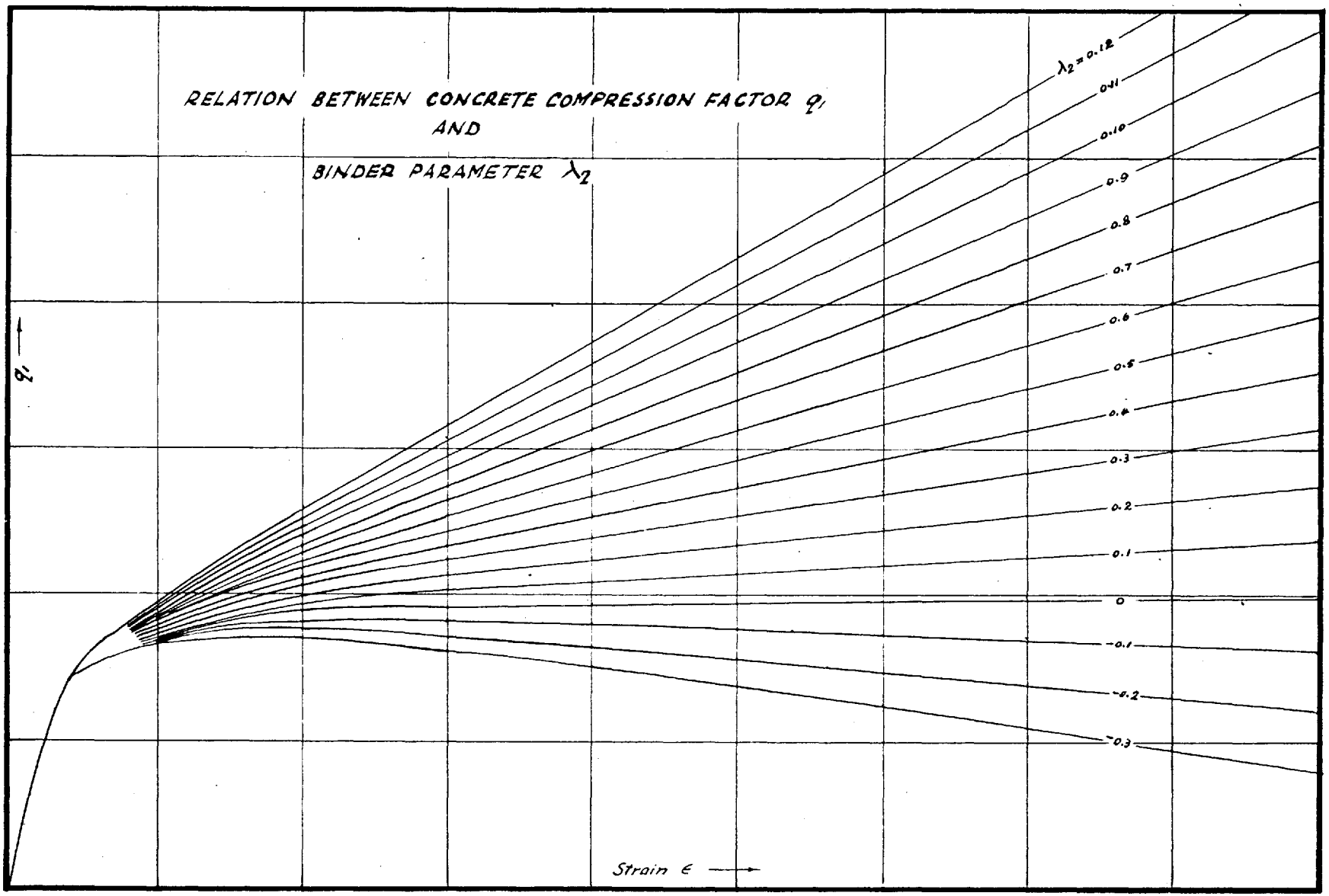

RELATION BETWEEN CONCRETE COMPRESSION FACTOR q_1
AND
BINDER PARAMETER λ_2
$\lambda_2 = 0.12$
0.11
0.10
0.9
0.8
0.7
0.6
0.5
0.4
0.3
0.2
0.1
0
-0.1
-0.2
-0.3
q_1
2.5
2.0
1.5
1.0
0.5
0
Strain ϵ
0.01
0.02
0.03
0.04

Fig. 4.

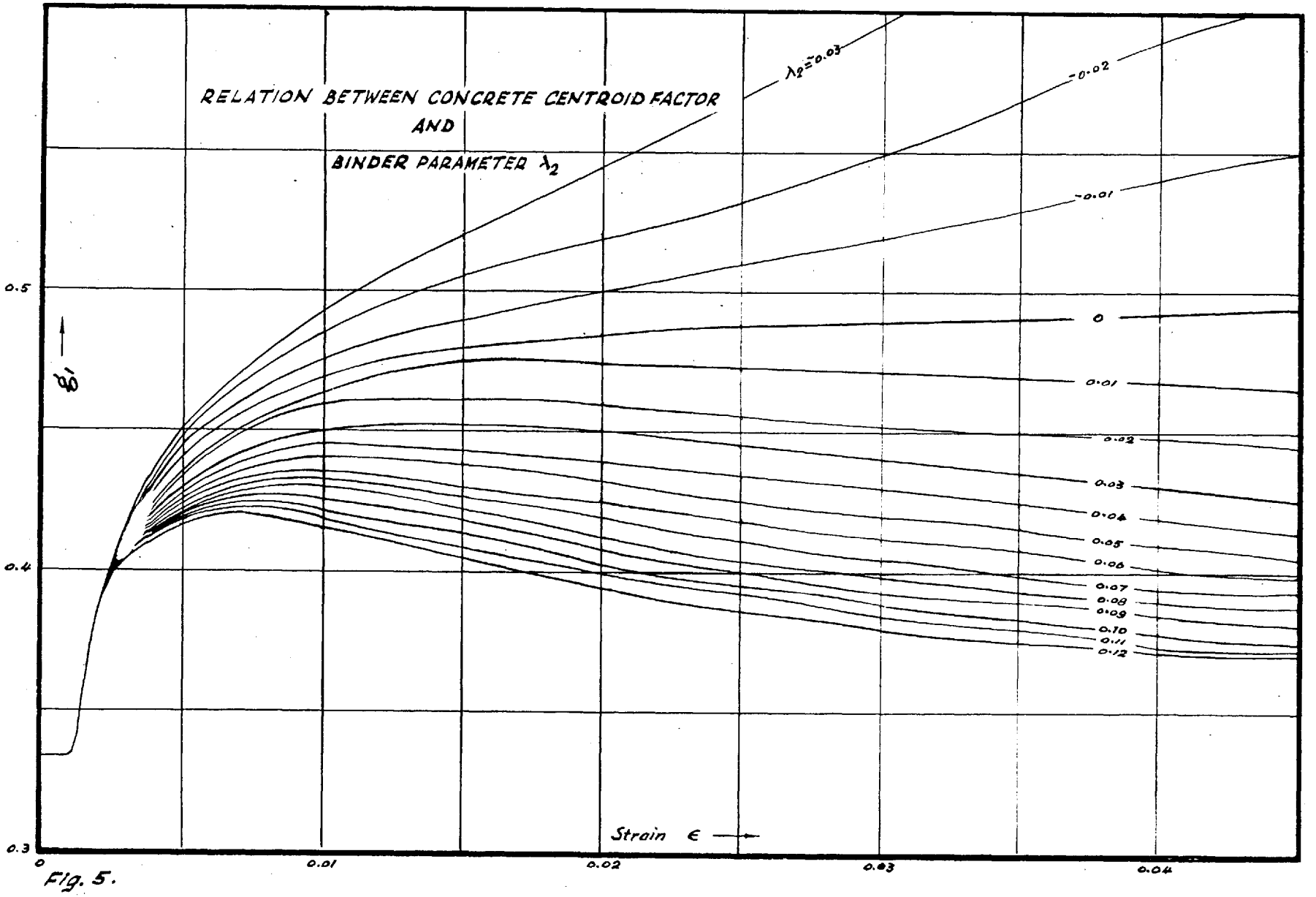

RELATION BETWEEN CONCRETE CENTROID FACTOR
AND
BINDER PARAMETER λ_2
$\lambda_2 = 0.03$
0.02
0.01
0
0.01
0.02
0.03
0.04
0.05
0.06
0.07
0.08
0.09
0.10
0.11
0.12
$\bar{y}$
0.5
0.4
0.3
Strain ϵ
0
0.01
0.02
0.03
0.04

Fig. 5.

These values are in good agreement with the findings of Smithies[20], who by the direct method of bending simulation, found that the stress-strain curve was nearly linear up to a strain of 0.0091 with a corresponding stress of 0.8 f_p, for a similar concrete of $f_p = 3600$.

The above figures give

$$\gamma_1 = 1.39.$$
$$\gamma_2 = 1.59.$$
$$E_e = 943.f_p$$
$$\lambda_1 = 0.1472.$$
$$\lambda_2 = -0.076. \text{ (for unbound concrete)}$$

Bound Plastic Range.

For reasons mentioned above, it is unsatisfactory to use the graphical differentiation process to determine the stress-strain relationship in this range, where very high deformations are encountered.

The only satisfactory method is to find, by trial, the values of λ_2 and γ_2 which give the best load deformation curve matching the actual curve obtained experimentally. The theoretical curves may be calculated by the equilibrium equations given in a later section, and are plotted together with the experimental results in Figs.25 to 49.

For a sufficient number of tests, the relationship between λ_2 and γ_2, and lateral binding may be established by this method of analysis.

To facilitate the trial process of determining values of λ_2 and γ_2, various values may be assumed and the corresponding g_1 and q_1 values plotted as in Figs.4 & 5, for various values of strain.

Stress-Strain Curve by Direct Method.

The method of Bending Simulation for directly determining the stress-strain curve of concrete in flexure was proposed by Professor A.L.L. Baker [3], and consists of subjecting a short length of concrete to variable stresses across the section by means of small individual hydraulic rams in the special testing machine. When the distribution of strains across the section is so adjusted that it represents the pattern of strain of a beam under bending, the corresponding stress distribution is obtained from the ram pressure readings. Some results were obtained by Smithies [20], and further research with this machine is still continuing.

The author would suggest that to check the validity of this method, beams of comparable size should be cast

with each bending simulation specimen, and tested in circular bending at the same time as the bending simulation test, and at the same rate of loading, so that the stress-strain curves obtained directly may be compared with those obtained analytically from the beam tests by the method described earlier.

If the stress-strain curve of plain concrete is shown to be accurately determined in this way, then it should also provide a direct method of investigating the stress-strain curves of bound concrete, for which analytical methods available are unsatisfactory.

PART III

THE STRENGTH AND DEFORMATION OF PLAIN AND BOUND REINFORCED CONCRETE.

Having established the generalized stress-strain relationship for bound and plain concrete as described in Part II, it is then possible to develop moment and force equilibrium equations which fully describe the strength and deformation of any reinforced concrete section at all stages of its loading history.

Basic Assumptions.

1. Plane sections remain plane in pure bending, or where distortion due to shear forces is negligible.
2. The stress-strain relationship is known for a given concrete, which for simplicity is assumed to be identical for flexure as for axial load.
3. The stress-strain relationship for steel reinforcement follows a trapezoidal curve, with ultimate strain hardening behaviour, and is identical for compression as for tension.
4. The tensile strength of concrete is neglected.
5. The failure of a section is brought about by the concrete attaining its ultimate strain, beyond which it fails to sustain a steady load.

Since the most general case is that of a section subjected to combined bending and axial load, this will be considered first.

Section Under Bending and Axial Load.

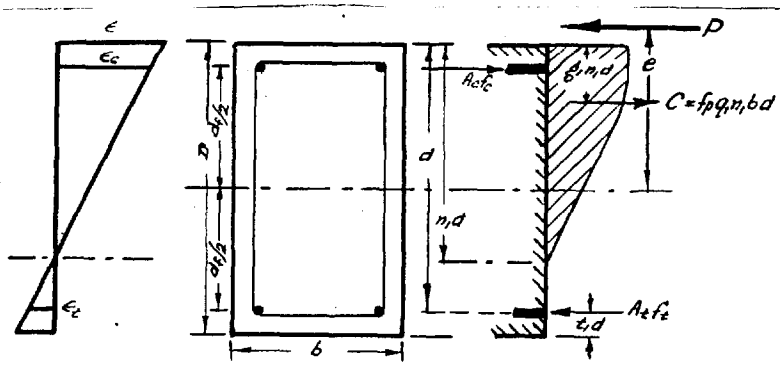


Fig. III.1.

Referring to Fig. III.1, equating moments about tension steel,

$$P(e + \frac{d_f}{2}) = C(1 - n_1 g_1)d + A_c f_c d_f$$

$$= f_p . q_1 n_1 b d^2 (1 - n_1 g_1) + A_c f_c d_f$$

----------(III.1)

Equating all forces,

$$P = C + A_c f_c - A_t f_t$$

$$= f_p . q_1 n_1 b d + A_c f_c - A_t f_t \quad ---(III.2)$$

For linear strain distribution,

$$\frac{\epsilon}{\epsilon_o} = \frac{n_1}{n_1 - t_1} \text{ , or } \quad f_c = \epsilon E_s \frac{n_1 - t_1}{n_1} \quad ----(III.3)$$

and after yield $f_c = f_y$

Also $\frac{\epsilon}{\epsilon_t} = \frac{n_1}{1-n_1}$, or $f_t = \epsilon E_s \frac{1-n_1}{n_1}$ -----(III.4)

and after yield, $f_t = f_y$

The eccentricity e denotes the total eccentricity, i.e., the sum of the nominal eccentricity e_o and the deflection. A method for determining the deflection is given later.

To solve the section completely by equations III.1 and III.2 entails the solution of the familiar cubic equation in n_1, which is rather tedious. A practical procedure is to find the value of n_1 by successive approximation by the following sequence:

For a particular value of ϵ, the values of g_1 and q_1 are known from Figs. 1, 2, 4, 5. Using a first guess value of n_1, a value of P is obtained by considering equations III.1, 3, and 4. Substituting this value of P, f_c and f_t in equation III.2, and solve for n_1 as unknown, thus completing the first cycle. Using this derived value of n_1 as a new guess value, the process is repeated until the derived value of n_1 equals the preceding guess value. In the first trial cycle, the eccentricity due to deflection can be neglected, using only the nominal value e_o. The deflection term is introduced when an approximate

value of n_1 is determined.

Note that to allow for the area of concrete displaced by the compression steel, the effective compression steel stress is given by

$$f_c = f_s - f$$

where f is the concrete stress corresponding to the strain ϵ_c.

Condition of $n_1 > \frac{D}{d}$.

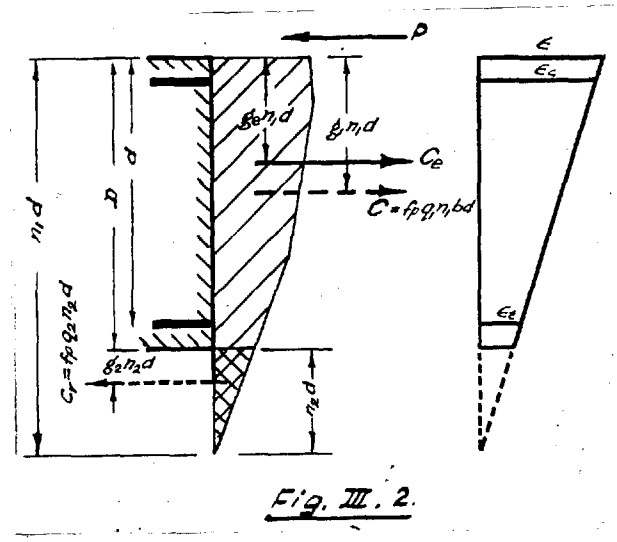


Fig. III. 2.

When the neutral axis is outside the section, a condition which may occur in a reinforced concrete member under bending and high axial load, and in prestressed concrete, it is clear from Fig.III.2 that the concrete compression and centroid factors q_1 and g_1 for a particular value of strain ϵ must be modified to equivalent compression and centroid factors q_e and g_e.

If C_e denotes the equivalent resultant force, then equating concrete forces:

$$C_e = C - C_r$$

$$= f_p q_1 n_1 bd - f_p q_2 n_2 bd$$

$$= f_p bd(q_1 n_1 - q_2 n_2)$$

and defining $C_e = f_p . q_e . n_1 db$, we have

$$q_e = \frac{q_1 n_1 - q_2 n_2}{n_1} \qquad \text{----------(III.5)}$$

Taking moments of concrete forces about O,

$$C_e . g_e n_1 d = C . g_1 n_1 d - C_r\left[n_1 - n_2(1-g_2)\right]d$$

$$= f_p bd^2\left\{g_1 q_1 n_1^2 - q_2 n_2\left[n_1 - n_2(1-g_2)\right]\right\}$$

giving $$g_e = \frac{g_1 q_1 n_1^2 - q_2 n_2\left[n_1 - n_2(1-g_2)\right]}{(q_1 n_1 - q_2 n_2)\, n_1} \qquad \text{---(III.6)}$$

or substituting (III.5) into (III.6) gives

$$g_e = \frac{g_1 q_1 n_1^2 - q_2 n_2\left[n_1 - n_2(1-g_2)\right]}{q_e n_1^2} \qquad \text{---(III.6a)}$$

and $$n_2 = n_1 - \frac{D}{d}$$

The values of q_2 and g_2 may be found in the same way as for q_1 and g_1, for the corresponding strain ϵ_b.

Hence the equilibrium equations for cases where $n_1 > D/d$ now become

$$P\left(e + \frac{df}{2}\right) = f_p q_e n_1 bd^2(1 - g_e n_1) + A_c f_c d_f \qquad \text{---(III.1a)}$$

and $$P = f_p q_e n_1 bd + A_c f_c - A_t f_t \qquad \text{-----(III.2a)}$$

Condition of Tension Steel Yield;

At steel yield, equation (III.2) becomes

$$P = f_p q_1 n_1 bd + A_c f_c - A_t f_y \qquad \text{--------(III2c)}$$

and equation (III.1) remains unchanged. Since the compression steel A_c has not yielded, f_c must be determined from the compatability equation (III.3) and hence a cubic equation is still involved.

Condition of Compression Steel Yield.

If the tension steel remains elastic, the general equations for this condition become.

$$P\left(e + \frac{d_f}{2}\right) = f_p q_1 n_1 bd^2 (1 - n_1 g_1) + A_c f_y d_f$$

and $$P = f_p q_1 n_1 bd + A_c f_y - A_t f_t \cdot$$

The solution involves a cubic equation.

Condition of Yield of Compression and Tension Steel.

In this case both the steel stresses are known without the compatability equations, giving

$$P\left(e + \frac{d_f}{2}\right) = f_p q_1 n_1 bd^2 (1 - n_1 g_1) + A_c f_y d_f$$

$$P = f_p q_1 n_1 bd + A_c f_y - A_t f_y,$$

$$n_1 = \frac{(d - \frac{d_f}{2} - e) + \sqrt{(d - \frac{d_f}{2} - e)^2 + \frac{4 g_1 d}{q_1 f_p}\left\{p_c f_y (\frac{d_f}{2} - e) + p_t f_y (e + \frac{d_f}{2})\right\}}}{2 g_1 d}$$

------(III.7)

This value of n_1 from the quadratic may then be substituted into (III.2) to find the load P .

For symmetrical reinforcement, $p_c = p_t = p_s$, and combining equations (III.7) and (III.2),

$$P = f_p bd \frac{q_1}{2g_1}\left[(1 - \frac{e_s}{d}) + \sqrt{(1 - \frac{e_s}{d})^2 + \frac{4g_1}{q_1} p_s \frac{f_y d_f}{f_p d}}\right]$$

------(III.8)

where $e_s = e + \frac{d_f}{2}$

Without compression reinforcement, $p_c = 0$, giving

$$P = f_p bd\left\{-p_t \cdot \frac{f_y}{f_p} + \frac{q_1}{2g_1}\left[(1 - \frac{e_s}{d}) + \sqrt{(1 - \frac{e_s}{d})^2 + \frac{4g_1}{q_1 f_p} p_t f_y \frac{e_s}{d}}\right]\right\}$$

For greater slide rule accuracy, this equation may be multiplied and divided by

$$-(1 - \frac{e_s}{d}) + \sqrt{(1 - \frac{e_s}{d})^2 + \frac{4g_1}{q_1} \cdot p_t \cdot \frac{f_y e_s}{f_p d}}$$, giving

$$P = A_t f_y \frac{(e_s + d) - \sqrt{(e_s - d)^2 + \frac{4g_1 \cdot f_y e_s}{q_1 \cdot f_p b} \cdot A_t}}{(e_s - d) - \sqrt{(e_s - d)^2 + \frac{4g_1 \cdot f_y e_s}{q_1 \cdot f_p b} \cdot A_t}}$$

--------(III.9)

Sections Under Pure Bending.

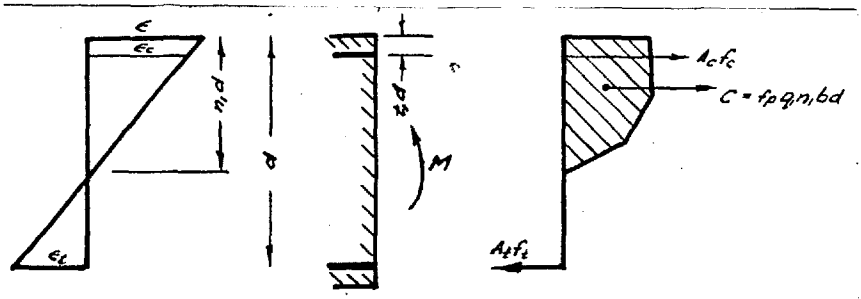


Fig. III.3.

Referring to Fig. III.3, equating all forces gives $f_p q_1 n_1 bd + A_c f_c = A_t f_t$ ---------(III.10)

and taking moments about the neutral axis,

$$M = f_p q_1 n_1^2 bd^2 (1 - g_1) + A_c f_c (n_1 - t_1)d + A_t f_t (1 - n_1)d$$

-------(III.11)

The compatability equations (III.3) and (III.4) also apply to this case.

The general equation for n_1, for any stage of load corresponding to a strain ϵ, is obtained by substituting equations (III.3) and (III.4) into (III.10),

$$n_1 = \frac{\epsilon E_s}{2 f_p q_1}\left[\sqrt{(p_c + p_t)^2 + \frac{4 f_p q_1}{\epsilon E_s}(p_c t_1 - p_t)} - (p_c + p_t)\right]$$

------(III.12)

For no compression reinforcement, $p_c = 0$, and

$$n_1 = \frac{\epsilon E_s}{2 f_p q_1}\left[\sqrt{p_t^2 + \frac{4 f_p q_1 p_t}{\epsilon E_s}} - p_t\right]$$ ------(III.12a)

and for symmetrical reinforcement, $p_c = p_t = p_s$,

$$n_1 = \frac{\epsilon E_s}{2f_p q_1}\left[\sqrt{4p_s^2 + \frac{4f_p q_1}{\epsilon E_s}.p_s(t_1 + 1)} - 2p_s\right] \quad ---(III.12b)$$

When the reinforcement steels yield, so the corresponding compatability equations are dissolved, as shown earlier.

Expressing the neutral axis factor in terms of strain gives

$$n_1 = \frac{\epsilon}{\epsilon + \epsilon_t}$$

and for a balanced yield,

$$n_1 = \frac{\epsilon_y}{\epsilon_y + \frac{f_y}{E_s}}$$

The Analysis of Circular Sections.

Hitherto the strength and deformation equations have been only derived for rectangular sections. For circular sections, the determination of the concrete resultant force and its line of action is very involved, especially when $n_1 > 1$.

Hognestad [16] assumes for such cases that the neutral axis depth may be considered to be $q_1 n_1 d$, from which the corresponding segment area of compression A is determined. The concrete resultant force is then found from $C = A.f_p q_1 n_1 d$, the line of action being located at the geometric centroid of the segment.

The author has found that this approximation is justified for the single ultimate load-stage only, and also only for sections in which $n_1 < 1$. For interpreting the complete loading history of the section, and where n_1 is high, this approximation method incurs serious error.

While a better method of analysis was still left to be desired, it was thought that , for the purpose of analysing the results of the author's tests on spirally bound cylinders, a sufficiently accurate approximation is achieved by assuming the circular

section to be replaced by an equivalent rectangle, the dimensions of the rectangle being obtained by equating:

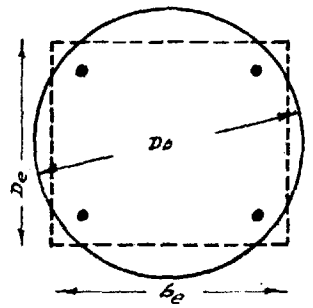


Fig. III.4.

i. The two areas;

ii. The two second moment of areas,

giving $D_e = 0.866\ D_o$

and $b_e = 0.908\ D_o$.

The strength and deformation equations are then applied to the equivalent rectangle, the steel reinforcement positions being unchanged, and the concrete cover having the same value as that of the circular section.

The theoretical curves given in Figs.35 to 41 were obtained in this way.

Determination of Deflections.

Deflection increases the eccentricity of a member subjected to combined bending and axial loads. When applying equations (III.1) and (III.2) to find the strength and deformation of such members, the deflection must therefore be known and included in the eccentricity term, as mentioned earlier.

Any member will deflect when a lateral load is introduced, the magnitude depending on the load and the rigidity of the member. In very slender members loaded axially and laterally, the moment due to the deflection multiplied by the axial load will still further increase the deflection appreciably.

Taking the case of a pin-ended uniform strut, axially loaded and point-loaded laterally at the centre as in Fig.III.5, the familiar expression for the maximum bending moment at the centre is

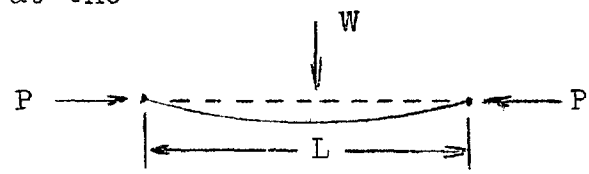


Fig.III.5.

$$M_o = \frac{W}{2}\sqrt{\frac{EI}{P}}.\ \tan\sqrt{\frac{P}{EI}}$$

Expanding this in series form,

$$\tan\theta = \theta + \frac{1}{3}\theta^3 + \frac{2}{15}\theta^5 + \text{-----}$$

$$\text{gives } M_o = \frac{WL}{4} + \frac{WL^3}{48EI}.P\left\{1 + \frac{\pi^2 P}{10P_e} + \frac{17\pi^4}{1680}.\left(\frac{P}{P_e}\right)^2 + \text{---}\right\}$$

$$\doteq \frac{WL}{4} + \frac{WL^3}{48EI}.P \qquad \text{in cases where}$$

higher terms may be neglected.

In most structural members, especially those of reinforced concrete, the slenderness ratios are not generally high, so that this approximation is sufficiently accurate for practical purposes.

The above equation shows that the total bending moment is found as the sum of the moment due to the lateral load, and the moment due to the axial load multiplied by the deflection causedby the lateral load.

In the above case, the deflection is

$$\delta = \frac{WL^3}{48EI}$$

$$= \frac{ML^2}{12EI}$$

and from the relation $M/EI = \epsilon/n_1 d$, we have

$$\delta = \frac{\epsilon L^2}{12 n_1 d} \qquad \text{----------(III.13)}$$

Since the stress-strain relationship is fully known, the deflection may be found for any value of ϵ and n_1 from the equations (III.1) and (III.2).

When part of the beam is plastic, EI is no longer constant, and although the precise value of the deflection

may still be determined, the process would be extremely tedious, since the change of EI along the length of the member in the plastic stage is generally difficult to be found. In such cases, it is probably simplest to use the mean of the elastic and plastic EI values.

For cases of very slender columns and where moments due to deflections are of high proportions, a more accurate determination of deflections is necessary. It is understood that this problem is being studied in fuller detail by Bassi [21].

Similarly, for the case of members subjected to bending and axial loads in single curvature bending only, as in Fig. (III.6), the deflection is given by

$$\delta = \frac{\epsilon L^2}{8 n_1 d} \qquad \text{---(III.14)}$$

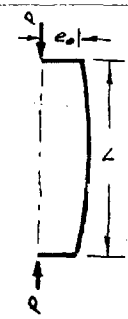


Fig. III.6

In this instance, since the member is subjected to a fairly uniform bending moment throughout its length, EI is also fairly constant throughout for both the elastic and plastic conditions.

Sections Under Axial Load.

This condition does not only exist in axially loaded columns, but also at sections such as the point of contraflexure O O shown in Fig.III.7 in columns subjected to bending and direct load.

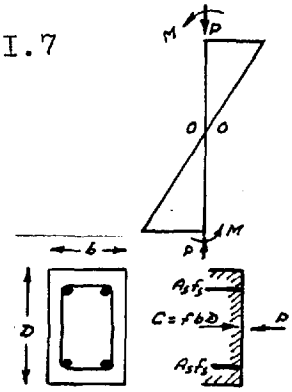


Fig. III. 7.

Referring to Fig.III.7, equating forces gives

$$P = f.bD + A_c f_c + A_t f_t \qquad \text{--------(III.15)}$$

and since concrete stress-strain is related by $f = \varphi(\epsilon)$,

$$P = \varphi(\epsilon)bD + (A_c + A_t)\epsilon E_s$$

or $$\frac{P}{bD} = \varphi(\epsilon) + (p_c + p_t)\epsilon E_s \qquad \text{----------(III.16)}$$

As reinforcement is usually symmetrical, $p_c = p_t = p_s$,

$$\frac{P}{bD} = \varphi(\epsilon) + 2p_s \epsilon E_s \qquad \text{----------(III.16a)}$$

Note that the steel ratio p_s is in this case expressed in terms of the overall depth D and not d as in the analysis for bending.

If the reinforcement is not symmetrical, the centroid of internal forces may not be at the geometrical centre-line, but would be on a line which the resultant of all internal forces cuts the section. This point

lies between the mid-depth and the geometrical centroid of the reinforcement, and the section will be truly axially loaded if the load is applied at that point. For such a section, the true centroid of internal forces will remain constant in position in the elastic range, but in the plastic range, the plastic centroid changes with change in load, since the ratio of steel to concrete forces in the section no longer remains constant.

Spalling in the Bound Plastic Condition.

Since effective triaxial compression from lateral binding commences after the ordinary crushing strength and deformation of the plain concrete has been exceeded, it follows that any concrete cover outside the lateral binding will have spalled off in the bound plastic range.

In practice, a certain depth of concrete cover is always provided to protect the reinforcement, and thus some sudden loss in strength takes place when the spalling load is attained, due to loss of concrete compression area. This reduction in area must be allowed for in considering the strength and deformation of bound concrete.

Test observations have shown that it is sufficiently accurate to assume the effective core of bound concrete to be the area enclosed by the lateral binding, as shown in Fig.III.8. The portions of the concrete cover which are still intact where the spalling strain has not been exceeded, still remain part of the effective concrete compression area.

Fig.III.8 shows the progressive stages of the spalling of concrete cover of a laterally bound section under bending load:

(a) shows the commencement of spalling when the compression edge of the section attains the plain concrete ultimate strain ϵ_o;

(b) shows the increasing depth of spalling when lower fibres in turn attain the value of strain ϵ_o, resulting in the gradual reduction of effective depth;

(c) shows further increase in the depth of spalling under further load, until all the cover up to the core boundary on the compression edge is lost. Any further loading would not resdlt in further decrease in effective depth, but will still continue to reduce the concrete compression area, due to reduction in effective breadth.

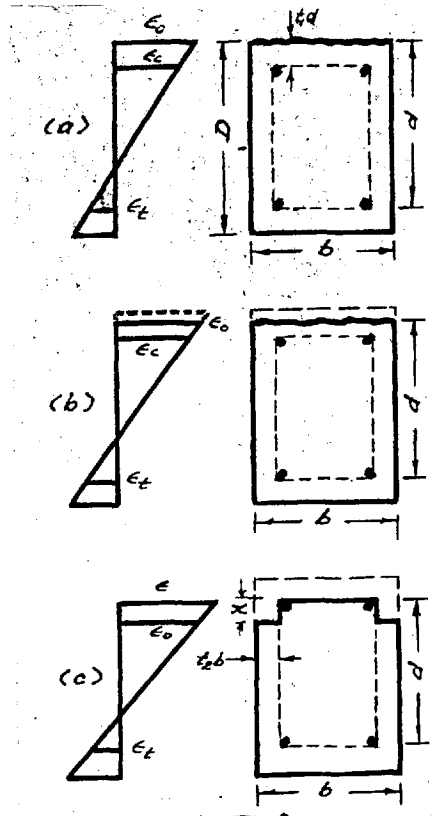


Fig. III. 8.

Referring again to Fig. III. 8, the effective depth d_e may be shown to be

$$d_e = \left(1 + \frac{\epsilon_o - \epsilon_c}{\epsilon_c + \epsilon_t}\right) d_f \qquad \text{----------(III.17)}$$

for the condition $d_f < d_e < d$, i.e., within case (b).

For condition (c), where $\epsilon_c > \epsilon_o$, and $b_e < b$,

$$d_e = d_f,$$

and equating the effective area to the equivalent area,

$$b_e . d_f = b\left(1 - \frac{2.t_2 x}{d_f}\right) d_f$$

gives the equivalent breadth as,

$$b_e = b\left[1 - 2.t_2 \frac{\epsilon - \epsilon_o}{\epsilon + \epsilon_t}\right] \quad \text{----------(III.18)}$$

The above equations enable values of d_e and b_e to be determined for the appropriate condition of spalling. The strength and deformation of bound sections may then be analysed by substituting these values in equations (III.1) and (III.2).

For axial loading, the strain is uniform over the entire section, so that once the spalling strain ϵ_o has been attained, the equivalent dimensions are simply

$$b_e = b - 2t_2 b$$

and $$d_e = d_s.$$

PART IV

THE BEHAVIOUR OF PLASTIC HINGES.

It was indicated in Part I that plastic hinge action commences at critical sections where peak regions of the bending moment diagram occur.

The required hinge rotation θ as defined in the Plastic Hinge Theory is first found by considering the modified elastic equations for plasticity and using a trial and adjustment procedure to obtain the most economic ultimate distribution of bending moments.

The available hinge rotation that can be developed at a hinge at the plastic moment value of resistance is then found by considering the deformation of the critical sections from

$$\theta = \frac{l_p s_p}{n_1 d} \qquad \text{----------(I.2)}$$

and the hinge is satisfactory if the required value does not exceeded the available value.

It was also shown in Part I that the above equation offers a practical design rule, but does not fully represent actual behaviour. In order to apply this design rule correctly, investigations have then to be made of the actual behaviour.

Basic Definitions.

In accordance with the relation between the Plastic Hinge Theory and actual behaviour, examined in Part I, the following definitions may be proposed:

1. A plastic hinge is defined as that region along a member under the influence of peak bending stresses, within which the strength and deformation has at every section exceeded its elastic value.

2. The available hinge rotation is the total change of slope in excess of the corresponding elastic change of slope over the length of the plastic zone, with reference to the plastic moment.

3. The strains within a plastic zone fall between two limits:

(a). The yield strain ϵ_y, at which plastic deformation commences with any further increase in load. The moment of resistance at this condition is defined as the yield moment M_y.

(b). Any higher value of strain not exceeding the ultimate value ϵ_u; the moment of resistance at this condition is the plastic moment M_u.

For (a), since the yield strain of concrete is about 0.00088 from test observations, and about 0.0013 for mild steel, the problem is considerably simplified

by assuming a common value of yield strain $\epsilon_y = 0.0010$. This implies that yielding commences at any section when the strain of 0.0010 is exceeded, for tension or compression. For other different concretes and steels, other suitable common values may be adopted.

For (b), the ultimate strain of concrete ϵ_u found in the author's tests had an average value of 0.0035. For laterally bound concrete, strain exceeding 0.015 may be reached. The tension steel is assumed to be able to accommodate indefinitely large strains in most usual cases so long as the concrete has not crushed. The effects of bond-slip and crack distribution at very high steel strains are not considered here, but may be allowed for by the use of F factors as in Professor A.L.L. Baker's Plastic Theory. In bound sections where the concrete strain is very high and the neutral axis value small, steel fracture may occur, but this condition seldom exists in practice. For compression reinforcement, lateral ties must be close enough to avoid early plastic failure by the bars buckling.

The Length of the Plastic Zone h .

For a ductile material with imperfect elasto-plastic properties, in which

$$0 < M_y/M_u < 1,$$

plasticity must take place over a finite length when the member is subjected to a varying bending moment as shown in Fig.IV.1. The length over which plasticity occurs will now be determined.

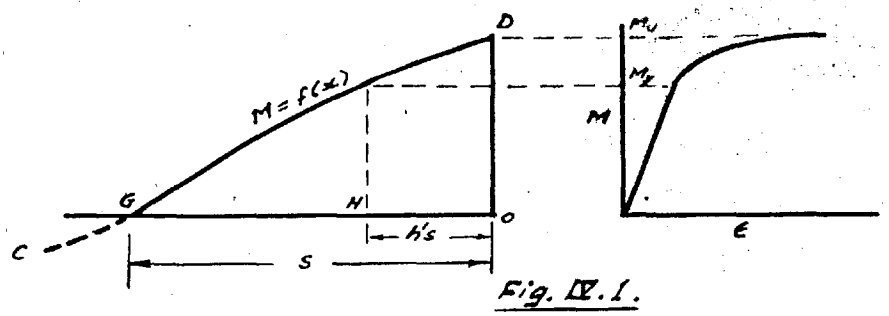


Fig. IV.1.

Case of Bending Only. Consider a length of member OGF which could be part of a beam with support section at O, where plastic rotations are developed along OH = h = h's, under a bending moment CGD which may be expressed as $M = f(x)$.

Differentiating, $\frac{dM}{dx} = f'(x)$,

and thus $h' = \frac{1}{s} \int_{s(1-h')}^{s} ds$

or $$h' = \frac{1}{s}\int_{M_y}^{M_u}\frac{dM}{f'(x)}. \qquad \text{--------(IV.1)}$$

For concentrated loading, the bending moment diagram is linear and may be expressed as

$$M = \frac{M_u}{s}.x$$

and $$dM = \frac{M_u}{s}\,dx$$

giving $$h' = 1 - \frac{M_y}{M_u} \qquad \text{----------(IV.2)}$$

In most cases, it is sufficiently accurate to assume that the B.M. diagram is linear within the length of the bending moment intercept, s .

The bending moment intercept s is a fraction of the whole length of a framework member. For instance, in the interior span of a continuous beam with a central point load, the value of s is $\frac{1}{4}$, and for usual columns is $\frac{1}{2}$, for the condition of fully equalized moments. The value of s for a given member is shorter for higher moment redistribution.

Using the general equations III.1 and III.2, and IV.2, the length of the plastic zone have been calculated for a medium strength concrete and various percentages of steel, and plotted in Fig. 6.

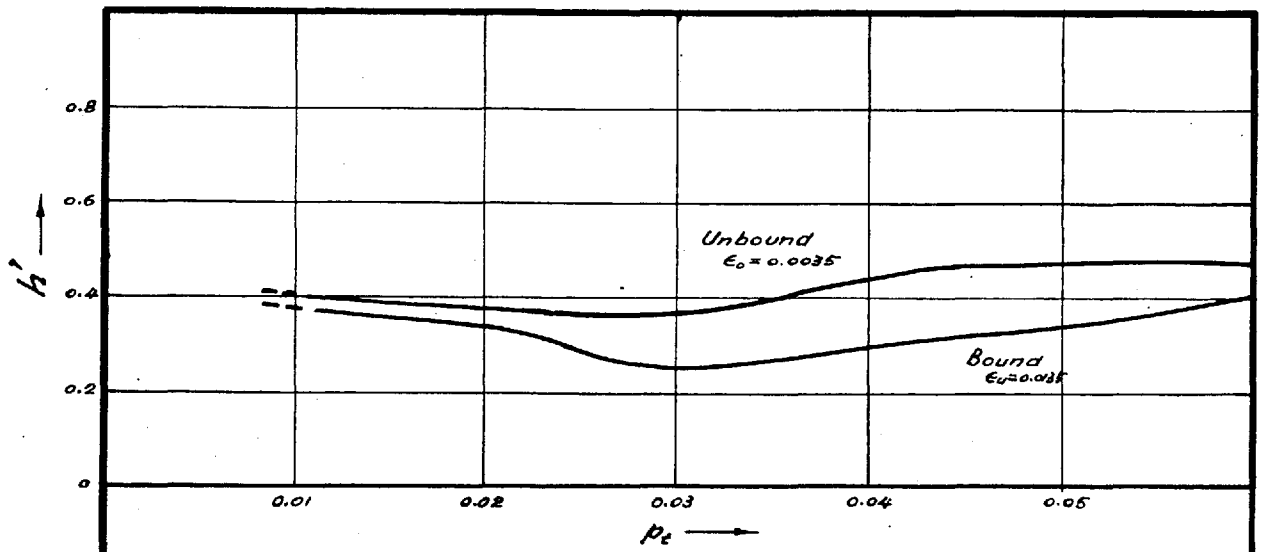


Fig. 6. RELATION BETWEEN LENGTH OF PLASTIC ZONE AND TENSION STEEL RATIO FOR MEMBERS IN BENDING ONLY.

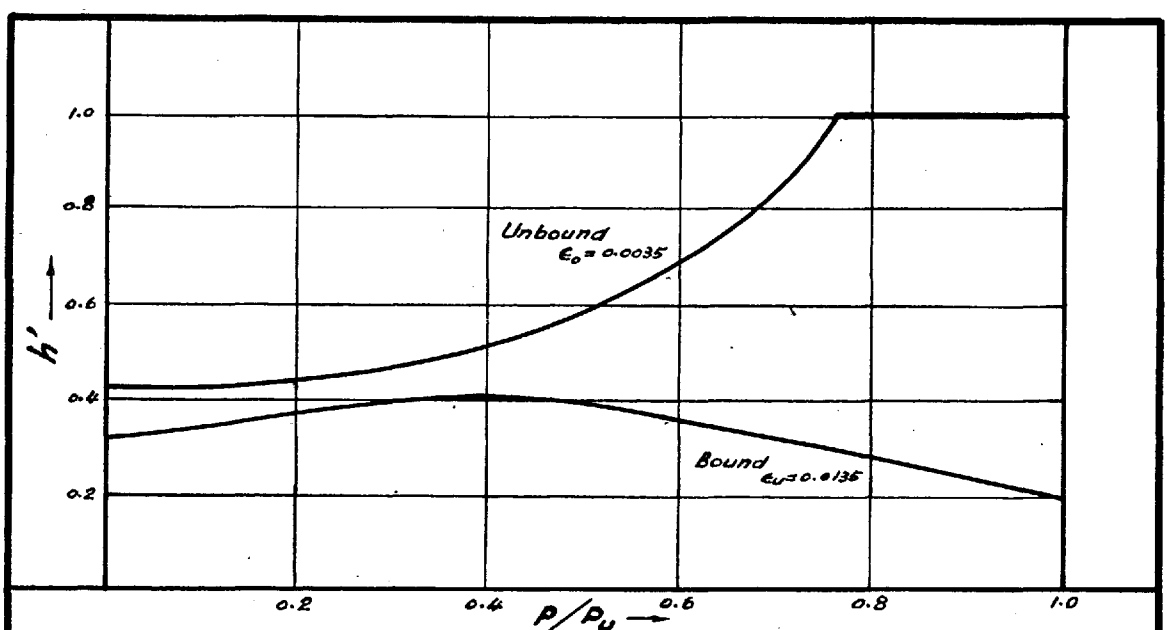


Fig. 7. RELATION BETWEEN LENGTH OF PLASTIC ZONE AND RATIO OF AXIAL LOAD.

It will be seen that for both under-reinforced and over-reinforced beams, the plastic zone length does not vary appreciably, having an average value of $h' = 0.4$. For uniformly distributed loading, taking into account the parabolic moment diagram, the corresponding value would be 0.228. It is possible that bond-slip may shorten slightly the plastic zone for under-reinforced beams, but this was not taken into account in the curves of Fig.6.

For laterally bound beams, the curve was calculated assuming that a binding used permitted an ultimate strain of $\epsilon_u = 0.0135$, and $\lambda_2 = 0.024$, and a depth of cover $t_1 = 0.12$. The reduction of area due to concrete cover being spalled off was allowed. The curve is seen to show a similar form to that of the plain concrete beams, with a slightly lower average value of $h' = 0.32$. The effect of spalling will be discussed later.

Case of Combined Bending and Axial Loads. Expressing the total bending moment as

$$M = P.e \ ,$$

where e denotes the nominal eccentricity plus the deflection of the particular section, equation (IV.2) becomes

$$h' = 1 - \frac{e_y}{e_u} \qquad \text{---------(IV.3)}$$

The influence of axial load on the length of the plastic zone has been examined and plotted in Fig.7 for the concrete and reinforcement assumed as in Fig.10, by considering equation (IV.3) and the equations (III.1) and (III.2). The axial load is expressed by the dimensionless parameter P/P_u, where P_u is the ultimate strength of the column under a pure axial load.

Unlike the case of beam hinges, the plastic zone increases in length with increasing axial load. It is clear that when the value of the axial load is alone sufficient to cause yield in the column at the point of contraflexure OO (Fig.IV.2) then the whole column has yielded since every other section along GO is at a higher strain, and hence

$$h' = 1, \text{ for } P_y < P < P_u.$$

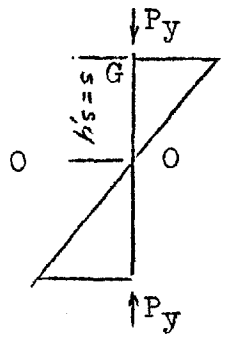


Fig.IV.2

For the case of plain unbound columns, the curve in Fig. 7 shows how the plastic zone spreads, as explained above.

For the case of laterally bound column hinges, it will be noticed that the plastic zone is increased for increasing axial loads at low values of load only, while at higher values of P, the value of h' is decreased

for further axial load increments. This is because the binding chosen for this example, giving $\epsilon_u = 0.0135$ and $\lambda_2 = 0.024$, gave values of P_u after allowing for spalling, which were lower than the unspalled value of P_y, so that no yield could occur at the point of contraflexure in the bound condition, and hence h' could not reach the value 1 .

In most columns in practice, the percentage of steel, depth of cover, strength of concrete, and the practical ratio of lateral binding that may be used, are such that h' will usually be less than 1 in the bound condition.

The Effective Rotation of Plastic Hinges.

It was shown in Part I that the hinge rotation as defined by the Plastic Hinge Theory, can be expressed by

$$\theta_k = \int_0^{h_k} \frac{M}{EI_s}\, ds \quad - \int_0^{h_k} \frac{M}{EI_e}\, ds \qquad \text{--(I.6)}$$

for the k^{th} hinge.

Equation (I.6) can be readily integrated if the relation $M/EI = f(x)$ can be expressed mathematically.

If the relationship is not known or is discontinuous, h_k can be divided into small segments over which EI values can be taken as constant, and the value of θ_k may then be obtained by summation:

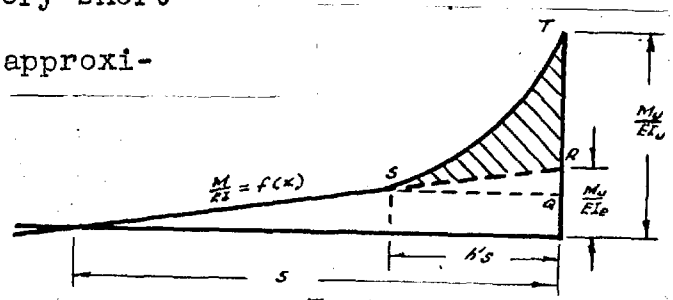
$$\theta_k = \sum_0^{h_k} \frac{M}{EI_s}\, \delta s \quad - \sum_0^{h_k} \frac{M}{EI_e}\, \delta s \qquad \text{--(IV.4)}$$

Both equations (I.6) and (IV.4) are very tedious to apply in practice. It is far simpler to obtain the elastic M/EI diagram experimentally, integrating graphically to obtain the area, and thus obtain values of constants in terms of the ultimate unit rotation M_u/EI_u. The value of θ_k may then be readily determined.

Practical Equation for Available Hinge Rotation.

Referring to Fig. IV.3, and in accordance with equation(I.6), it is clear that the effective rotation is given by the hatched area STR.

The length of RQ is very short compared with SQ, so that approximately SR = SQ = h's.



Area $\overline{STR}$ may be expressed by

$$h's.TR.\beta \quad ,$$

where β is a constant depending on the form of curvature distribution, and may be termed the curvature distribution factor. Also, $TR = M_u/EI_u - M_u/EI_e$, so that the rotation equation becomes

$$\theta_k = \beta h'_k . s . M_u \left[\frac{1}{EI_u} - \frac{1}{EI_e}\right] \quad ---(IV.5)$$

If equation (IV.2) for the length of plastic zone is also introduced, then

$$\theta_k = \frac{M_u s}{EI_e} . \beta \left[1 - \frac{M_y}{M_u}\right]\left[\frac{EI_e}{EI_u} - 1\right] \quad ---(IV.6)$$

The determination of θ_k is thus reduced to the work of finding the moments and rigidities of the member for the elastic condition and the ultimate fully plastic condition only. The experimental determination of β values is discussed later.

Main Factors Governing the Available Plastic Rotation.

Tension Reinforcement.

As was pointed out by Professor Baker [3,4], under-reinforced sections which yield mainly by steel plasticity, can develop high plastic rotation values before failure, since for a given value of ϵ_u, very small neutral axis depths occur before failure, so that

$$M_u/EI_u = \epsilon_u/n_1 d$$

will be high.

For heavily reinforced sections, the neutral axis depth at failure will be relatively higher, giving smaller plastic rotations, unless higher strains can be safely accommodated by the use of lateral binding.

The relation between tension steel ratio and the available plastic hinge rotation has been studied and plotted in Fig.8, from a worked example assuming concrete and steel properties as given in Fig. 10. The curves show that the increase of steel quickly decreases the rotation value. This is in agreement with other results. [8, 17].

Compression Reinforcement.

Consideration of equation (III.1) and (III.2) will show that, since compression steel yields long before

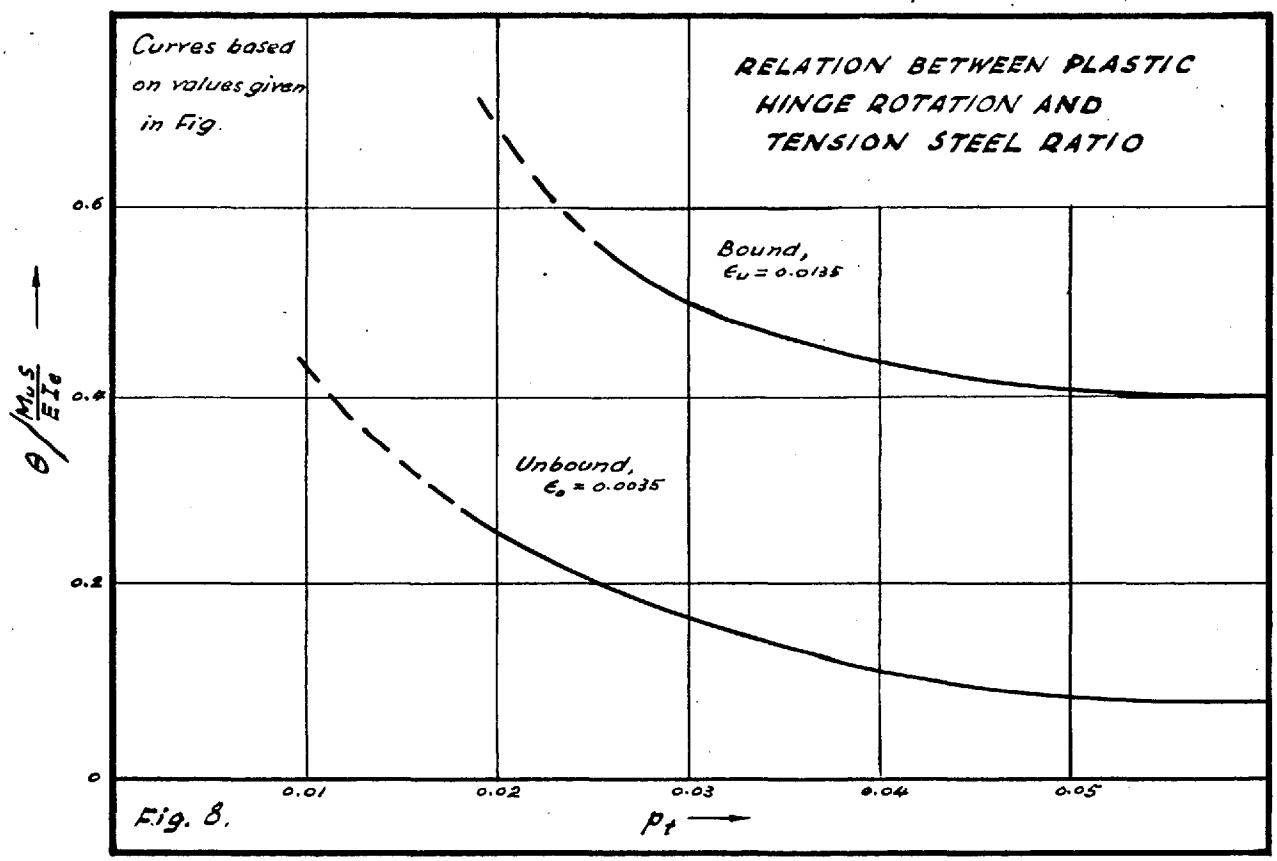

Curves based on values given in Fig.
RELATION BETWEEN PLASTIC HINGE ROTATION AND TENSION STEEL RATIO
Bound, $\epsilon_u = 0.0135$
Unbound, $\epsilon_u = 0.0035$
$\theta / \frac{M_u S}{E I_e}$
p_t
0.6
0.4
0.2
0
0.01
0.02
0.03
0.04
0.05

Fig. 8.

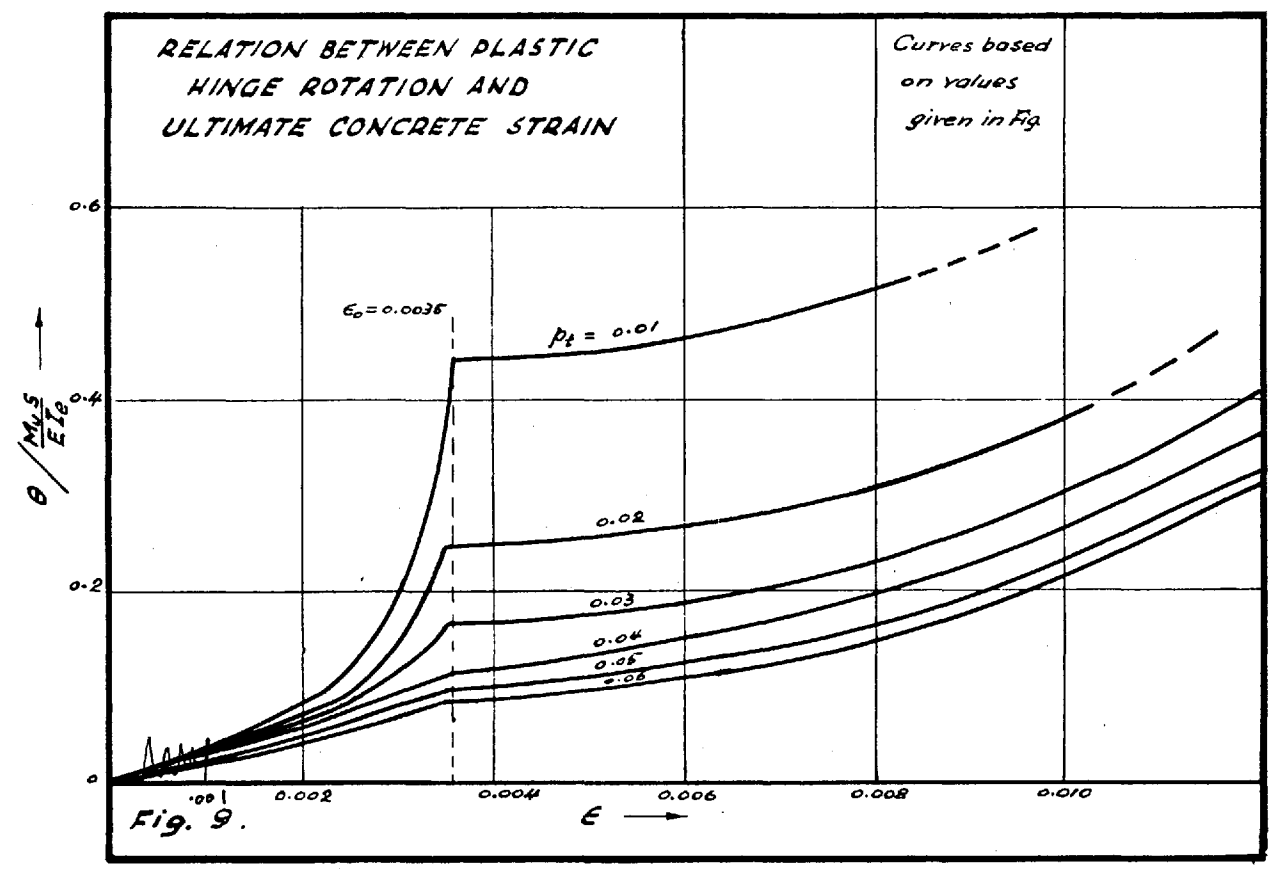

RELATION BETWEEN PLASTIC HINGE ROTATION AND ULTIMATE CONCRETE STRAIN
Curves based on values given in Fig.
$\epsilon_u = 0.0035$
$p_t = 0.01$
0.02
0.03
0.04
0.05
0.08
$\theta / \frac{M_u S}{E I_e}$
ϵ
0.6
0.4
0.2
0
.001
0.002
0.004
0.006
0.008
0.010

Fig. 9.

the ultimate strain of plain concrete is reached, it cannot help the concrete to increase the ultimate compressive strain. However, high compression steel ratios for a given concrete strength and tension steel, will strengthen the compression zone and cause the virtual tension steel ratio to be decreased, hence tending to result in tension failure and therefore giving higher rotation value.

Also, for bound concrete, if the compression steel is adequately bound to prevent premature buckling, then a high compression steel ratio would tend to cause the member to behave more and more like a structural steel member, so that in the limit, if the amount of compression steel completely displaces the concrete, it becomes a steel member. Since steel members are capable of accommodating high plastic rotations under an approximately constant load, it will be seen that high compression steel ratios would tend to increase the plastic rotation of bound sections, and the drop of load due to spalling would tend to be minimised.

Concrete Strength.

In a review of previous work on the ultimate strain of different concretes, Hognestad[16] showed that very diverse conclusions have been obtained, and that

it is probably simplest to assume that a constant average value holds for the range of concrete strengths which occur in practice.

However, for a given steel ratio, a stronger concrete strengthens the compression zone and therefore tends to cause initial tension yield, resulting in a higher θ value.

In bound concrete, a high concrete strength for a given section and binding will give a very large drop of load when the spalling load is attained, especially when the compression steel ratio is low, and is usually an uneconomical arrangement.

Axial Load.

The presence of axial load superimposed on the bending load causes the neutral axis depth to be increased. For a given ultimate strain, the ultimate rotation is small since $\epsilon_u/n_1 d$ is small.

In the limit, as the total eccentricity of loading approaches zero, so the curvature and rotation, ignoring the occurence of buckling, also tend to zero. It would thus appear that very small available rotations are obtained in such worst cases. Fortunately, the plastic zone is greatly lengthened for high axial load, thus allowing considerable plastic rotations to

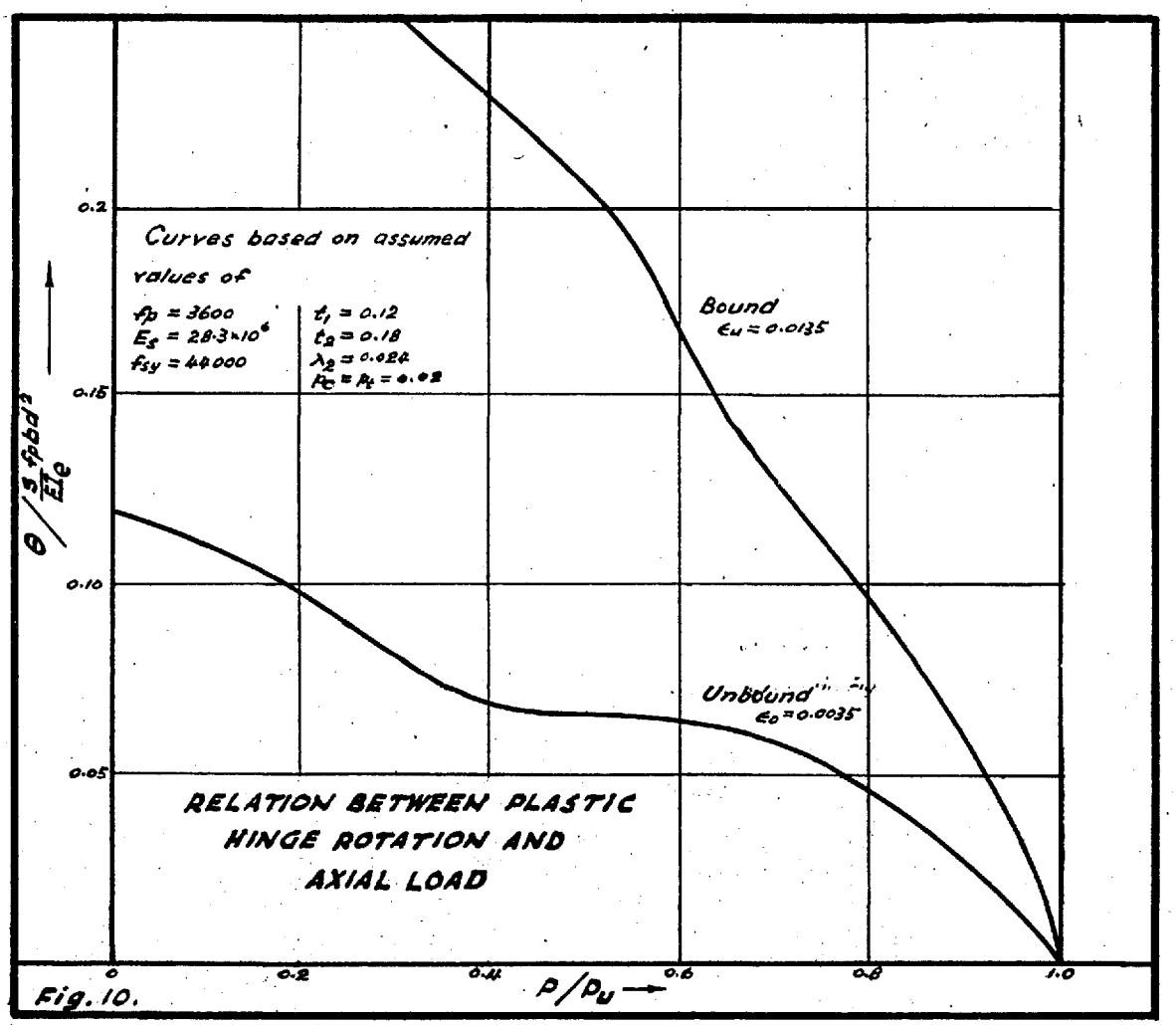

Curves based on assumed values of
f_{cp} = 3600
E_c = 28·3×10⁶
f_{sy} = 44000
t_1 = 0.12
t_2 = 0.18
λ_2 = 0.024
$p_c = p_t$ = 0.02
Bound
ϵ_u = 0.0135
Unbound
ϵ_u = 0.0035
RELATION BETWEEN PLASTIC HINGE ROTATION AND AXIAL LOAD
$\theta / \frac{3 f_{cp} b d^2}{E I_c}$
P/P_u
0.2
0.15
0.10
0.05
0
0.2
0.4
0.6
0.8
1.0

Fig. 10.

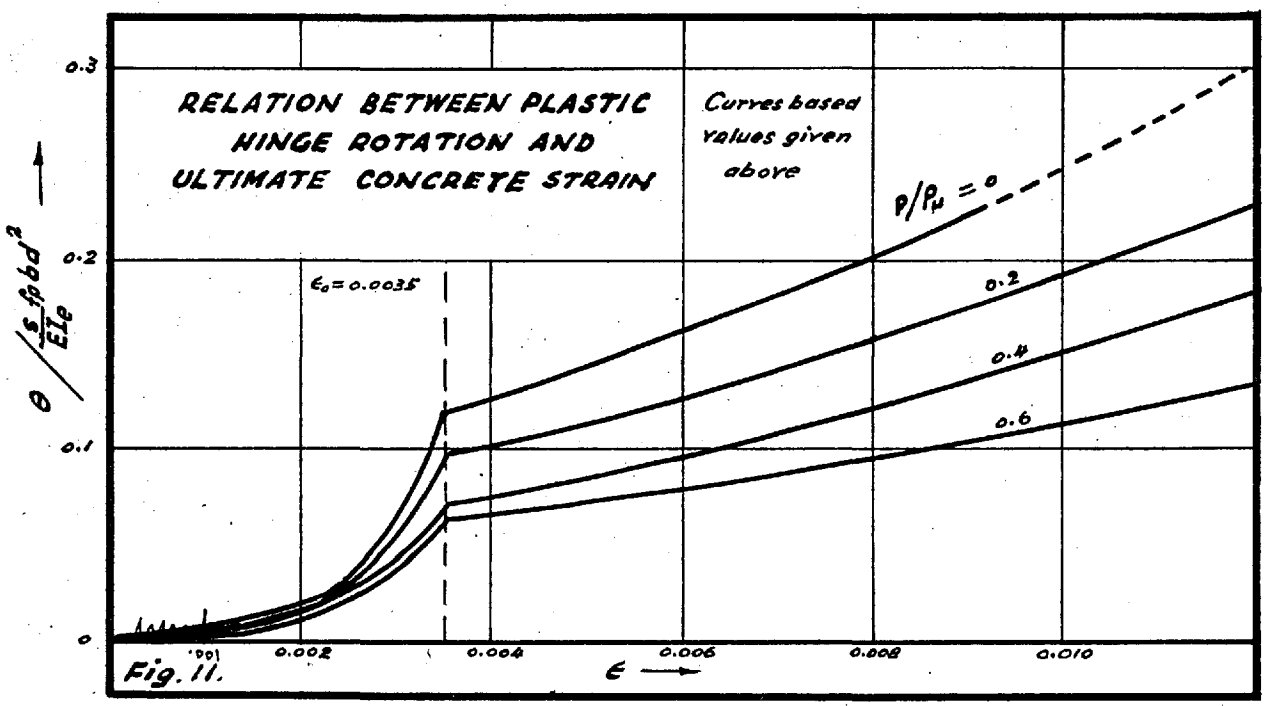

RELATION BETWEEN PLASTIC HINGE ROTATION AND ULTIMATE CONCRETE STRAIN
Curves based values given above
ϵ_u = 0.0035
P/P_u = 0
0.2
0.4
0.6
$\theta / \frac{3 f_{cp} b d^2}{E I_c}$
ϵ
0.3
0.2
0.1
0
0.002
0.004
0.006
0.008
0.010

Fig. 11.

be developed over a large region.

The relation between axial load and θ has been studied by the example worked out and plotted in Fig.10. It is seen that at high values of P/P_u, the available rotation decreases rapidly with small increments of P . Since a symmetrically reinforced section will yield initially in tension when subjected to pure bending only, the θ value at very low values of P/P_u are high.

The use of binders is shown to increase the available θ value considerably.

Lateral Binding.

It was indicated in Part II that the strength and deformation of plain concrete can be considerably increased by using lateral binding. The stress-strain relationship was shown to be satisfactorily represented by the proposed curve.

Even with very heavy ratios of lateral binding, a sudden small drop of load is inevitable when the concrete strain exceeds its ultimate value ϵ_o , due to the spalling of concrete cover which is always provided for corrosion protection. On further loading, and accompanied by large deformations, the strength of the section may be further increased, or may gradually drop, depending on the efficiency of the binding, and,

in the case of columns, also on the rate of increase of bending moments due to deflections. When bending moments due to deflections are appreciable, the actual bending moment resisted may increase, while the external load resisted is decreased.

In most practical cases, it will be found that within the range of concrete strengths, steel ratios, lateral binding ratios, and slenderness ratios, the strength of the member in the bound plastic range will generally be less than the strength attained just before spalling.

Figs. 9 & 11 give curves showing the relationship between θ and the ultimate strain ϵ_u. Comparing Fig. 9 with Fig.11, the gradient of the θ-ϵ curves are much flatter for sections under pure bending in the bound range of strains.(Note difference in scales). This shows that lateral binding is more efficient for column hinges.

Spalling and the Plastic Zone.

As illustrated in Fig.IV.4, since M_u' is generally

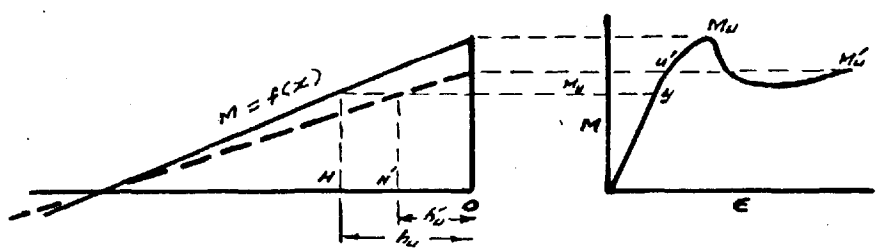


Fig. IV. 4.

less than M_u, we obtain $h_u' < h_u$; that is, the plastic zone is decreased due to spalling. It will be noticed that between the load-stages M_u and M_u', plastic unloading occurs between H and H', since OH is plastic at the M_u-stage. This is ignored for simplicity, it being assumed that on unloading the same $M-\epsilon$ curve is retraced. The error involved is not serious, since u'y on the $M-\epsilon$ curve does not deviate much from a straight line.

Spalling and Curvature Distribution.

It is a well-known phenomena that when a member is subjected to a varying bending moment such as shown in Fig.IV.5, spalling occurs when the ultimate strain ϵ_o of the concrete cover is exceeded at the point O, taking place not only at the point O, but propagating along the member for some distance OR = $r_1 s$.

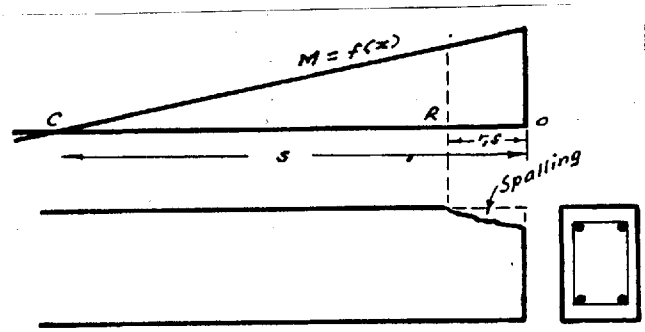


Fig. IV. 5.

It follows therefore, that since a strain gradient is present along the member, there must exist a lower limit of strain at which the propagation of spalling ceases. The author's tests indicate that this lower

limiting strain ϵ_r is around 0.0020 to 0.0025.

With these considerations, it was found that where the axial load resulted in a value of $h' < 1$, the value of $r_1 = 0.20$, and is found to be rather insensitive to different values of h'. This means that spalling spreads over a distance of one-fifth of the bending moment intercept.

In the limit, when the member is subjected to a purely axial load, it is clear that when spalling occurs, it will extend over the entire length of the member, since there is no strain gradient.

No quantitative data from previous investigators seems to be available regarding the propagation of spalling, although observations described and illustrating photographs [22] indicate that the value of $r_1 = 0.20$ finds reasonable verification.

The propagation of spalling and the accompanying weakening of the member, results in a shortened plastic zone and the concentration of the change of curvature within the spalled length $r_1 s$, as shown in Fig.IV.6, since in the relation $M/EI = \epsilon/n_1 d$, the value of ϵ_u is very high due to binder action, and

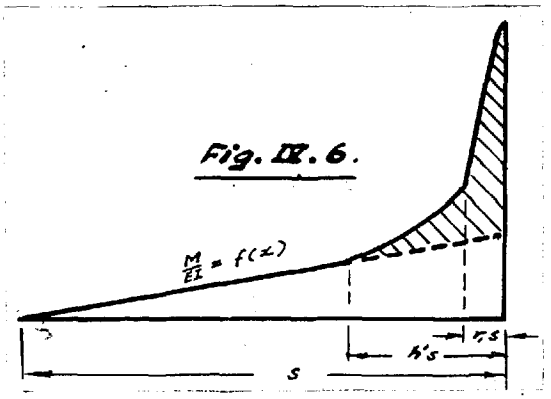


Fig. IV. 6.

$n_1 d$ is small as spalling increases the eccentricity of loading.

As will be expected, the value of β for spalled bound hinges is different from the value of β for plain unbound hinges. This is shown in the author's tests.

Procedure for Designing Plastic Hinges.

On the basis of the characteristics of plastic hinges already discussed, the following procedure indicates the method of design:

1. The required plastic hinge rotation θ at a particular hinge for an ultimate economic distribution of bending moments in the structure is first determined by applying the trial and adjustment method of the Plastic Hinge Theory. From this is also found the form of B.M. diagram, and the bending moment intercepts for the various plastic hinge regions.

2. From the assumed sections at the particular hinge, determine the values of yield moment M_y and ultimate moment M_u. As a first trial, assume the hinge to be unbound, having say,

$$\epsilon_y = 0.001 ,$$

$$\epsilon_u = 0.0035 .$$

3. From 1. and 2., determine the plastic zone length factor h', given by

$$h' = 1 - \frac{M_y}{M_u} \qquad \text{--------(IV.2)}$$

For beams under bending only, it is sufficiently accurate to assume an average value of $h' = 0.40$. For members with combined bending and axial loads, the value of h' may be found from equation (IV.3), or

obtained from curves such as those given in Fig.7. Alternatively, a rough value $0.4 < h' < 0.7$ may be assumed which should cover usual cases.

4. The plastic hinge rotation θ available at the particular hinge, is then determined from

$$\theta_k = \frac{M_u s}{EI_e} \beta \left[1 - \frac{M_y}{M_u}\right]\left[\frac{EI_e}{EI_u} - 1\right] \quad \text{---(IV.6)}$$

where EI values may be calculated from $EI = M.n_1 d/\epsilon$, and the value of β obtained from tests.

If the plastic zone is very long, and the properties of the sections change within this length, then the value of θ_k may have to be determined from equation (IV.4). However, this complication is unlikely in practice.

5. If the required θ value is not greater than the available θ value, then the plastic zone around the assumed hinge position is safe.

If the required rotation is greater than the available value, then the critical section at the assumed hinge will fail before the final redistribution of moments is attained. In such cases, the hinge must be redesigned by one of the following possible arrangements:

(a) Re-detail the critical section, so that it will have the same plastic moment value, but having a

low percentage of tension steel, thus giving higher available rotation.

(b). Employ close lateral binding to extend the stress-strain range of the concrete, thus giving higher θ values. Lateral binding may be designed by the type of curves given in Fig. 65 & 66. If the θ value so obtained is not less than the required value, the design is satisfactory. The binding should then be detailed to extend for not less than 1/5 of the bending moment intercept, since this is the distance of spalling propagation. For cases of very high axial load, where $h' = 1$, the required bound length may extend to the entire length of the bending moment intercept.

(c). If the available θ value obtained from the alternative arrangements (a) and (b) still give insufficient hinge rotation, the required rotation must be reduced, and the bending moment distribution for the structure re-adjusted by the methods given in the Plastic Hinge Theory.

Any one of the three alternative methods may provide the most economic solution in a particular case, so that no general rule is possible.

In beams, the method of under-reinforcing, if possible, is probably the simplest and most economic arrangement. In columns, where high axial loads are

present, this may not be possible. The weakening due to spalling is an important factor in bound hinges.

A more economic design may often result with only partial redistribution in certain members, in which very high hinge rotations can thus be avoided.

PART V

EXPERIMENTAL WORK

It has been shown that the relation between lateral reinforcement and bound concrete stress-strain curve constants must be determined from tests.

It is convenient to study such behaviour experimentally by conducting tests on bound concrete members subjected to compressive loading with small eccentricities, with varying ratios and types of binding, so that the effect of lateral binding on members under high compressive flexural strain may be studied.

The influence of axial load on the formation and behaviour of plastic hinges, which has been investigated analytically, also requires experimental data to determine the curvature distribution factors, and to observe the propagation of spalling in bound sections.

With these requirements in mind, the following series of tests were conducted:

Series B. This consisted of 9 short prisms, 6 inches square in section and 11½ inches long, reinforced with 4 - 5/8" bars, and laterally bound with various types of square ties with bent-in ends, of ¼", 3/16", and 1/8" diameters and of pitches from 1" to 4" .

These prisms were pin-ended and loaded by compression with an eccentricity of $\frac{1}{2}$".

Series C. 7 cylinders of 6 inch diameter and 12" long, also reinforced with 4- 5/8" bars, were tested by loading in compression with an eccentricity of $\frac{1}{4}$" .

The main variable was also lateral binding, where $\frac{1}{4}$", 3/16" and 1/8" diameter bars, and pitches from 1" to 4" were used in the spiral binding. By comparing the results of this series with those of series B, the efficiencies of rectangular and circular binders can be compared.

Series S. This was made up of 7 struts 52" long and 6" x $3\frac{5}{8}$" in section, symmetrically reinforced with 4- $\frac{1}{2}$" bars and laterally bound with rectangular welded closed links at a pitch of 3", except for specimen S3, which had a pitch of $1\frac{1}{2}$" .

The struts were loaded in a specially constructed testing frame by axial compression through pins at the ends, and also by a central lateral point load. This was intended to simulate the condition of a plastic hinge forming within the critical region of a column under a varying bending moment distribution and high axial load.

By varying the ratio of the bending to the axial

OUTLINE OF TESTS

Series	No.	Size	Reinforcement A_c	Reinforcement A_t	Binding Dia.	Binding Pitch	Eccentricity	Av. Cube Strength	Remarks
B	1	6"x6"x 11½"	2-5/8"ø	2-5/8"ø	¼"	1"	½"	5460	½"clear cover
	2	"	"	"	"	"	"	3980	No cover
	3	"	"	"	"	1"helix	"	3510	"
	4	"	"	"	"	2"	"	2910	"
	5	"	"	"	"	4"	"	2650	"
	6	"	"	"	3/16"	1"	"	3560	"
	7	"	"	"	"	2"	"	3100	"
	8	"	"	"	1/8"	1"	"	3320	"
	9	"	None	None	3/16"	1"	"	2970	"
C	1	6" dia.x 12"	2-5/8"ø	2-5/8"ø	¼"	3/4"	¼"	3540	"
	2	"	"	"	"	2"	"	2790	"
	3	"	"	"	"	4"	"	2900	"
	4	"	"	"	3/16"	1"	"	3960	"
	5	"	"	"	"	2"	"	3260	"
	6	"	"	"	1/8"	1"	"	3320	"
	7		None	None	3/16"	1"	"	2970	"
S	1	6"x3 5/8" x 52"	2- ½"ø	2- ½"ø	¼"	3"	W/P=1/21	4520	1/8"cl. cover
	2	"	"	"	"	"	1/10	4360	"
	3	"	"	"	"	1½"	1/18	5160	"
	4*	"	"	4-3/8"ø"	"	"	1/10	4440	"
	5	"	"	-	"	"	1/10	4400	"**
	6	"	"	"	"	"	1/10	3880	"***
	7	"	"	"	"	"	1/18	4450	"

Bent-in binders for series B.
Spiral binding for series C.
Welded binders for series S.

* Extra hinge reinforcement.
** After initial yield, P kept constant.
*** After initial yield, W kept constant.

load, the length of the plastic zone and the curvature distribution in different cases can be studied. The ratio of W/P ranged from 1/21 to 1/10 .

In strut S4 , special hinge reinforcement was inserted.

An outline of tests is given in the preceding page.

Concrete Quality

The concrete strength for series B and C was kept at around 3000p.s.i., while for series S the average value was 4000 p.s.i., both being the strength at 28 days.

The mix was approximately 1:2.4:3.6, using crushed 3/8" shingle for the coarse aggregate. The water-cement ratio was 0.68 for series B and C, and 0.5 for series S. This ensured a better flow of concrete in specimens of Series B and C, since there was hardly any concrete cover provided.

Normal Portland cement was used for series B and C, and Rapid Hardening Portland cement for series S .

All specimens were compacted by vibration, aided by some hand tamping. Moulds were stripped at 3 days, the concrete cured for a further week in wet hessian, and then left exposed to the laboratory air until testing at 28 days. 3 cubes and 3 cylinders accompanied each test specimen.

Reinforcement.

Ordinary smooth round mild steel reinforcement was used for the longitudinal steel in all test specimens, having a yield point of around 40000p.s.i. As almost all the longitudinal steel were to be subjected to compression, care was taken to use only very straight bars, so that no premature buckling would occur.

For lateral reinforcement, $\frac{1}{4}$", 3/16" and 1/8" diameter bars were used, all of mild steel. The 1/8" wire used was of the type normally employed for reinforcing shell roofs.

The stress-strain curves for all reinforcement used, are given in Fig. 12 and 13, and represent the average curves of 5 test pieces of each type of bar, which were tested in a "Buckton" 10-ton universal lever testing machine.

These tests showed that for longitudinal reinforcment, the stress strain curves for tension and compression were practically identical up to the strain-hardening condition. After strain-hardening, buckling invariably occurred in the test pieces, so that only the tension test pieces could record the strain-hardening behaviour.

Compression test pieces had a slenderness ratio

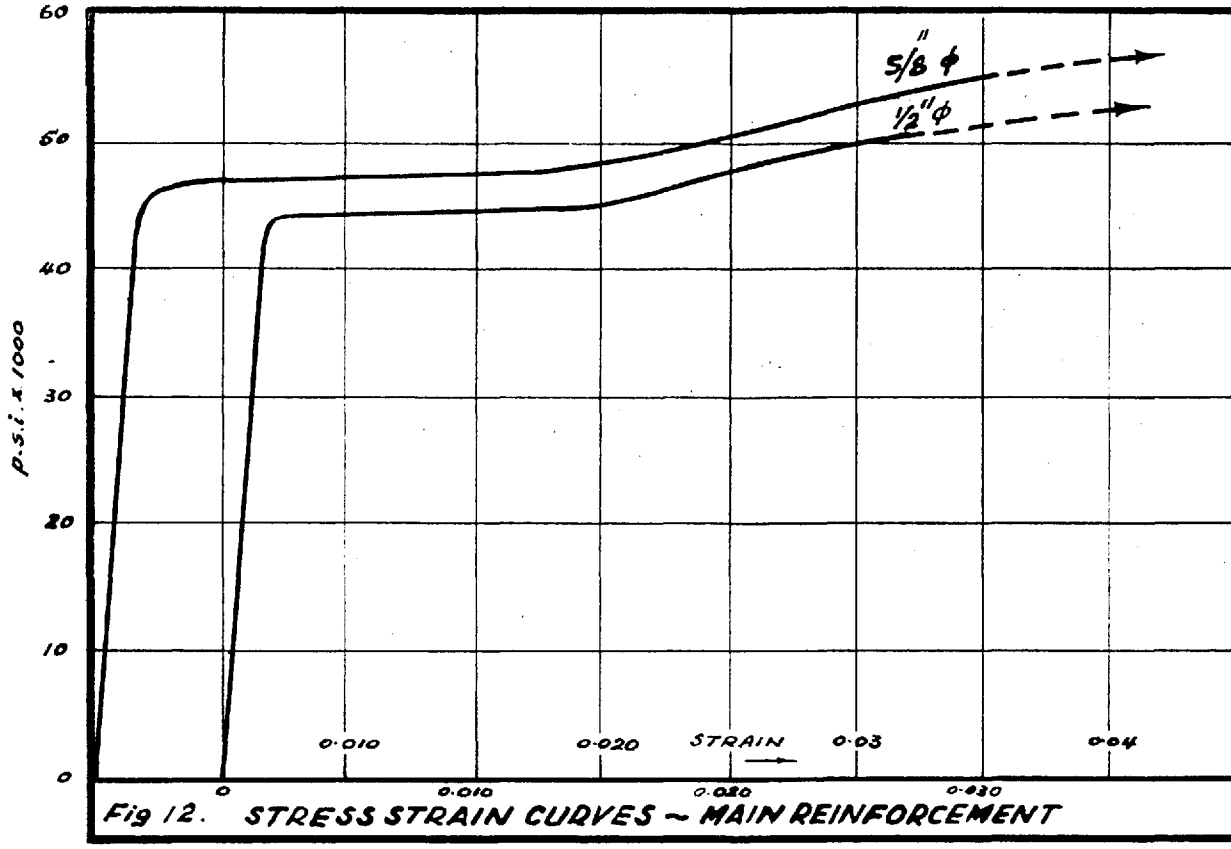


Fig 12. STRESS STRAIN CURVES ~ MAIN REINFORCEMENT

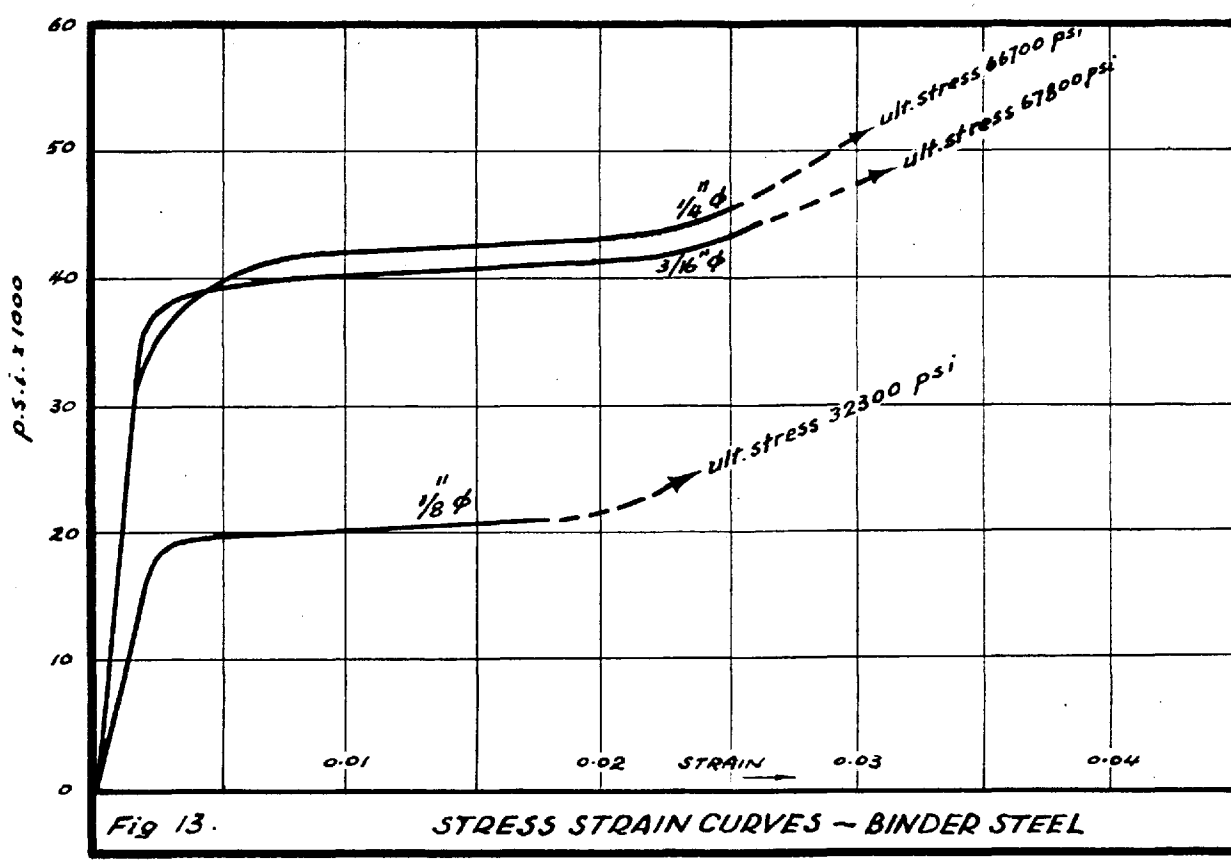


Fig 13. STRESS STRAIN CURVES ~ BINDER STEEL

of 4 , with ends carefully ground truly flat and parallel. 3 - $\frac{1}{2}$" electrical strain gauges were stuck on each test piece longitudinally around the circumference. Small trial loads were first run and adjustments made to the centering of the test-piece in the machine until a truly axial compression was indicated by the 3 strain gauges reading identically.

In tension tests, test pieces had about 12" clearance between jaws. Both electrical and mechanical gauges were used. Gauge points for the mechanical gauges were of two kinds: one by sticking small 1/16" thick, $\frac{1}{4}$" square plates drilled with a No. 60 drill hole on each plate as gauge points, and the other by welding small lugs made out of short lengths of 3/8" diameter reinforcement onto the test bar, and drilling No. 60 holes on the lugs as gauge points. This latter method was used in measuring all the strains of embedded reinforcement. Stress-strain tests on these two methods of strain measurement showed that spot welding small lugs for gauge points at intervals down to 2" did not materially affect the stress-strain properties of the reinforcement, and that it thus provided a satisfactory method of measuring steel strains.

Moulds.

Special care was taken in the design of moulds to ensure that they were rigid and true, since the strength of members with high axial loads are greatly affected by being out of true. Thus steel forms were used whenever possible.

The mould used for the short prisms of series B was made up of the straight backs of two lengths of 6"x 3" steel channels as sides, and bolted down onto a stiff wooden baseboard which formed the third side. Two 3/8" thick steel plates were bolted on to the baseboard and the ends of the channels as end-plates. These specimens were cast on their sides.

For the cylinders of series C, an ordinary test cylinder steel mould was used. The best mould was selected from a batch of 10 and the same mould used for all the specimens. These cylinders were therefore cast vertically.

In series S, the back faces of two long 6"x3" channels were used as sides, and also bolted onto a wooden baseboard. The back faces of the channels were carefully machined and each end faced off square. 3/8" steel plates were used as end-plates.

Fabrication.

Since loads were to be applied at the ends of the specimens in all the tests, it was necessary to ensure that the load would bear evenly on the concrete and the steel bars. For this, special external jigs which measured the exact overall lengths of the moulds were made. The main reinforcement bars to be used for the test specimens were first carefully straightened, and then faced off on a lathe, where with the aid of the appropriate jig, the bars were brought down to exactly the same length as the moulds. This ensured that the ends of the reinforcement and concrete were flush, resulting in an even distribution of load.

To ensure binders of identical size and shape, $\frac{1}{2}$" thick steel templates machined to the required internal dimensions and shape of the rectangular binders for specimens of series B and S, were made. Binders were then formed over these templates by hand with the aid of a hammer and a bench vise.

Spiral binding for the cylinders of series C was coiled by hand around a 5" diameter piece of lead pipe. When released, it uncoiled approximately to the required diameter, and could be re-adjusted

again to the correct size and shape.

All reinforcement was first assembled and tied into rigid cages before being placed in moulds. Binding was tied to the longitudinal steel by means of 2 mm. soft wire.

For the spirals of series C, the 4 longitudinal bars in each specimen were first positioned and aligned in a jig, 2 rings cut out from the spirals then welded round the bars near each end to lock them in position, and the spiral finally slipped in and secured.

In the struts of series S, special positioning holes were drilled through the end-plates; the ends of the main bars were drilled and tapped with 5 B.A. thread, and were secured in position against the end-plates by 5 B.A. screws after the required number of binders had been threaded in. The binders were then spaced and tied, and the whole cage finally bolted onto the steel mould at the end-plates.

Steel lugs for use as strain gauge points on the main bars were welded on before assembly, and any kinks in the bars due to local heating straightened out. The lugs were wrapped with a thin layer of plasticine to prevent bonding with the concrete.

Strain Measurement.

All straim measurements were made by using mechanical gauges applied by hand, of 8" and 2" gauge lengths. For small strains up to about 0.004, 2" and 8" Metzger gauges were used, but for higher strains up to about 0.025, (i.e., in the bound plastic range) a modified type of 8" gauge with a very long travel devised by J.M. Prentis, was used. The usual practice of checking instrument and temperature errors was made by taking readings on a dummy bar after each set of readings.

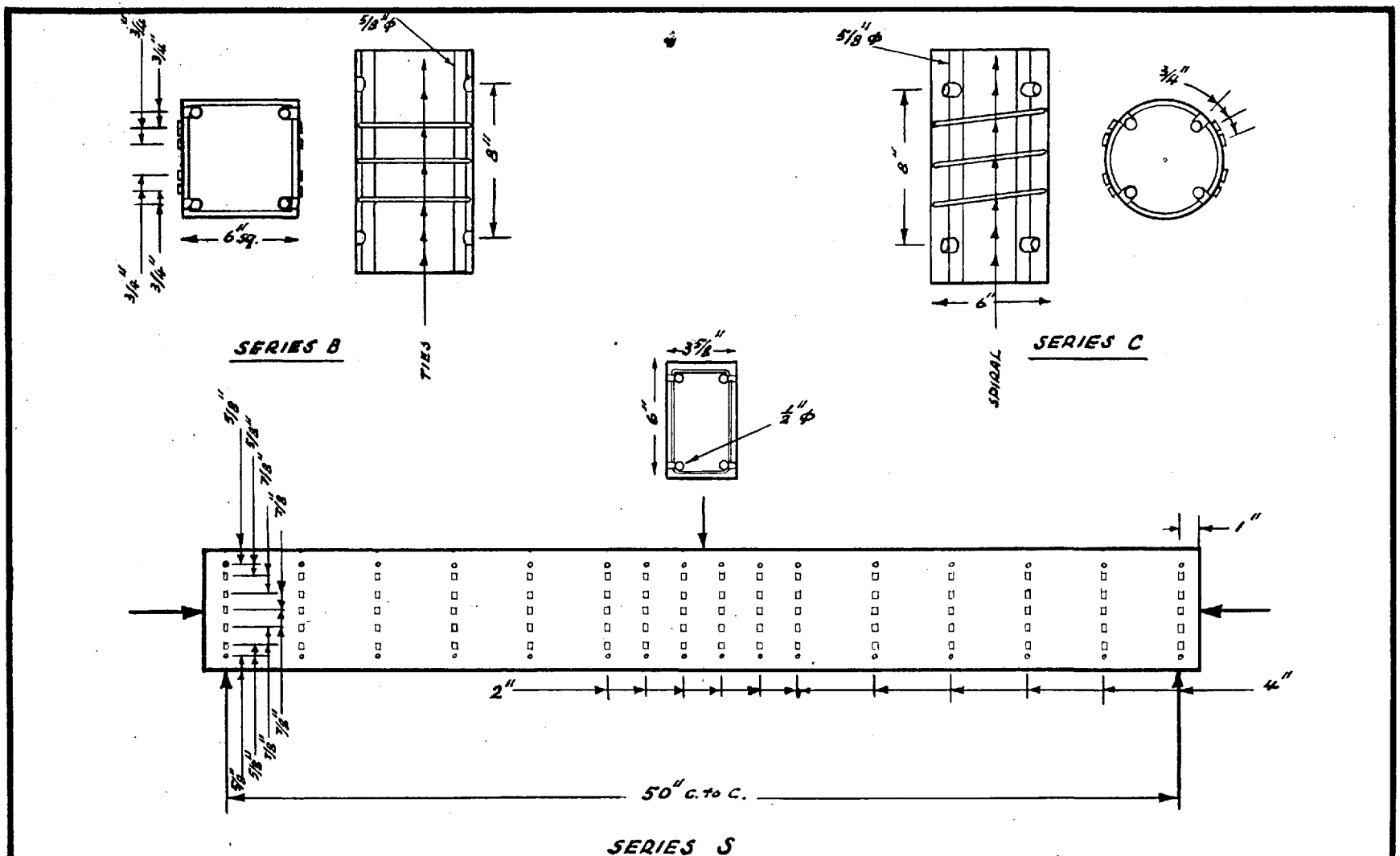
The use of electrical resistance strain gauges was considered unsatisfactory for this experimental work as strains in the bound plastic range far exceeding the working range of such gauges were to be measured, and moreover, great uncertainties accompanied their use in reinforced concrete work with regard to waterproofing, mechanical protection, and drift.

In series B and C, 6 pairs of gauge points were used to measure the strain across the section. During each load stage, 12 strain readings were taken, 6 on either face.

In series S, there were 10 sets of 8" gauge points at 4" intervals and 5 sets of 2" gauge points at 1"

intervals on each face of the struts. Each set consisted of 6 pairs of gauge points across the face of the strut (see Fig.14.). Hence for each load-stage, a total of 180 strain readings had to be taken.

All gauge points on concrete surfaces consisted of 1/16" thick, 3/8" square steel plates drilled with a No. 60 drill hole. They were stuck with a cellulose adhesive onto the concrete surface, the latter having been previously rubbed down and cleaned with acetone. The correct gauge length was set by means of a jig. After being stuck on, the gauge points were left to dry under an infra-red lamp for 24 hours and at least 3 more days were allowed to elapse before testing.



SERIES S

Fig. 14. STRAIN GAUGE LOCATION CHART

Testing Equipment.

Series B and C. For these short specimens subjected to eccentric compression, a hydraulic compression machine of 200 ton capacity normally used for testing cubes and cylinders, was employed.

As shown in Figs. 15 and 16, these specimens were capped at each end with a 2" thick steel end-plate, and loaded through rocker plates and semi-circular pin-joints. These pins were not fixed to the end-plates so that they could be placed to give any eccentricity.

As no further clearance was available in the machine, it was not possible to insert accurate load measuring devices such as proving rings or dynamometers directly between the loading ram and the specimen. Hence reliance had to be placed on the Bourdon pressure gauge which was connected to the hydraulic circuit of the machine. This gauge was carefully checked and calibrated from time to time.

Series S. These longer struts were to be loaded axially as well as with a lateral bending load. Because it was impractical to support the strut laterally and at the same time apply the axial load through the same pin-joints, it had to be supported from underneath

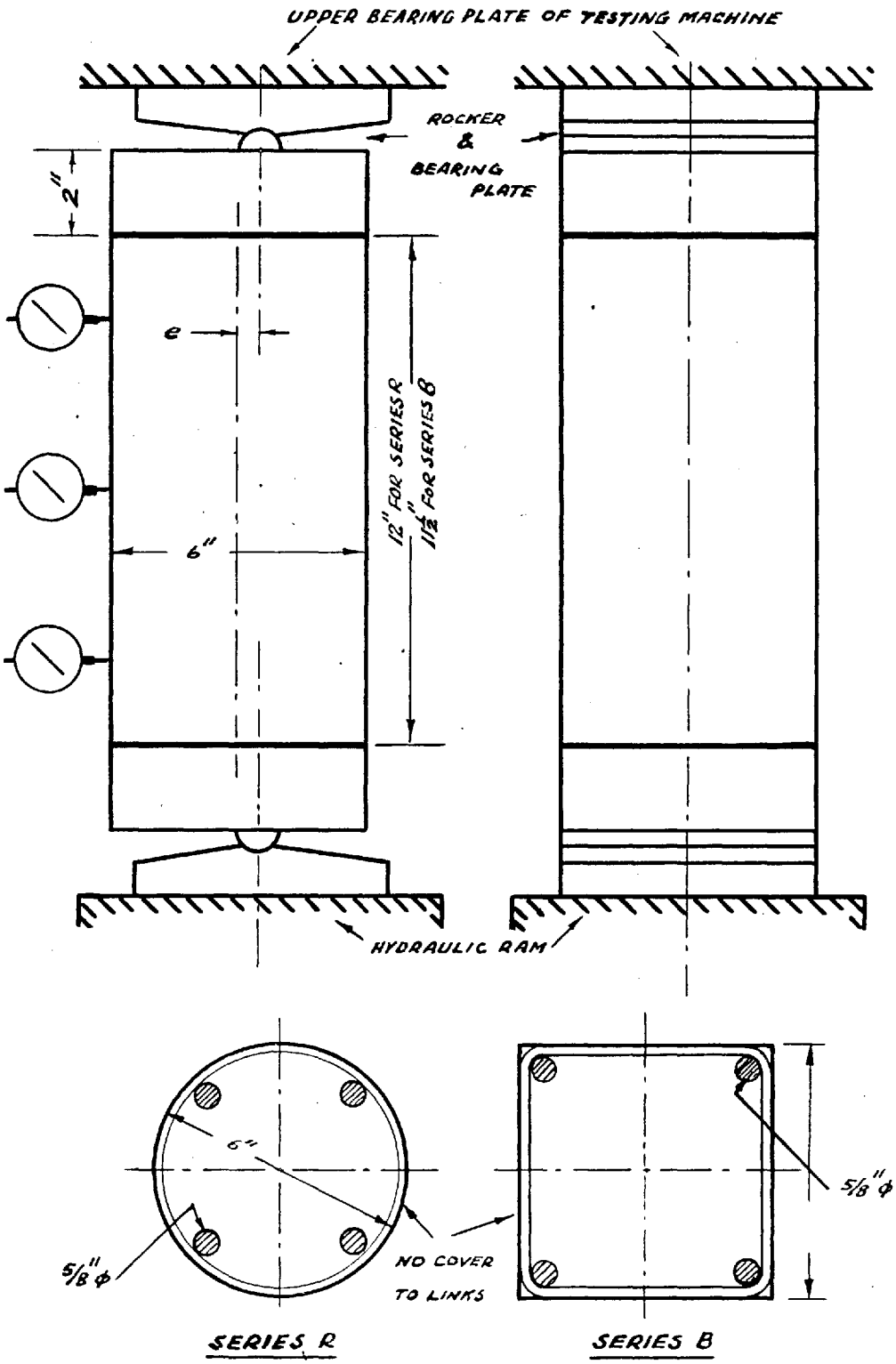


Fig. 15. TESTING ARRANGEMENT FOR PRISMS & CYLINDERS



Fig. 16 . Testing Arrangement for Series B & C.

near each end (similar to supports for a simply supported beam) to take the lateral load reaction, and loaded axially through a separate set of end-plates and pin-joints at each end, as shown in Fig.14 .

With this arrangement, it will be appreciated that under progressive loading, deflection will cause the axial loading pins to travel upwards if the bottom supports remained fixed in position, or alternatively, the bottom supports will be lowered if the axial loading pins remained stationary. No machine was available which fulfilled these requirements, and so a special testing frame had to be built for the purpose.

Since the axial loading part of the frame involved heavy hydraulic jacks, load-measuring capsules, and tie bars, due to the high axial load required, it was more convenient to anchor the axial load system, and construct a bending frame which could be made light enough to be readily suspended and counterweighted, so that it would be capable of "floating" weightlessly to follow the deflection movements. Many arrangements were attempted on these lines. The main difficulties encountered were to overcome "testing machine instability", and to arrange the tie-bars so that there was a minimum of obstruction to strain

and deflection measurements, and also to provide sufficient clearance to accommodate the floated bending frame.

The final arrangement shown in Figs. 17, 18, & 19, which was designed and built by the author, was successfully used. The movable crosshead at one end of the axial loading system permitted the extension of tie-bars under load to take place, but prevented any vertical movement. This was achieved by a set of steel rollers tightly mounted on a horizontal guide rail. The other fixed end consisted of a horizontally mounted 80-ton hydraulic jack which exerted the axial load.

The bending frame was made up of a girder of a pair of channels, with light hangers pinned at either end to hold up the test strut and take the lateral load reactions. A vertically mounted 10-ton jack provided the lateral load. The whole frame was hung up at the centre by a steel rope and counterweighted over a pair of pulleys, thus allowing the strut to "float" weightlessly. The pulley frictional force was about 30 lbs. representing only very small shear forces at the end-plates.

The load-measuring devices consisted of a 50-ton "Maclow-Smith" liquid-filled capsule, for the axial load, and a 10-ton proving ring for the lateral load.

SCALE: 1 INCH TO A FOOT

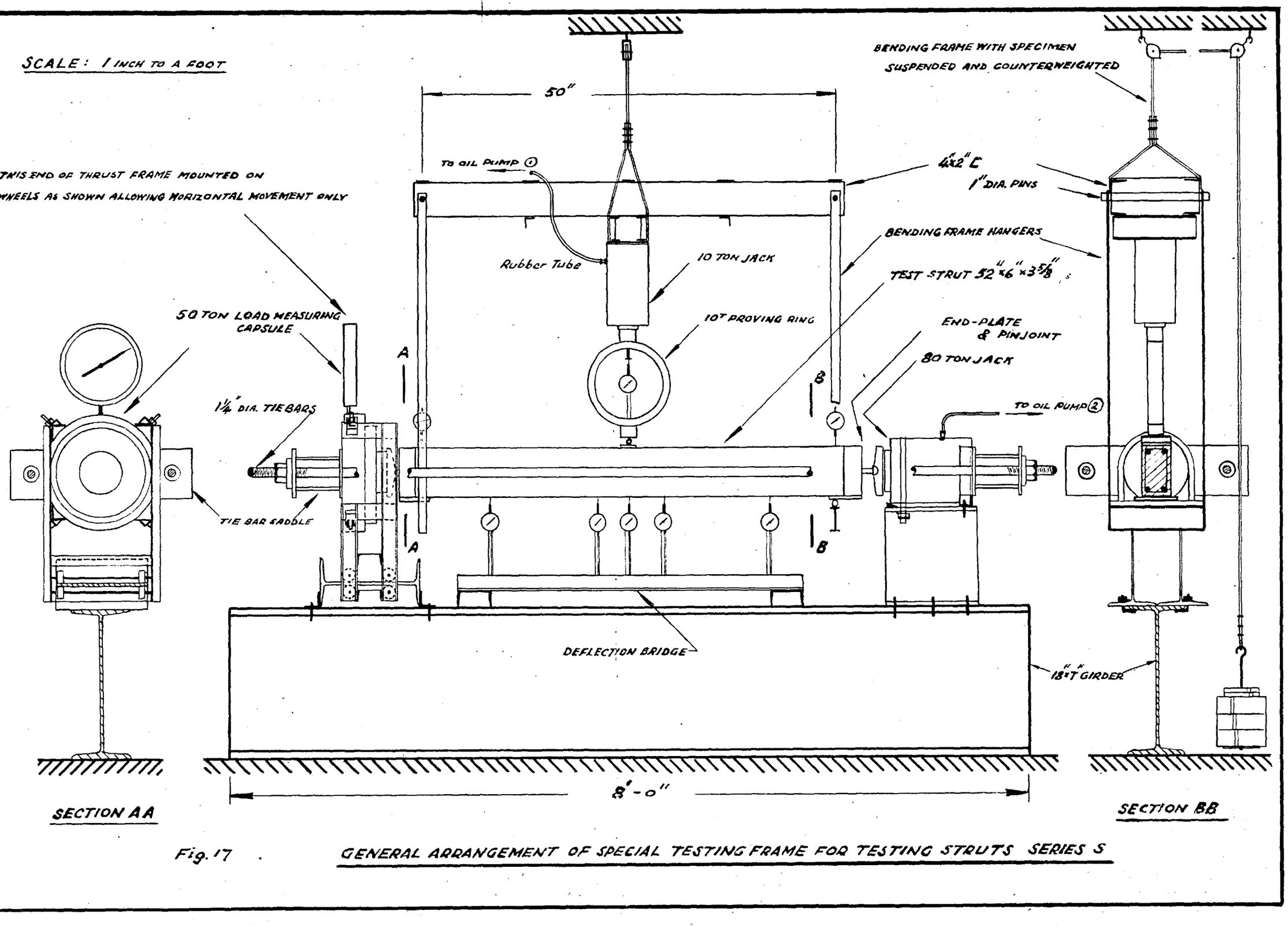


Fig. 17 . GENERAL ARRANGEMENT OF SPECIAL TESTING FRAME FOR TESTING STRUTS SERIES S



Fig. 18 . Testing Frame for Strut Tests of Series S .

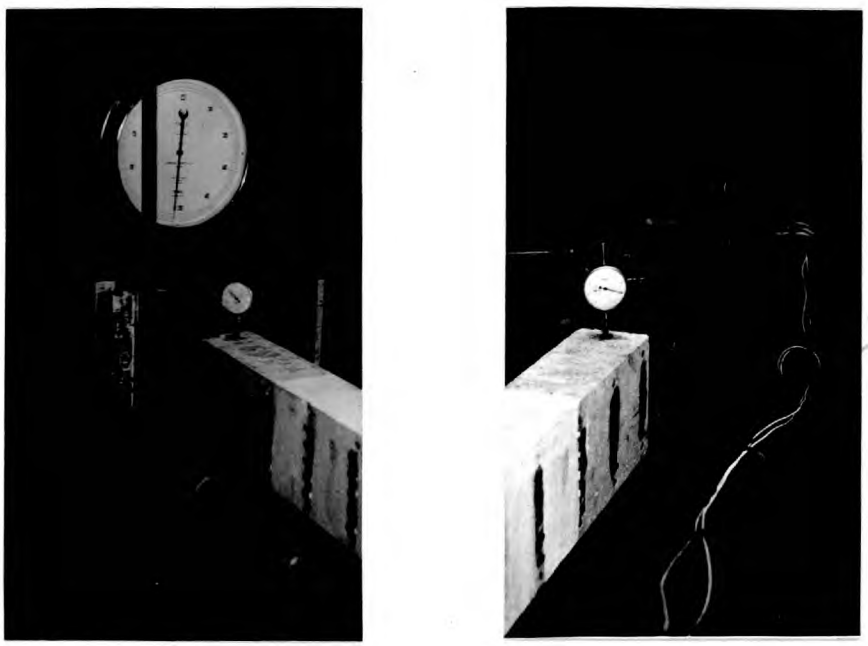


Fig. 19 . Axial Load Arrangement in Strut Testing Frame.

Testing Procedure.

Series B & C. After setting up the specimen accurately in the machine, a very slight load was applied to hold the specimen in place. Zero readings were then taken of strain gauges and deflection gauges.

Loading then proceeded by pumping up the ram, and after each increment of load, strain and deflection readings were taken. After the spalling stage, due to very high strains and creep, a slight increase in load was achieved only after considerable pumping.

As no abrupt failure took place in these bound specimens, loading was continued until excessive creep and spitting of the bound concrete prevented any further load to be steadily sustained, when the section was deemed to have failed.

Slight leakage of oil in the machine and creep usually caused a slight drop in load during the initial attainment of a new load stage. This was eliminated by allowing the load to settle for a while and then re-adjusting the load until a steady state was reached before readings were taken. Any further change in load during measurements was noted and the average value adopted.

One complete set of readings took about 8 minutes.

Series S. The testing frame was so designed that most of its component parts were automatically self-aligning. With the bending frame empty, the counterweight required to balance the bending frame alone was about 200 lb. When the strut, which weighed about 100 lb. was placed on the frame, a corresponding counterweight had to be added.

Prior to testing, numerous trial loads had to be run and the tie-bar anchoring nuts adjusted until identical strain readings on both faces of the strut indicated that the end load was truly axial.

After zero readings, loading was progressively applied in about 12 to 15 stages, and the usual measurements of strain and deflection were taken at each stage. The application of load called for two operators, synchronising the oil pumps so that the lateral and axial loads were at all times kept at the prescribed ratio.

Due to the large number of gauge points, each set of measurements took at least 20 minutes, and thus each specimen required a total testing time of about 6 hours, or one working day.

The remarks about the method of applying load increments for series B and C also apply here.

The Behaviour of Test Specimens.

General.

In all three series of tests, the following general properties were observed:

a. The ultimate crushing strain ϵ_o of the concrete used varied between 0.003 and 0.004, under the action of bending and axial loads.

b. Spalling commenced at sections where the concrete cover reached its ultimate strain ϵ_o, causing an abrupt drop of load due to the reduction in effective concrete compression area, and the increase in eccentricity of loading. In cases where a strain gradient existed along the length of a member, such as in the struts of series S, spalling was observed to propagate along the length of the member for a short distance until the maximum surface strain was reduced to about 0.002 to 0.0023.

c. Lateral binding had a marked contribution to the strength and deformation of reinforced concrete members after the ordinary crushing strength of the concrete had been exceeded. Prior to the spalling stage, very little difference in behaviour was observed which could be attributed to the influence of lateral binding.

d. Circular binding was distinctly more efficient in extending the strength and deformation capacity of bound concrete as compared to rectangular binders. No difference in efficiency was apparent between continuous square helices and separate tied square links.

e. The distribution of strains across the section of the specimens was approximately linear. (Fig. 34, 42, & 50) Some deviation from a straight line distribution was observed at low loads in the short prisms of series B and C; this is thought to be due to the small differences in length between the reinforcement bars and the concrete specimen lengths, causing slight uneven distribution of pressure on the steel and concrete, and also due to disturbance created by the frictional restraint of the end-plates on the ends of the specimens. In the struts of series S , it was shown from strain readings that the effects of this "end-error" was not felt at a distance of 6" away from the end plates. This error is decreased at higher loads, due to local yielding of the uneven bearing surfaces.

Series B.

As given in the Outline, 9 specimens of 6" square section and 11½" long were subjected to compression with an eccentricity of ½" with lateral reinforcement

as the variable.

The quantity of lateral binding used was such that, after spalling, the strength of the specimen could not be recovered to its value at spalling. Hence the spalling load was the maximum attained. However, the lateral binding enabled very large deformations to take place with only comparatively small changes of load.

The eccentricity of $\frac{1}{2}$" resulted in a neutral axis factor value of around 2 in the elastic range, and dropping to a value of about 1 as a result of spalling, deflection and plasticity.

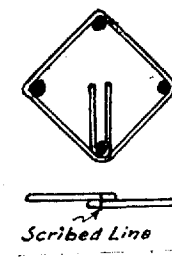
The spalling stage was generally reached at about the fifth or sixth loading stages and failure within 15 load stages. At the instant of spalling, a small drop of load took place, the magnitude depending on the depth of cover and concrete strength. In specimen B1 which was the pilot test and had the largest depth of clear cover of $\frac{1}{2}$", the drop of load was most marked, while in the other specimens with almost no cover, the drop in load was least felt. This may be seen by comparing Fig. 25 with Figs. 26 to 33 .

After spalling, small quantities of crushed concrete would fall from the spaces between adjacent binders, and distinct arching of bound concrete between the binders could be seen.(Refer to Figs. 21, 22)

After the specimens were considered to have failed, they were then subjected to a creep observation by sustaining a reduced load of about 70% of the ultimate load for about 2 hours, and showed that, even after assumed failure, these specimens could still resist considerable load without catastrophic collapse.

Specimen B3 , which was laterally reinforced with a continuous square helix, proved very difficult to fabricate, and was intended to show whether this type of binding had any advantage over tied links. As far as measurements have indicated, no difference was observed as compared with tied links.

A further effort was made to investigate whether tied links with bent-in ends would open up under high lateral pressures. To do this, the corners of one of the specimens (B4) were bared where the bent-in position of the binders occurred. A fine line was then scribed across the two overlapping corners, as shown in the accompanying diagram. An illuminated and graduated magnifying glass normally used for detecting cracks, was used to observe the two lines, which would move out of alignment if any opening-out of the binder occurred.



It was concluded that no opening-out of bent-in links would occur provided that the bent-in corner was embedded in the compression zone of the concrete, and that the bent-in legs were sufficiently long, say not less than the effective depth of the section.

Series S.

In this series 7 spirally bound 6" dia. x 12" cylinders were subjected to compression with $\frac{1}{4}$" eccentricity, also having lateral binding as variable.

The eccentricity of $\frac{1}{4}$" caused the neutral axis factor to have a value of about 4 in the elastic range, and falling to about 1 in the bound plastic range.

While the phenomena of deformation, spalling and arching action, etc., were observed to be very similar to those of the prisms of series B, it was apparent that the circular-shaped binder was distinctly more efficient than rectangular ones. This was shown by the fact that in most of the spiral specimens, although a similar abrupt drop of load took place at the spalling stage, it was eventually possible to attain load values exceeding the first maximum. Much higher strains could also be accommodated.

Due to the circular-shaped section, spalling com-

menced at very narrow strips on the edge of maximum compression, and propagated across the section at a much slower rate than was observed in Series B.

Other observations were similar to those of series B. In this series, all binding was of continuous spirals, so that no observations were made of the opening-out of ends of binders.

Series S .

7 struts 52" long and having a section of 6"x3$\frac{5}{8}$" were tested as laterally loaded, pin-ended struts. The ratio of W/P varied from 1/10 to 1/21 .

In struts S5 and S6 , W and P respectively were kept constant after the struts had reached the yield strain, and further load increments were applied with one jack only, the other load being kept constant.

In strut S4 , special hinge reinforcement was inserted as shown in Fig. 46, to study the effect of this reinforcement on the strength and deformation.

In strut S3 , the lateral binding of rectangular binders having welded ends, were at a pitch of 1$\frac{1}{2}$", while in all the other struts of this series, the binders were spaced at a pitch of 3" .

Prior to the spalling stage, the struts deflected in the form of a smooth curve, but after spalling,

accompanied by a drop in load, local weakening in the region of spalling caused most of the deformation to be concentrated in that region, with the result that the two halves of the struts appeared to be bent round very sharply near the centre, or indeed, a sort of hinge had been formed there. This may be seen from Figs. 23, and 58 to 64 .

Since the concrete cover in these struts was much deeper than that of series B and C, and also the deflections were higher due to the longer length of the struts, the drop of load due to spalling was much more acute.

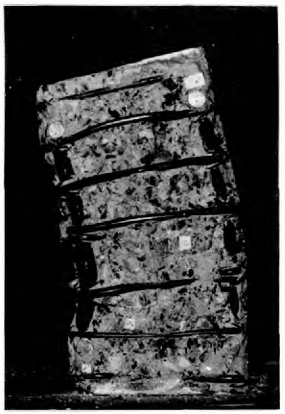
Unlike the shorter specimens, the struts could not be indefinitely strained to total destruction without dangerous signs of buckling sideways. Loading was therefore discontinued once the ultimate bound plastic strength of the struts was exceeded.



Fig. 20. Appearance of Typical specimens of Series B & C at Spalling Load.



B 3





B 5



B 6



B 7



B 8



B 9

Fig. 21 . Series B Prisms after Testing to Destruction.

(Photographs of B1 & B2 not available)



C 1



C 2



C 3



C 4



C 5



C 6



C 7

Fig. 22 . Series C Cylinders after Testing to Destruction.



Fig. 23 . Appearance of Typical Struts of Series S at Spalling Load.



S 1



S 2



S 3

Fig. 24 . Struts of Series S at Ultimate Load.



S 4



S 5

Fig. 24 . (Continued)



S 6



S 7

Fig. 24 . (Continued)

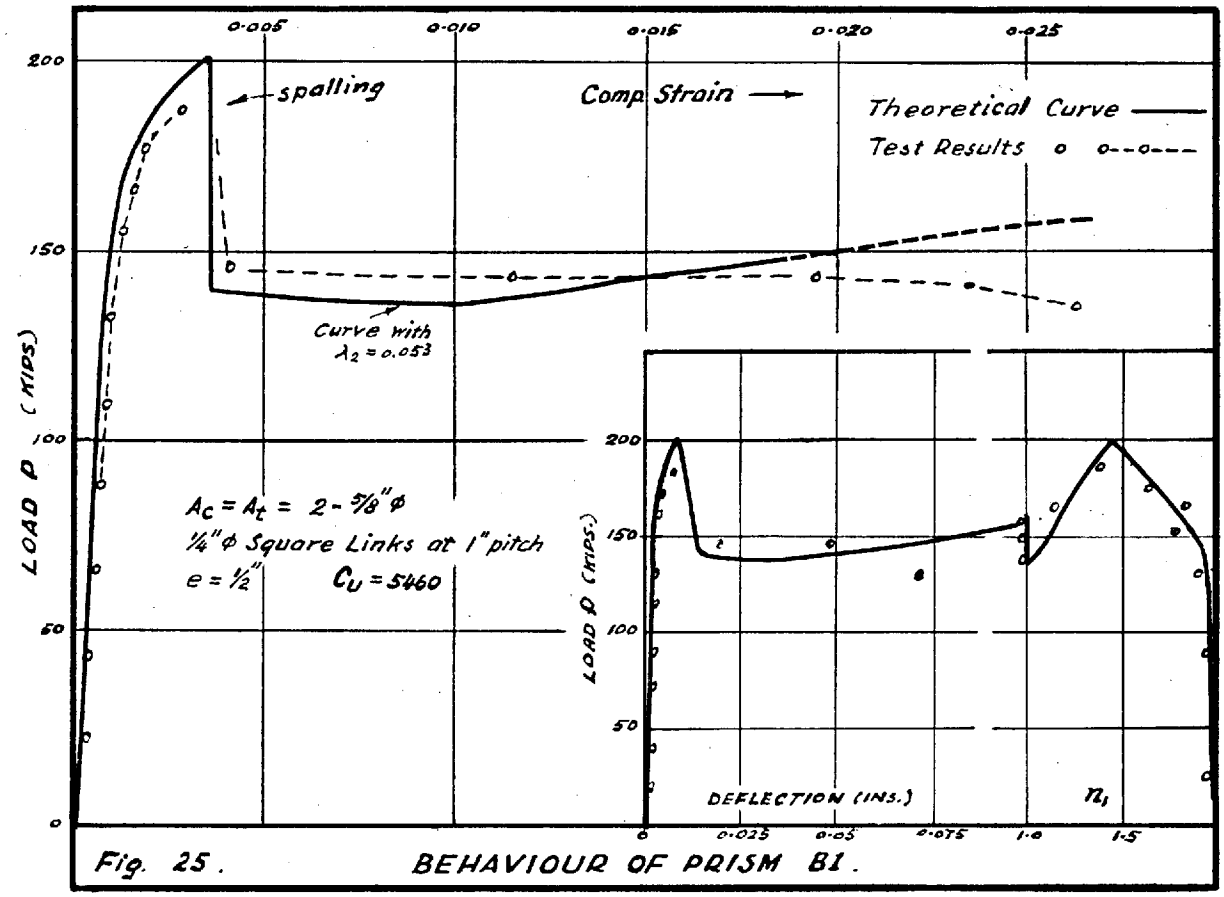


Fig. 25. BEHAVIOUR OF PRISM B1.

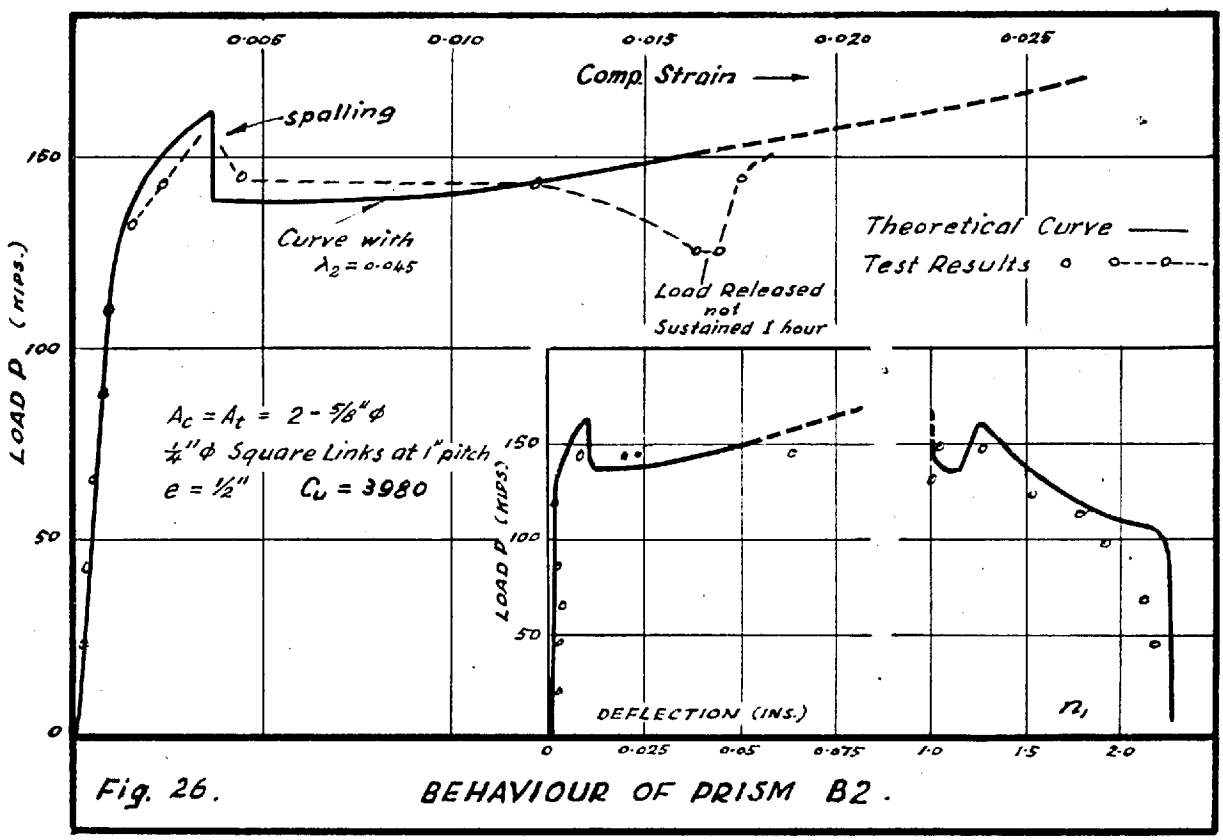


Fig. 26. BEHAVIOUR OF PRISM B2.

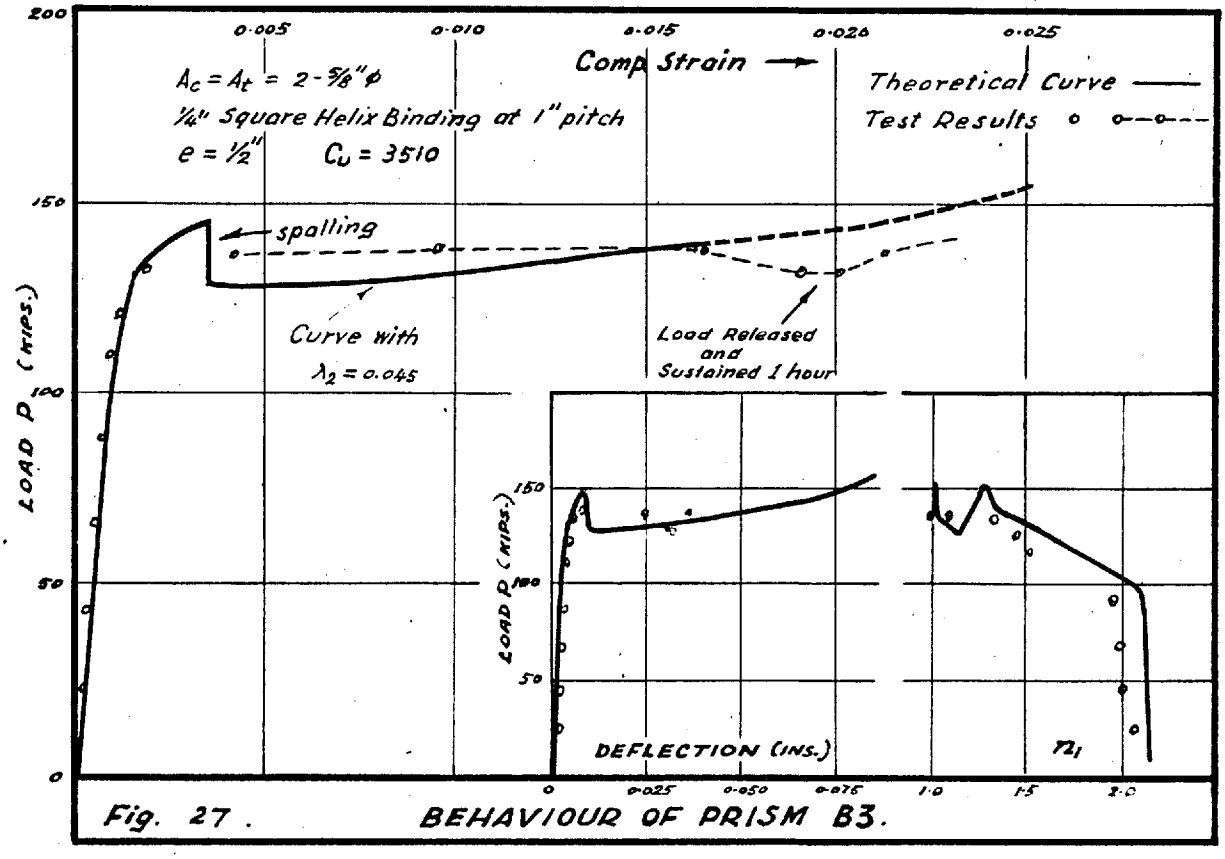


Fig. 27. BEHAVIOUR OF PRISM B3.

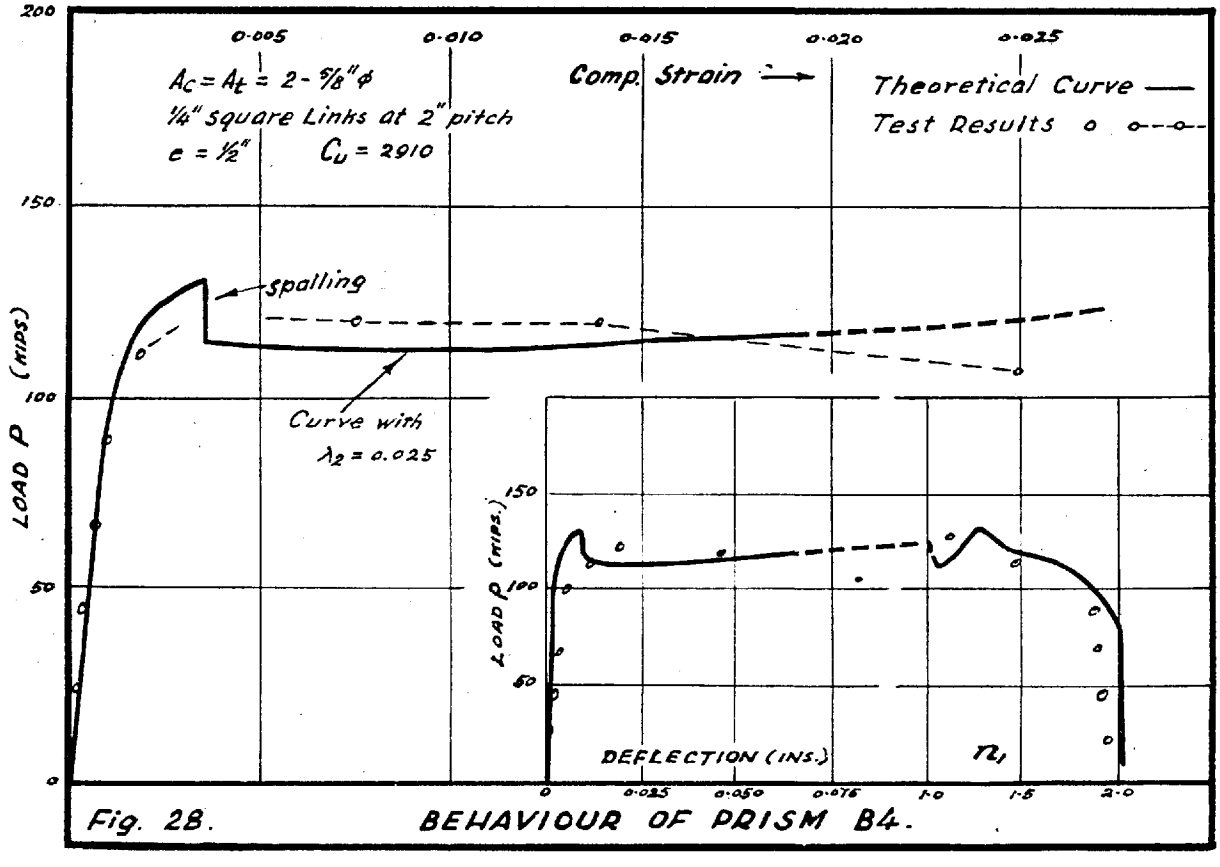


Fig. 28. BEHAVIOUR OF PRISM B4.

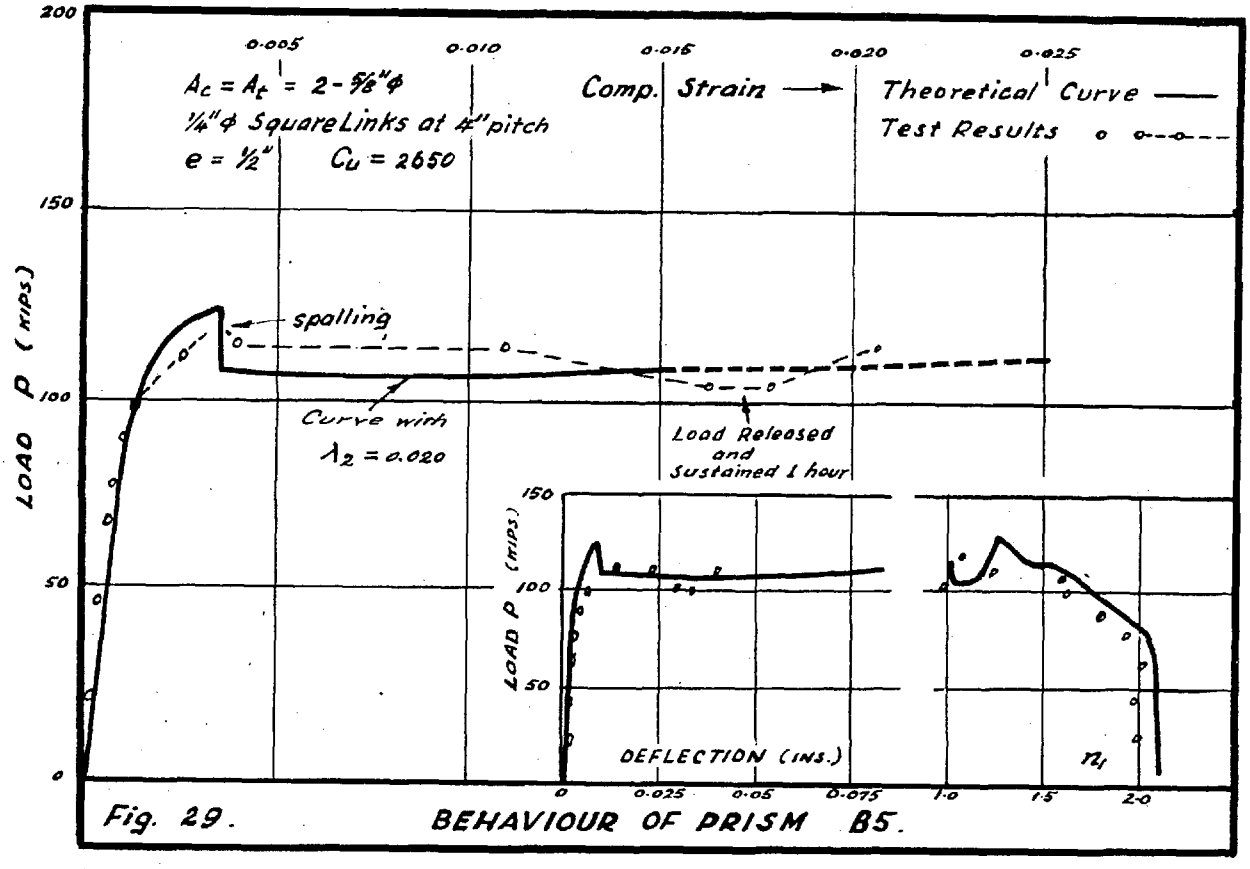


Fig. 29. BEHAVIOUR OF PRISM B5.

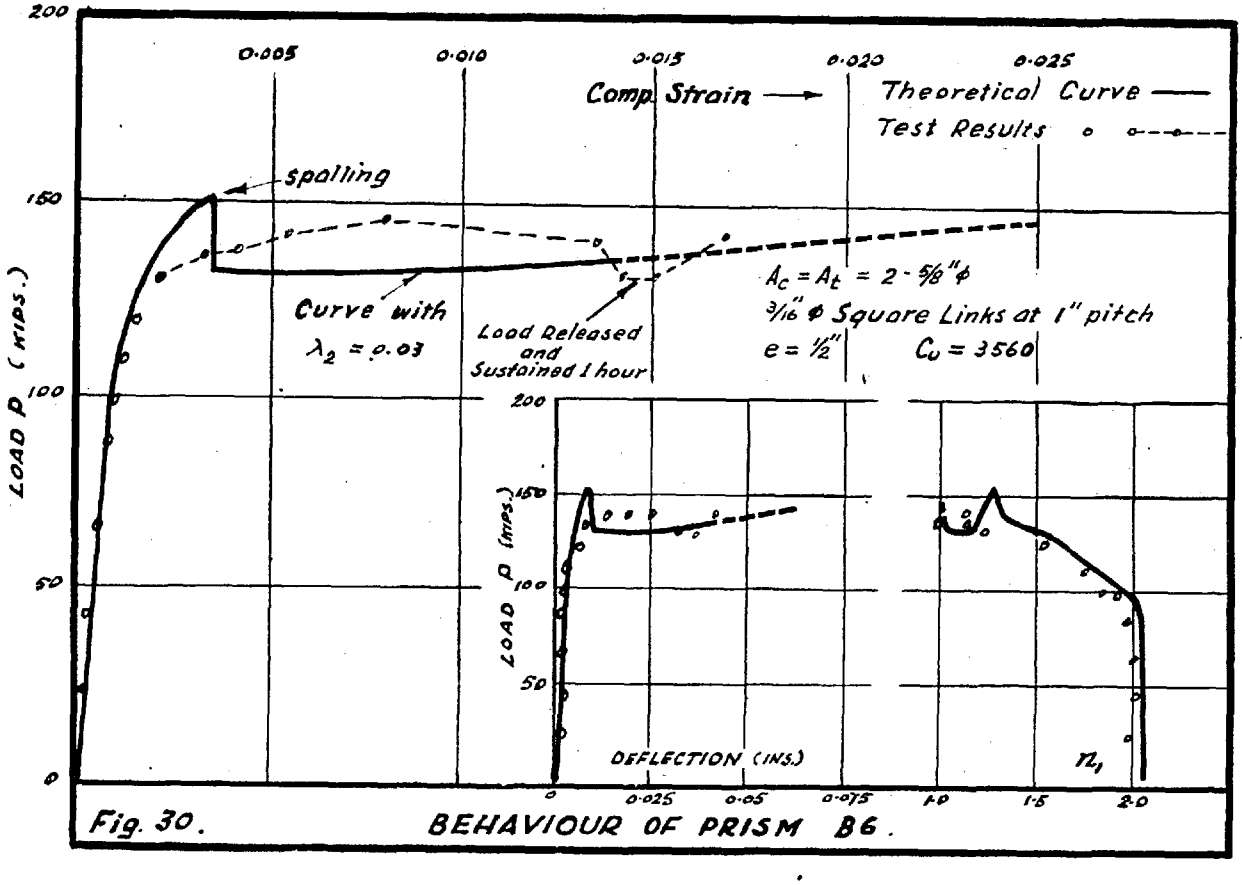


Fig. 30. BEHAVIOUR OF PRISM B6.

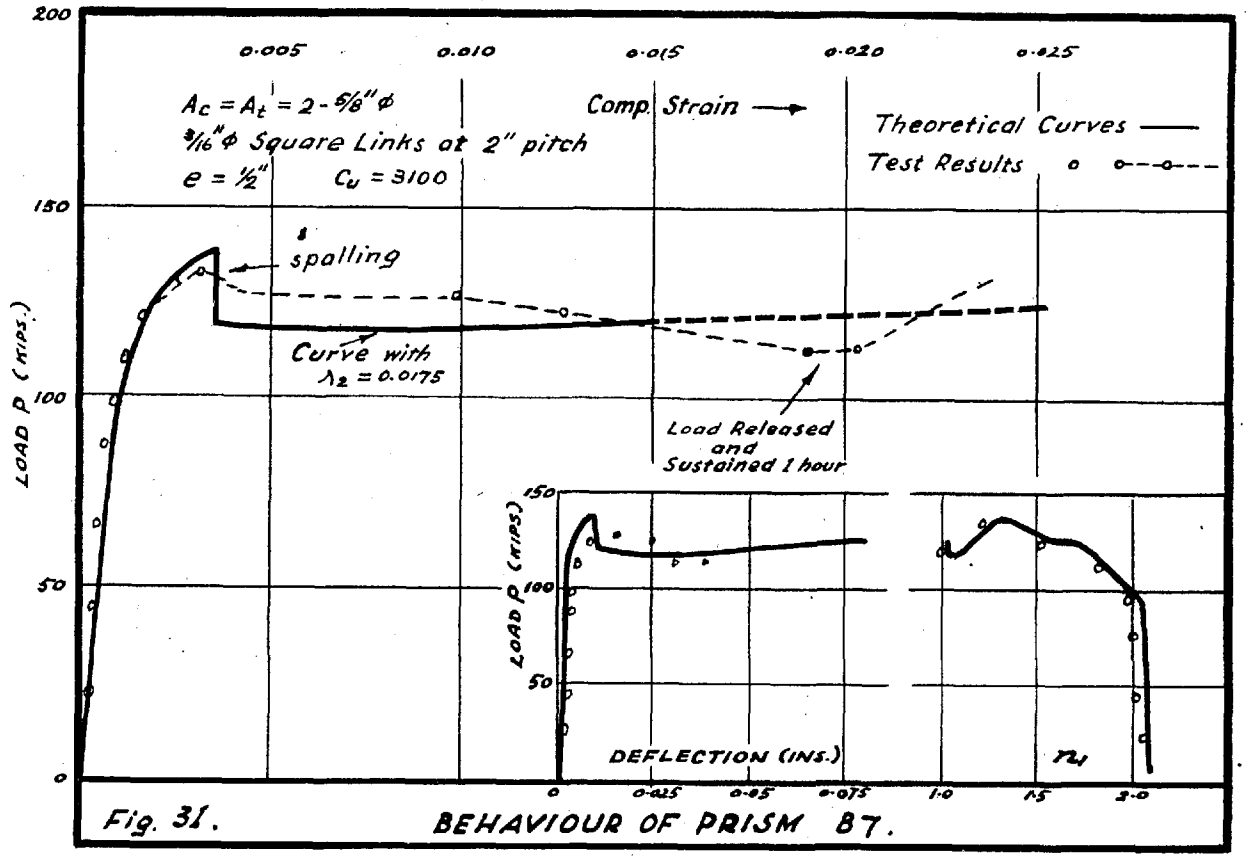


Fig. 31. BEHAVIOUR OF PRISM B7.

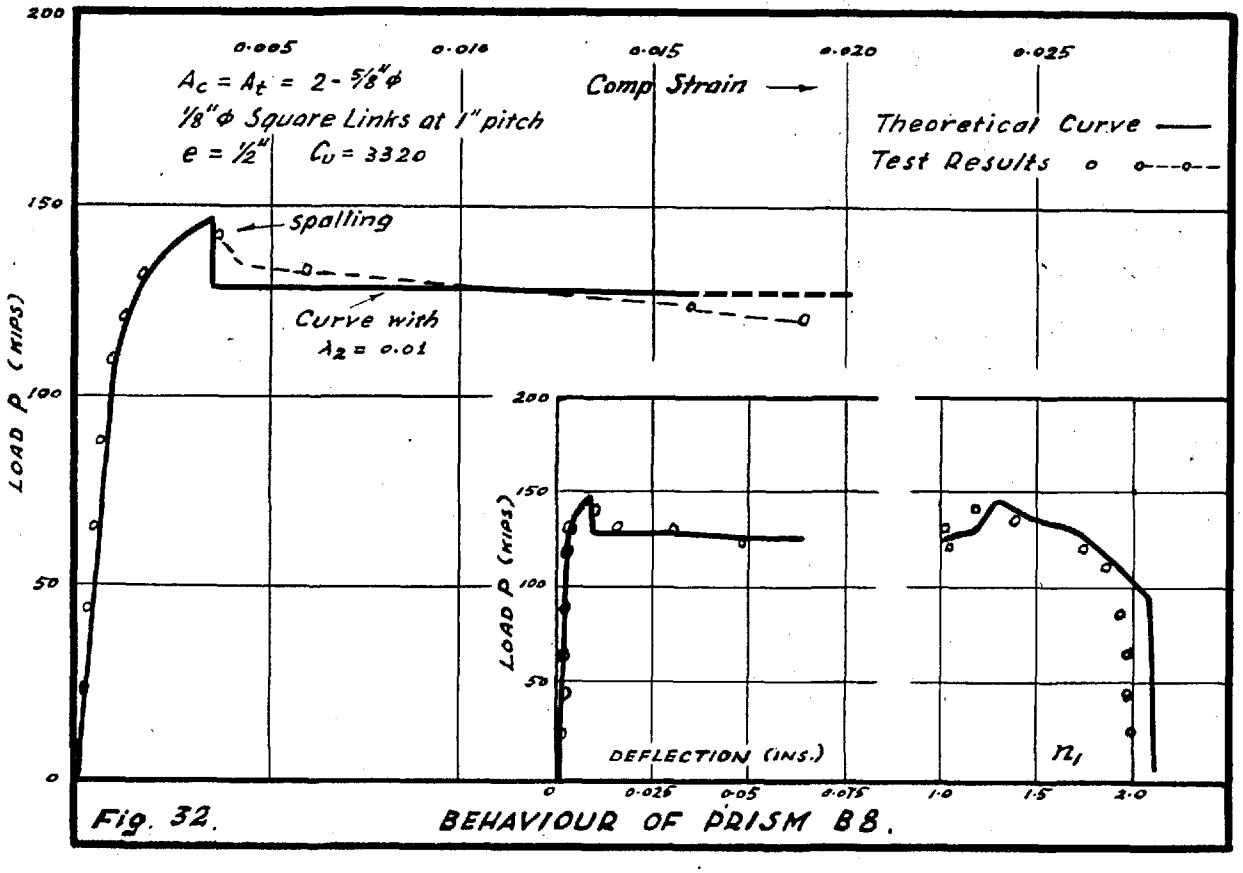


Fig. 32. BEHAVIOUR OF PRISM B8.

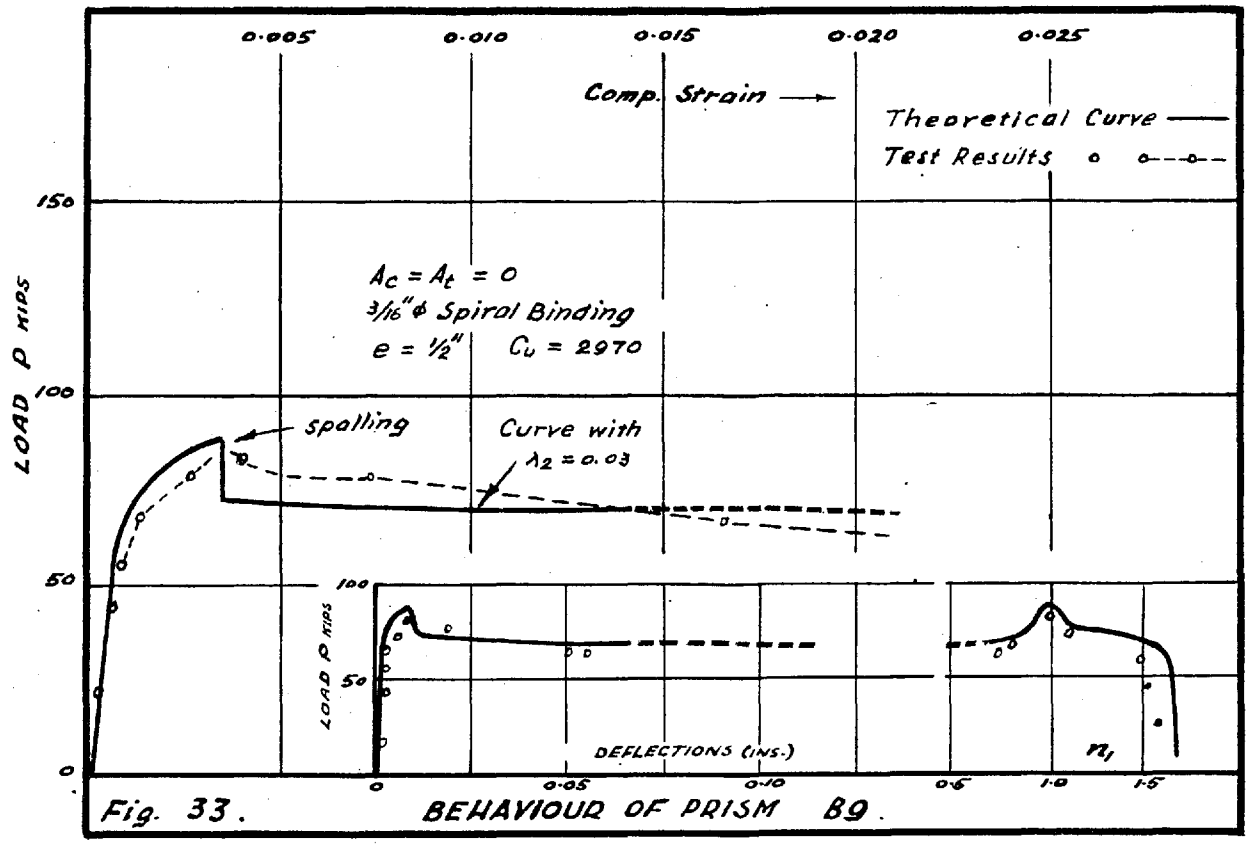


Fig. 33. BEHAVIOUR OF PRISM B9.

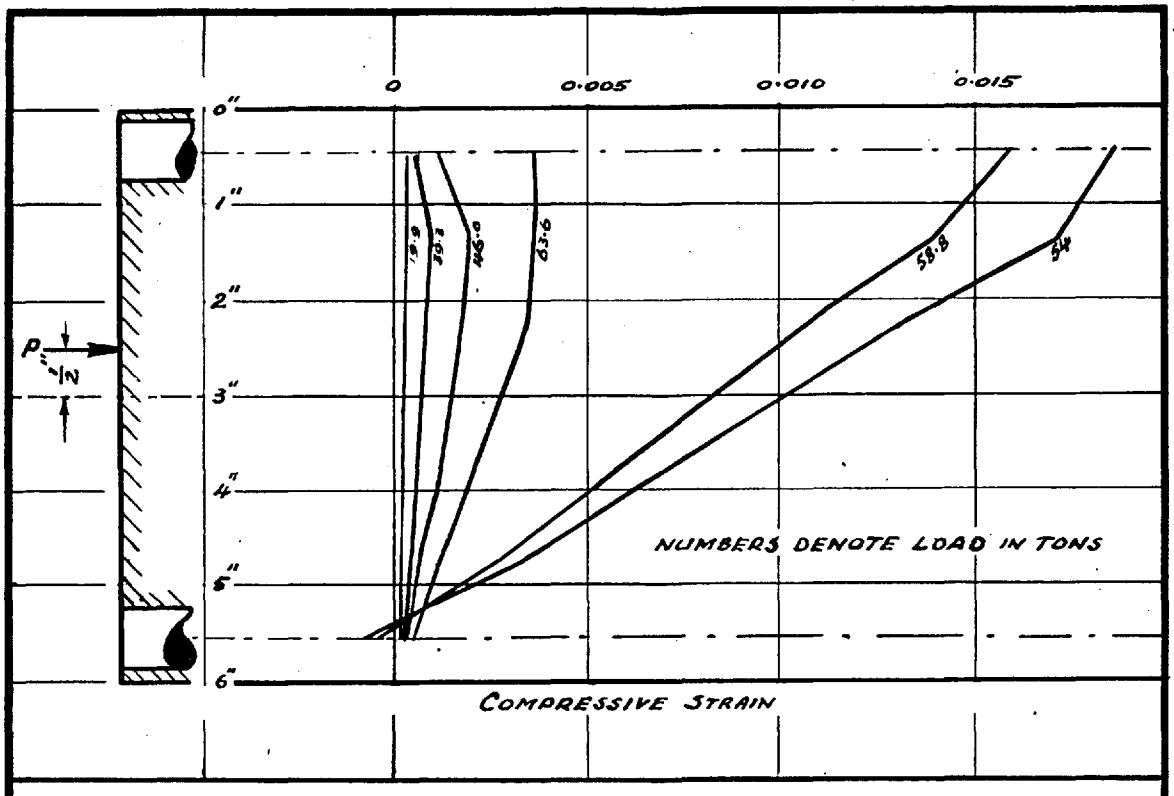


Fig. 34. TYPICAL STRAIN DISTRIBUTION ~ PRISM B8.

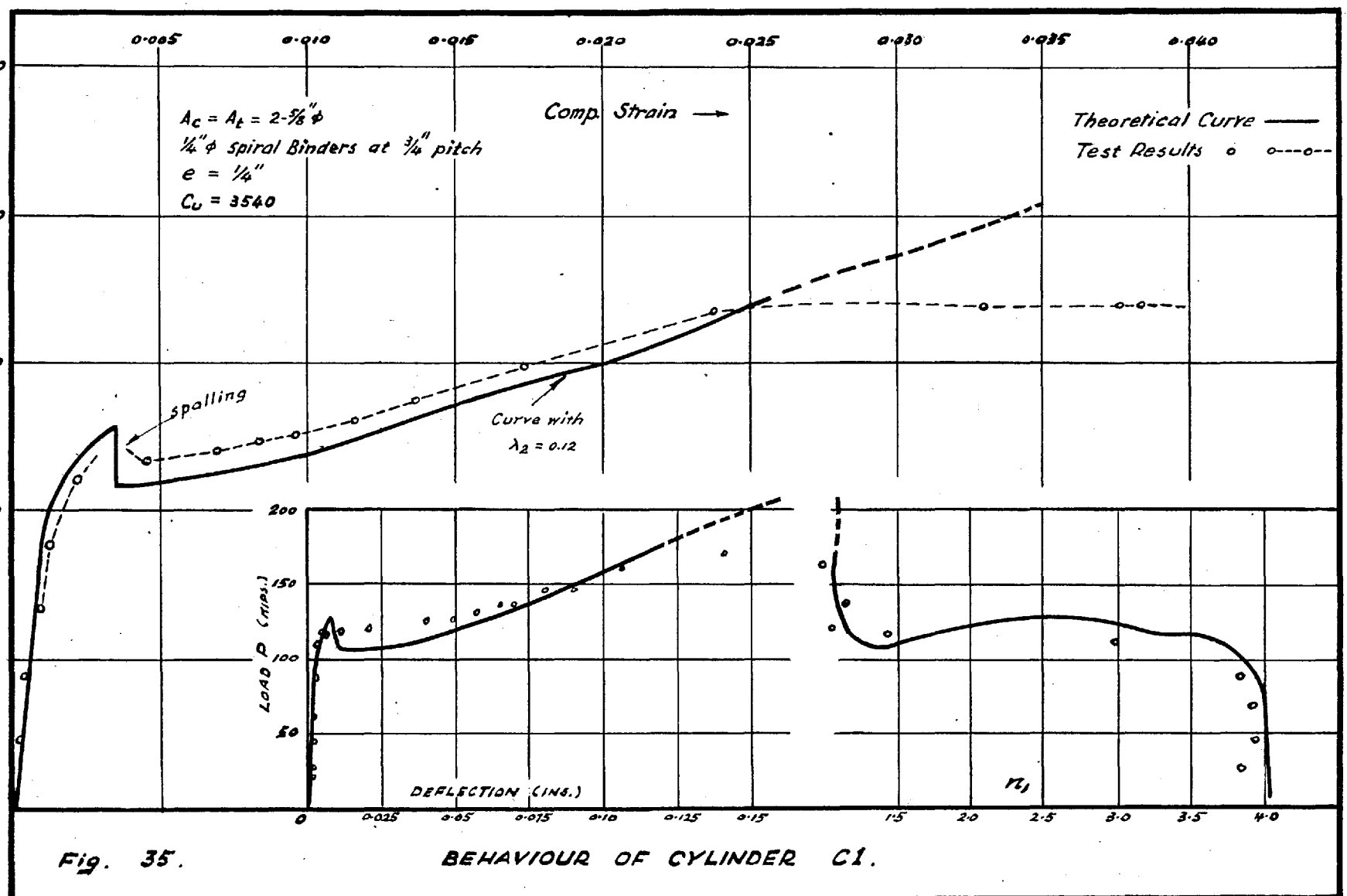


Fig. 35. BEHAVIOUR OF CYLINDER C1.

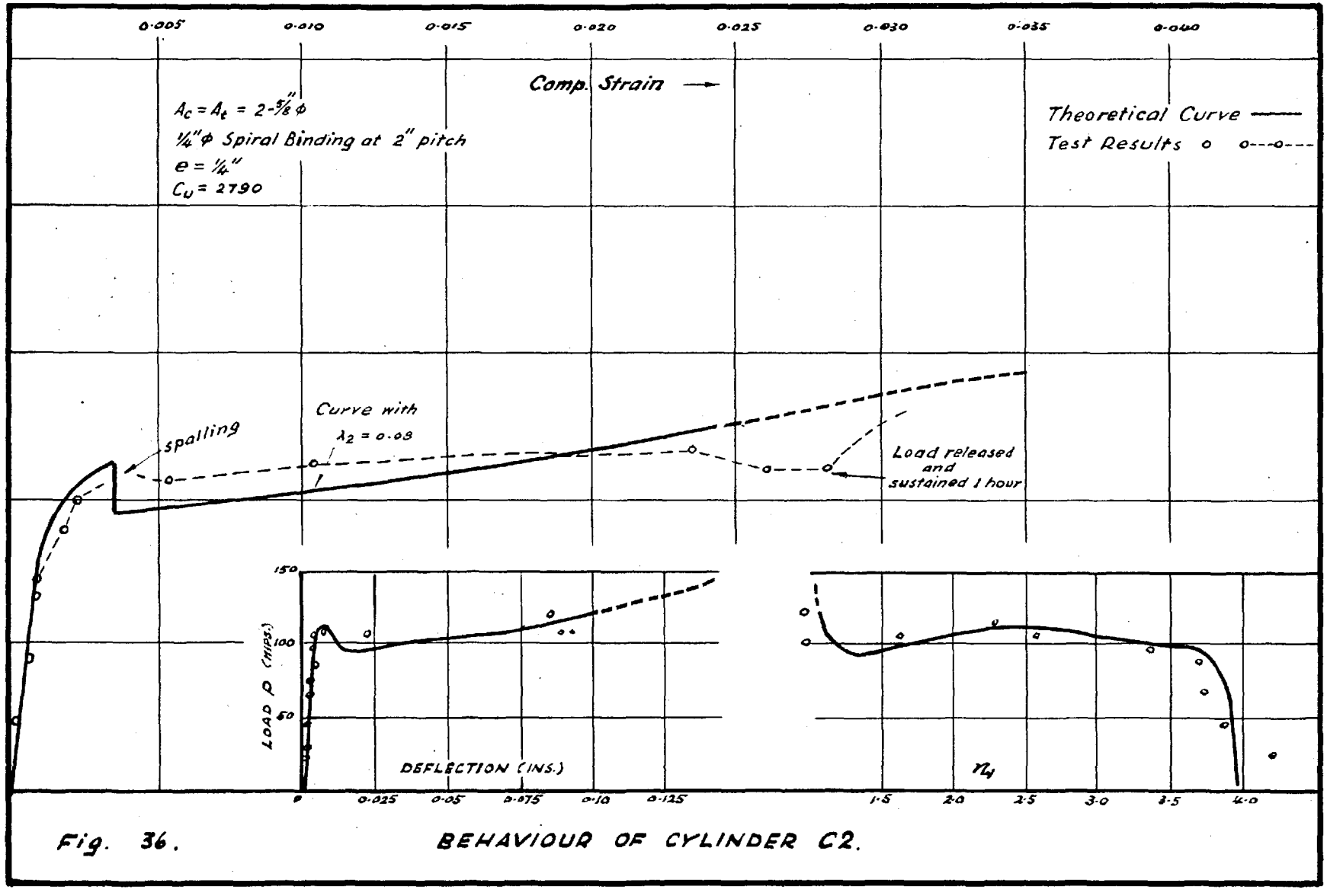


Fig. 36. BEHAVIOUR OF CYLINDER C2.

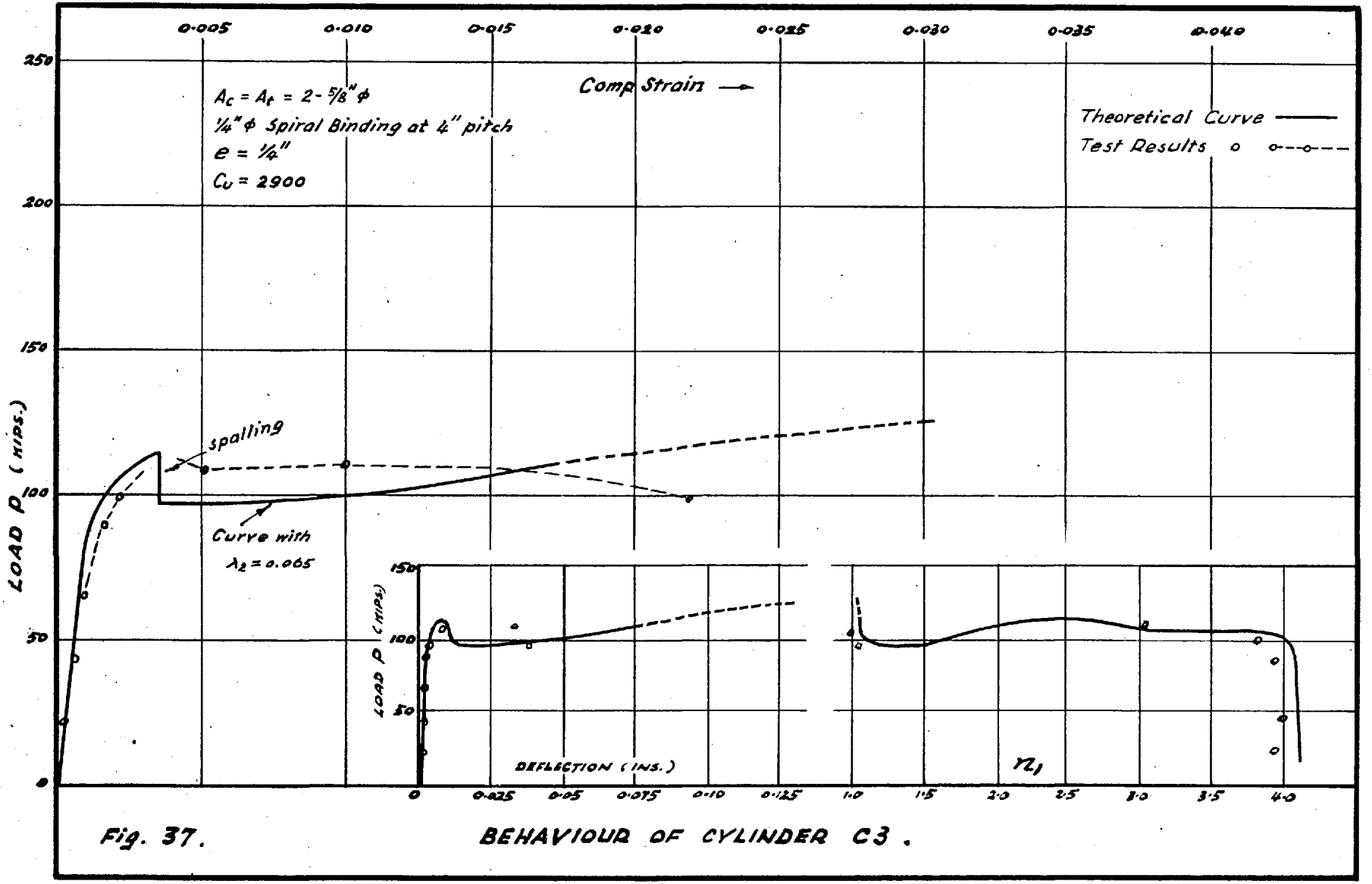


Fig. 37. BEHAVIOUR OF CYLINDER C3.

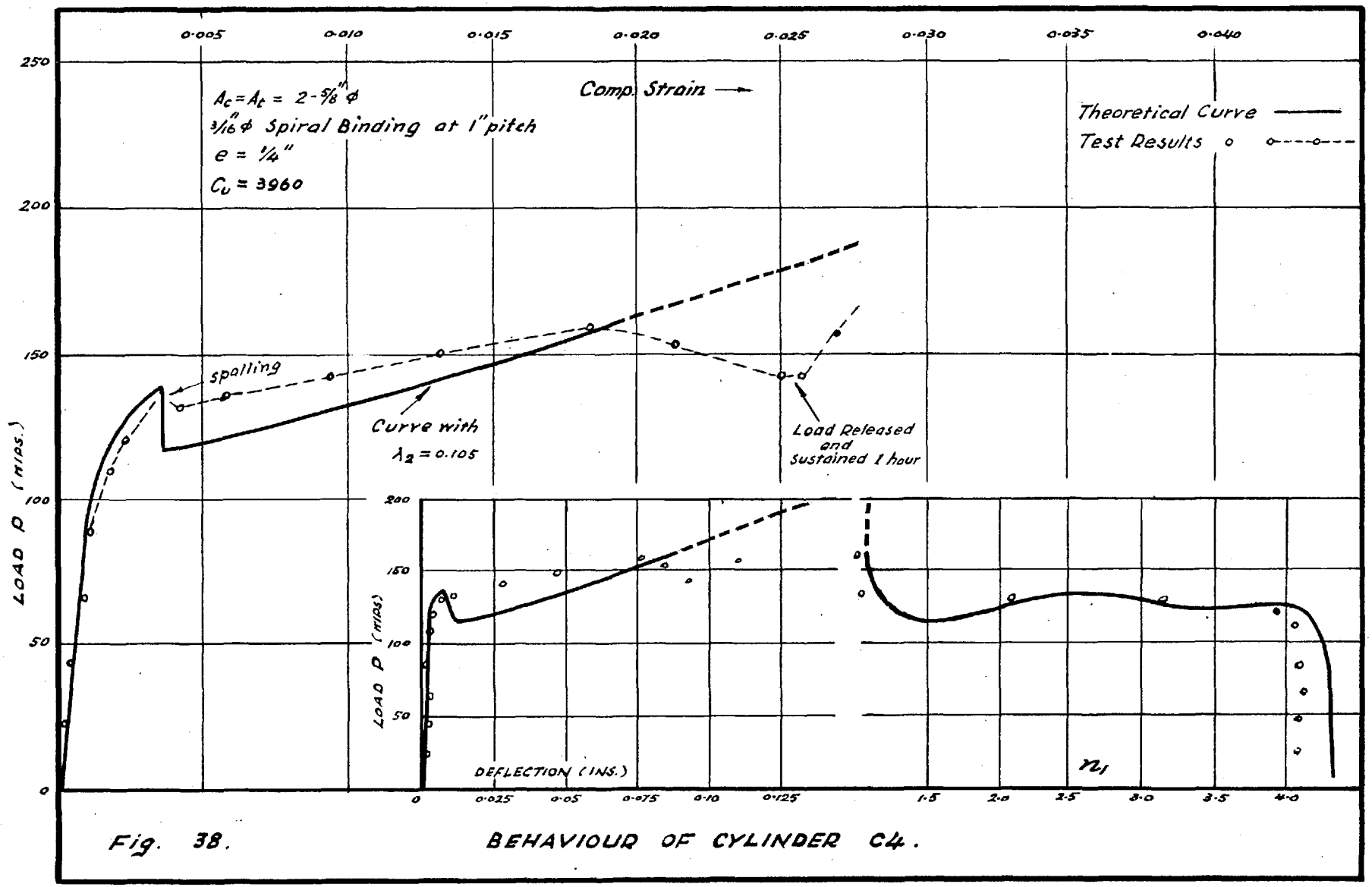


Fig. 38. BEHAVIOUR OF CYLINDER C4.

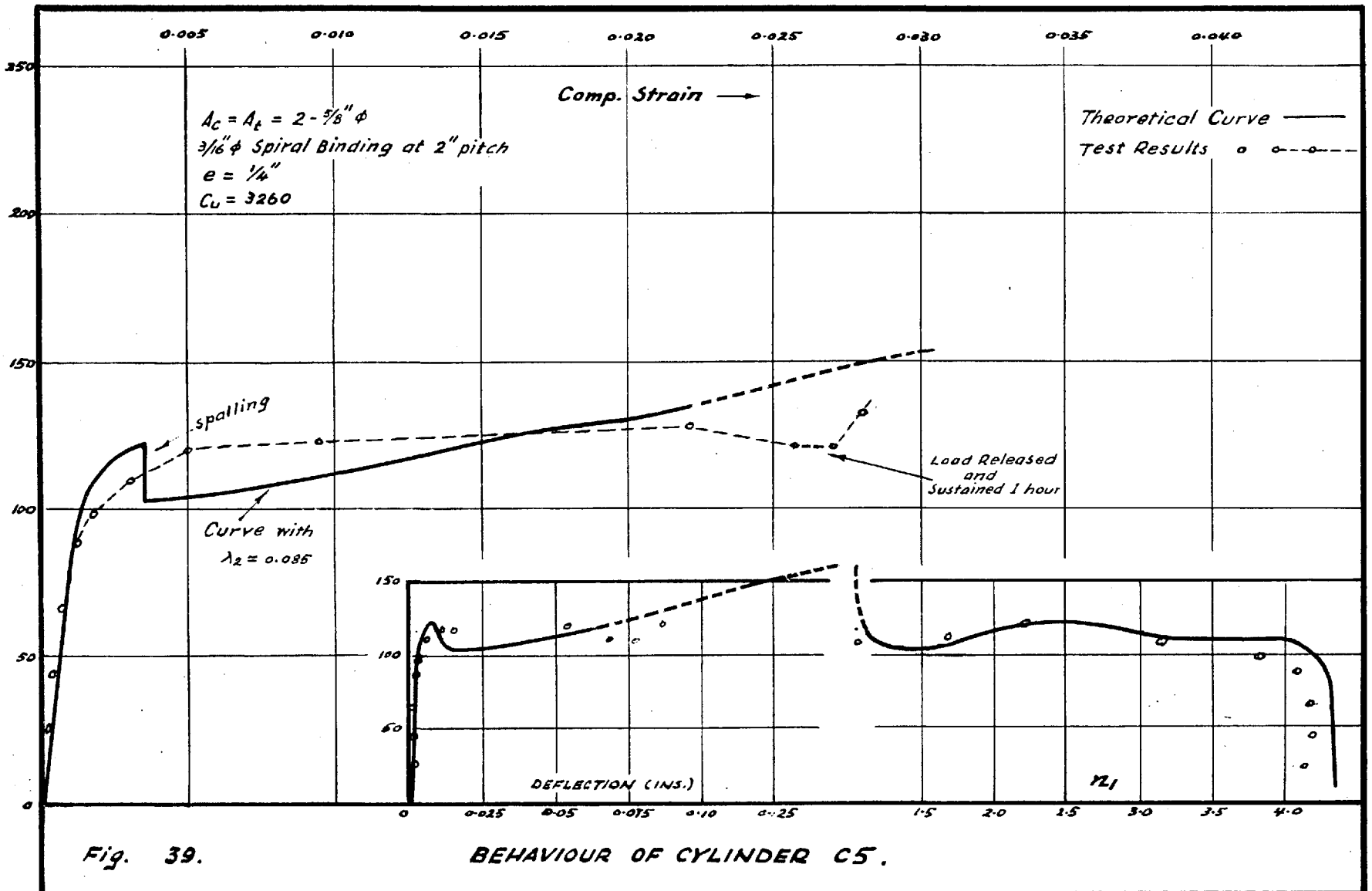


Fig. 39. BEHAVIOUR OF CYLINDER C5.

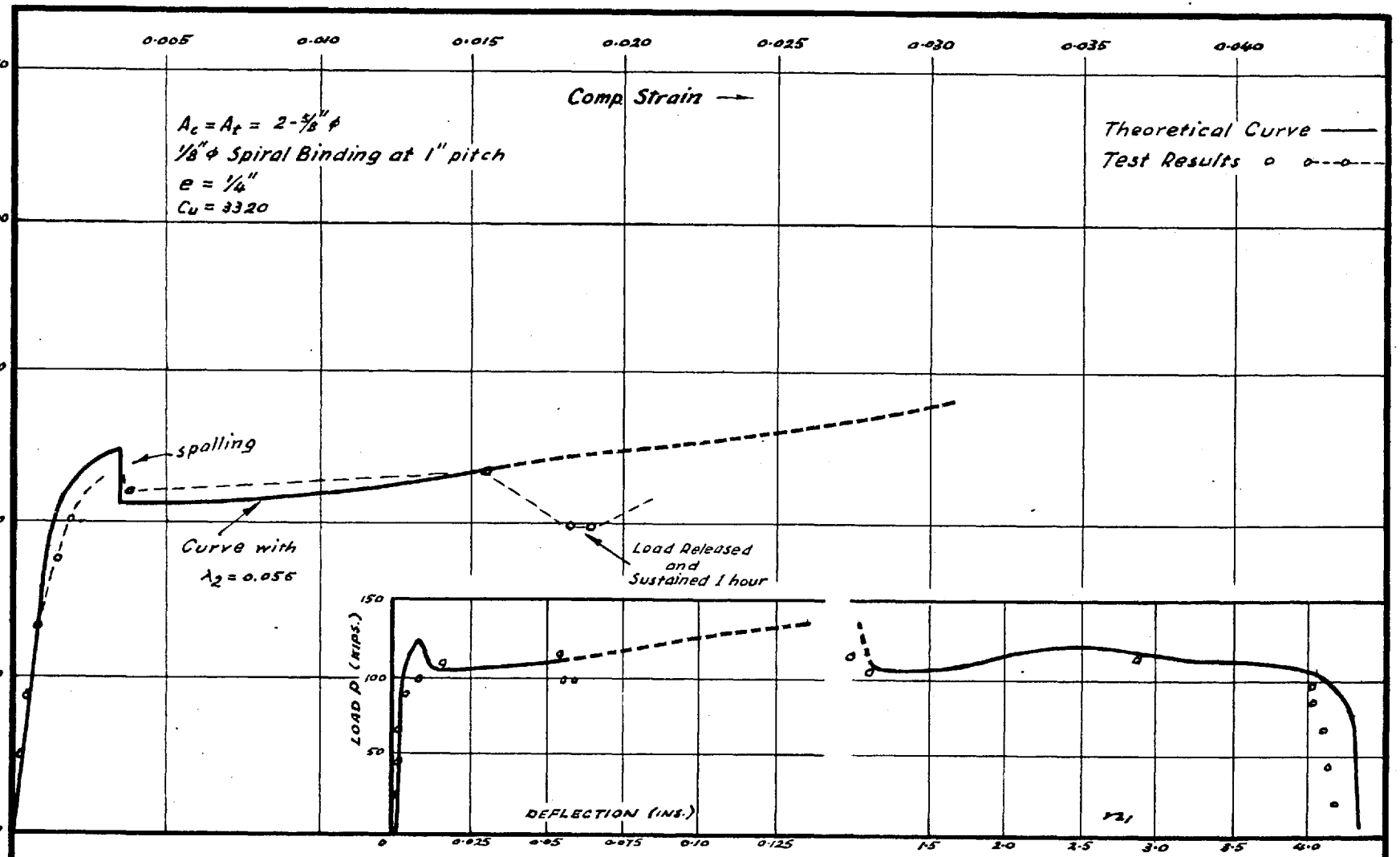


Fig. 40.

BEHAVIOUR OF CYLINDER C6.

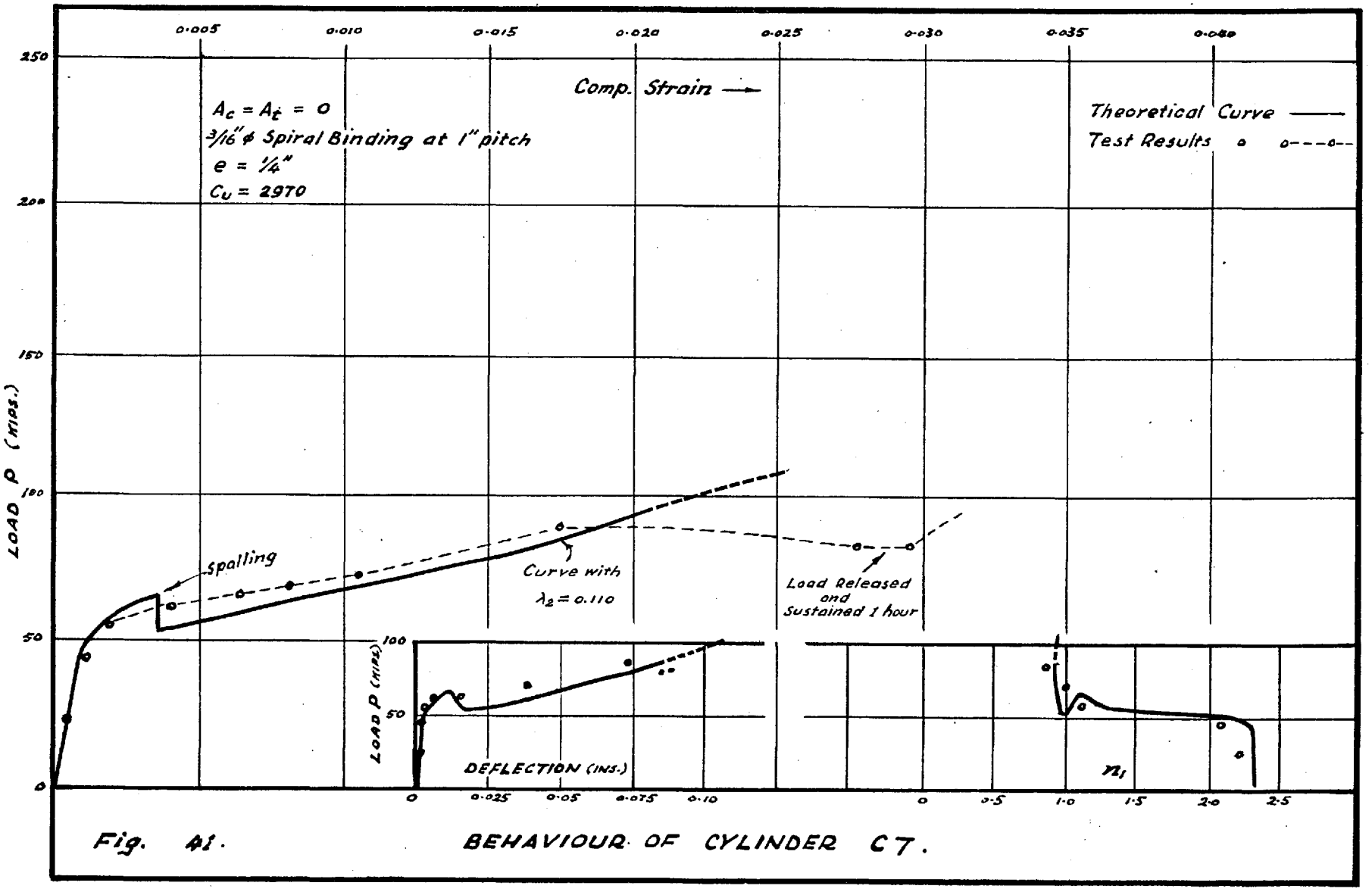


Fig. 41. BEHAVIOUR OF CYLINDER C7.

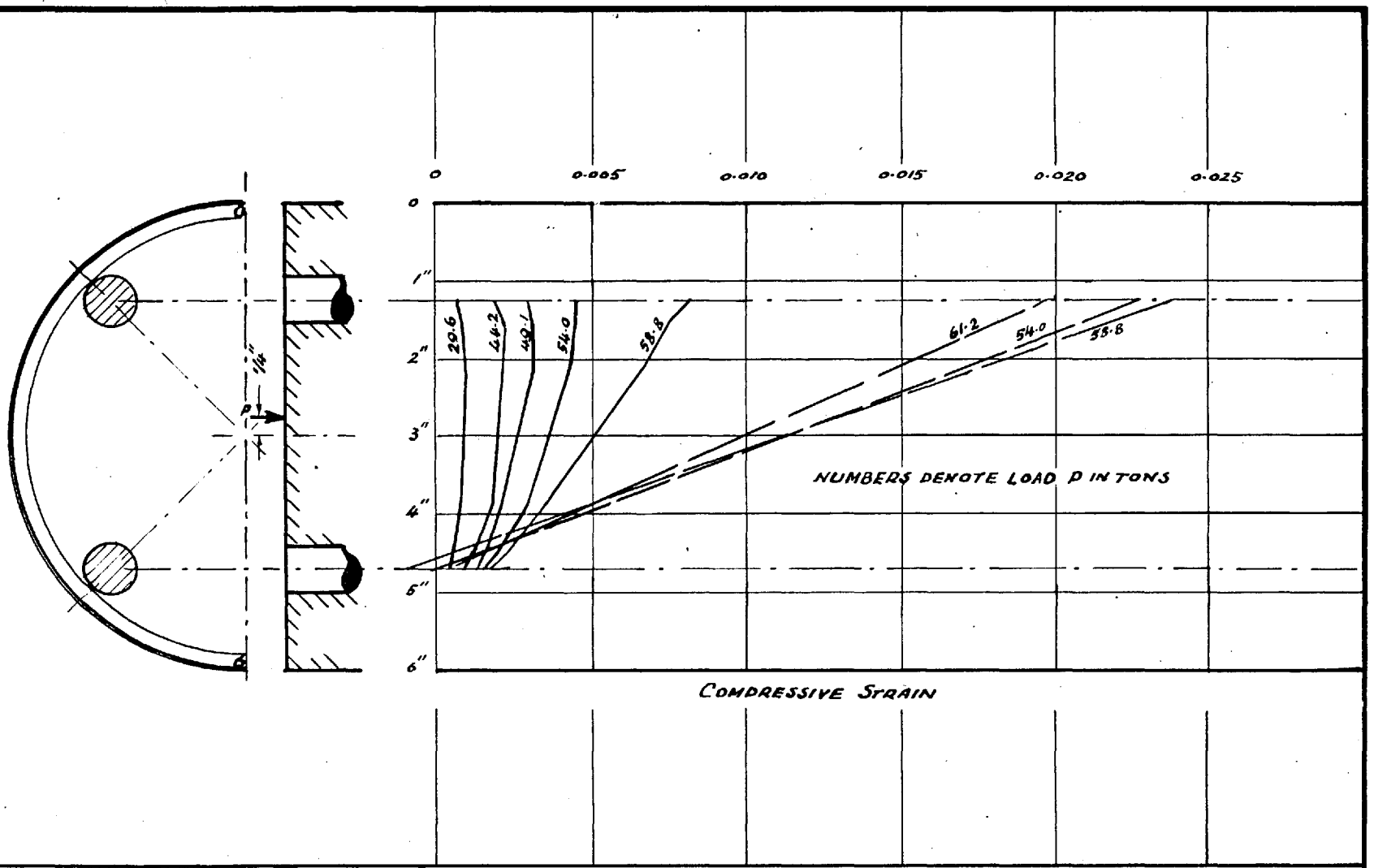


Fig 42. TYPICAL STRAIN DISTRIBUTION ~ CYLINDER C4.

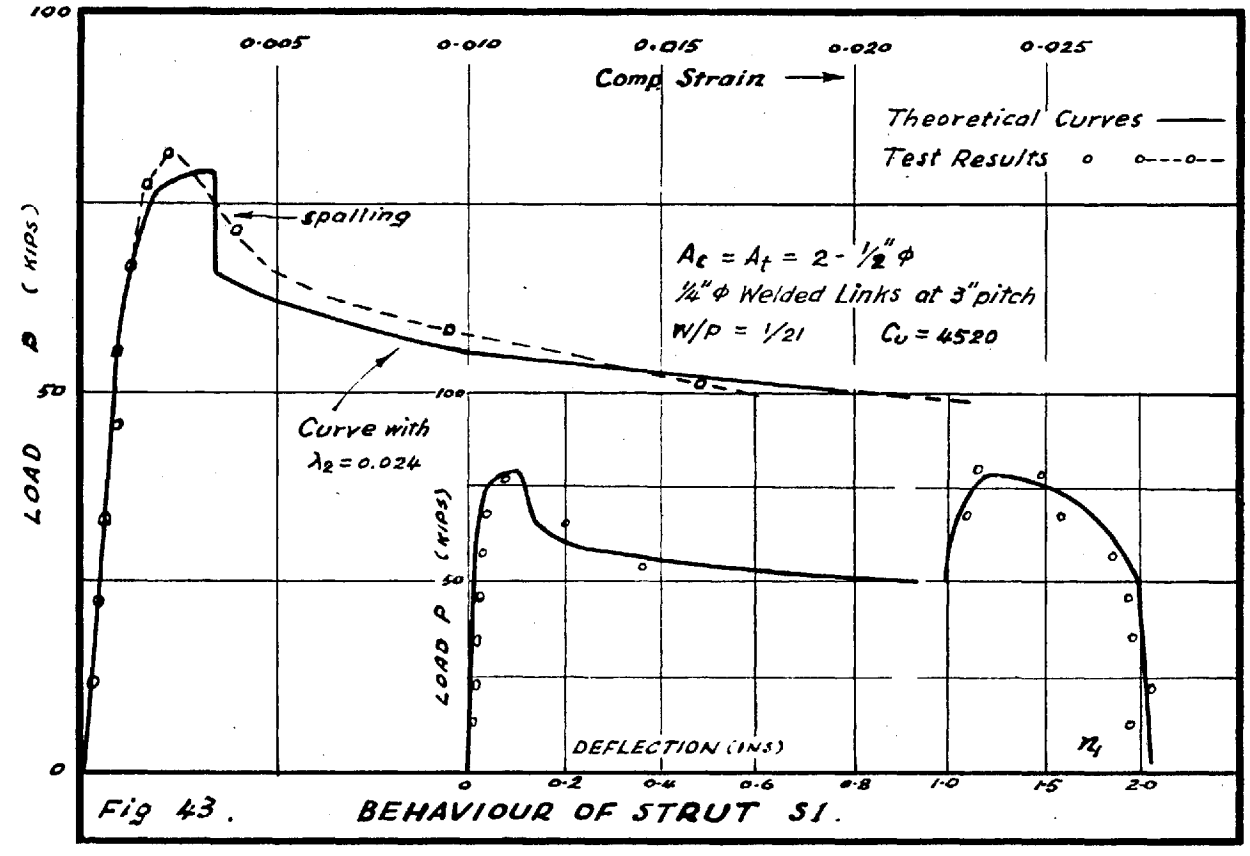


Fig 43. BEHAVIOUR OF STRUT S1.

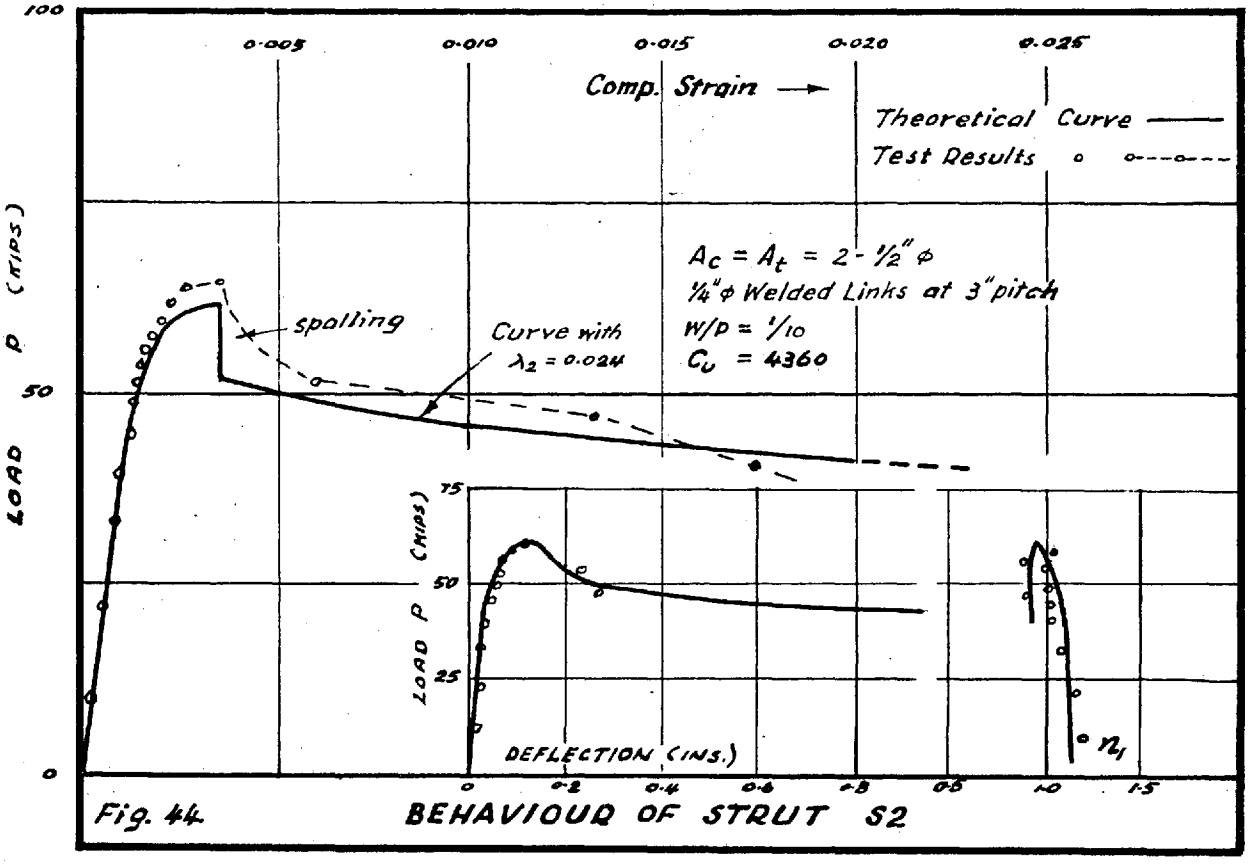


Fig. 44. BEHAVIOUR OF STRUT S2

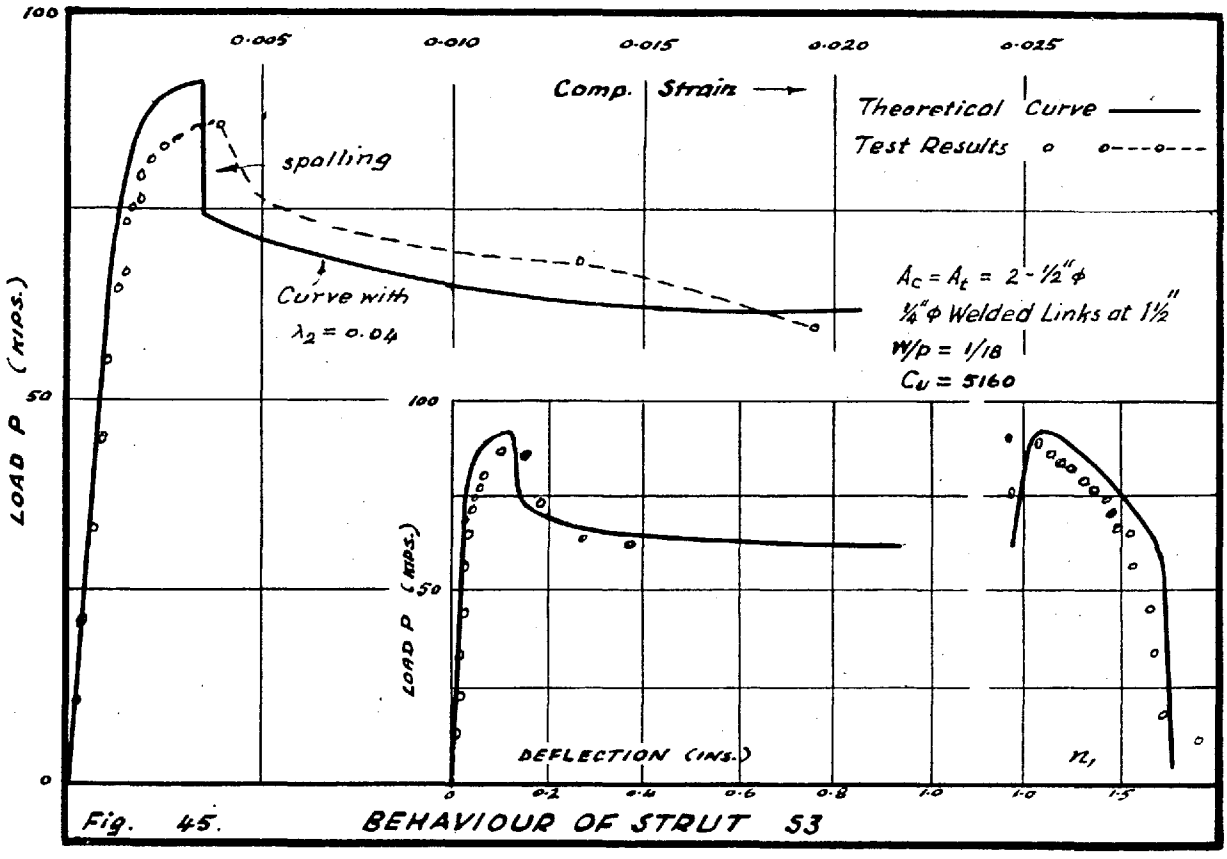


Fig. 45. BEHAVIOUR OF STRUT S3

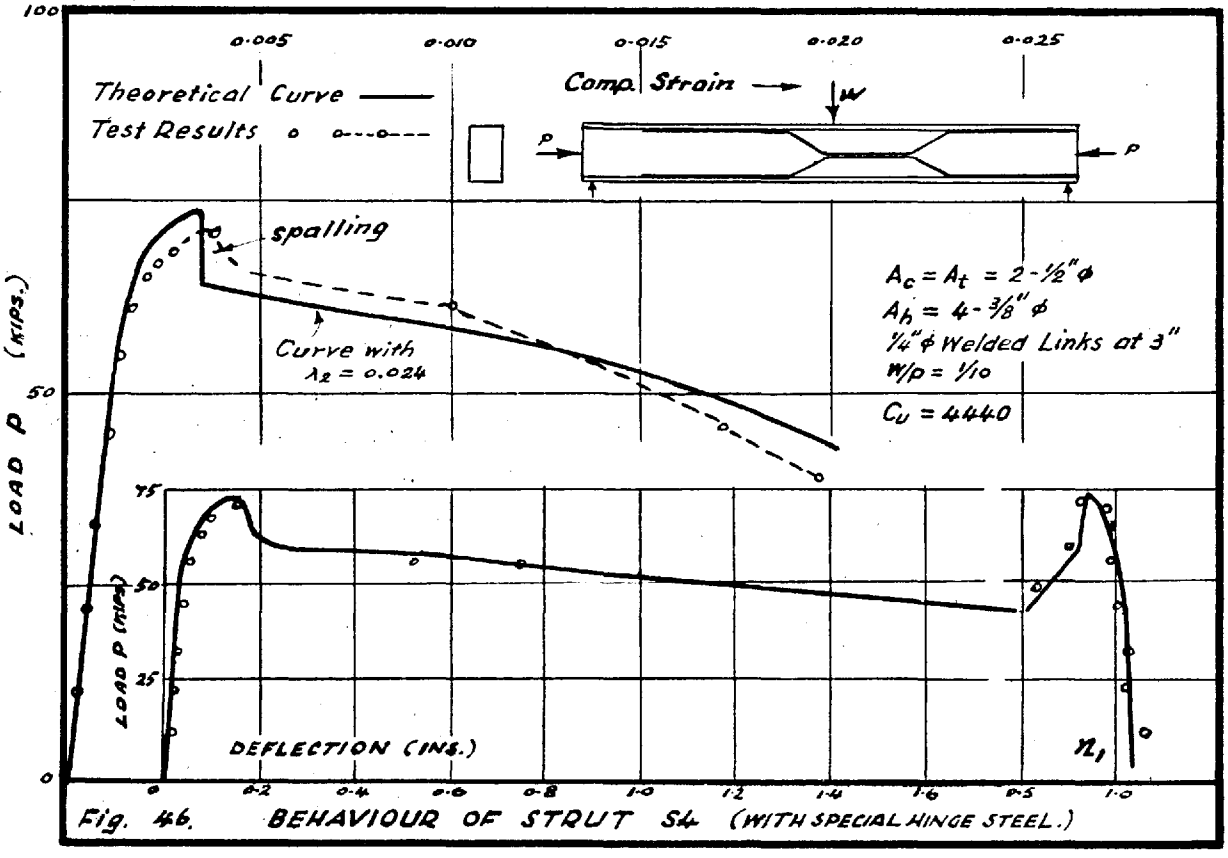


Fig. 46. BEHAVIOUR OF STRUT S4 (WITH SPECIAL HINGE STEEL.)

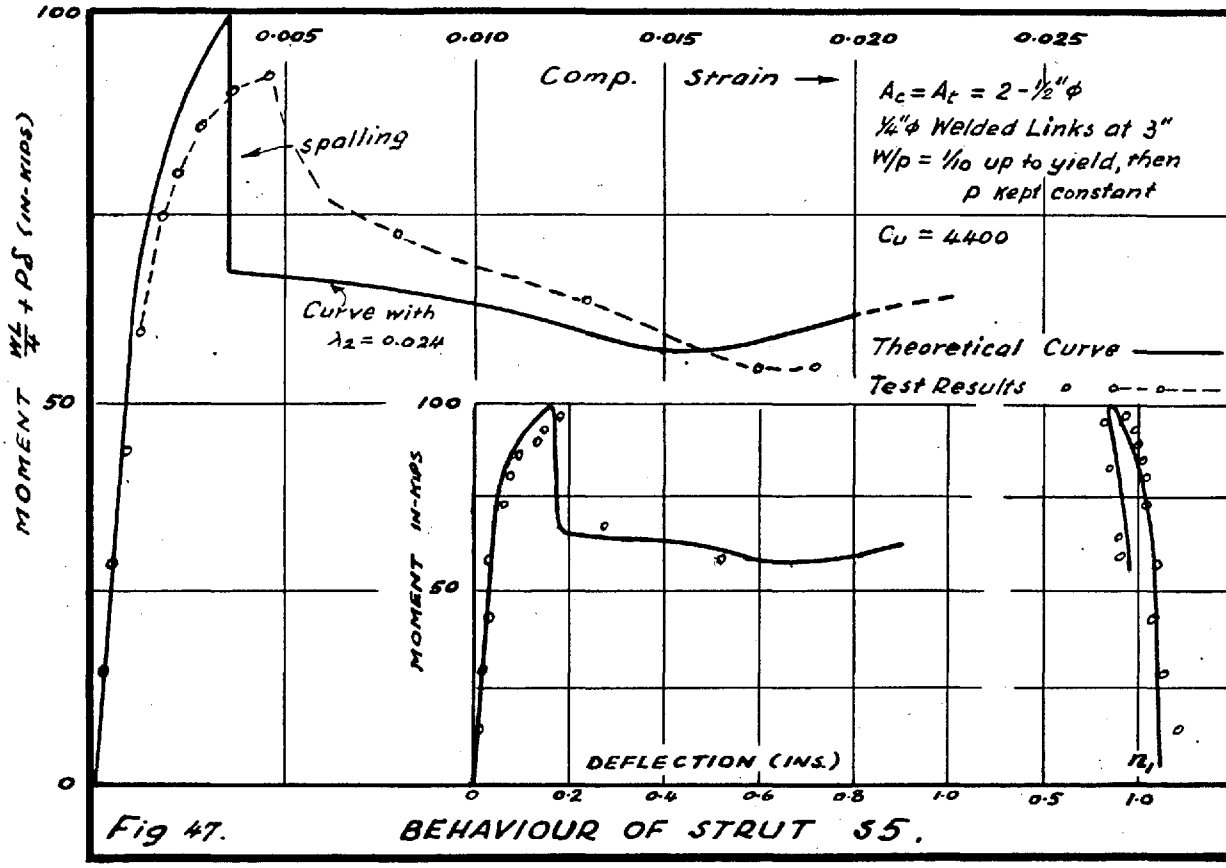


Fig 47. BEHAVIOUR OF STRUT S5.

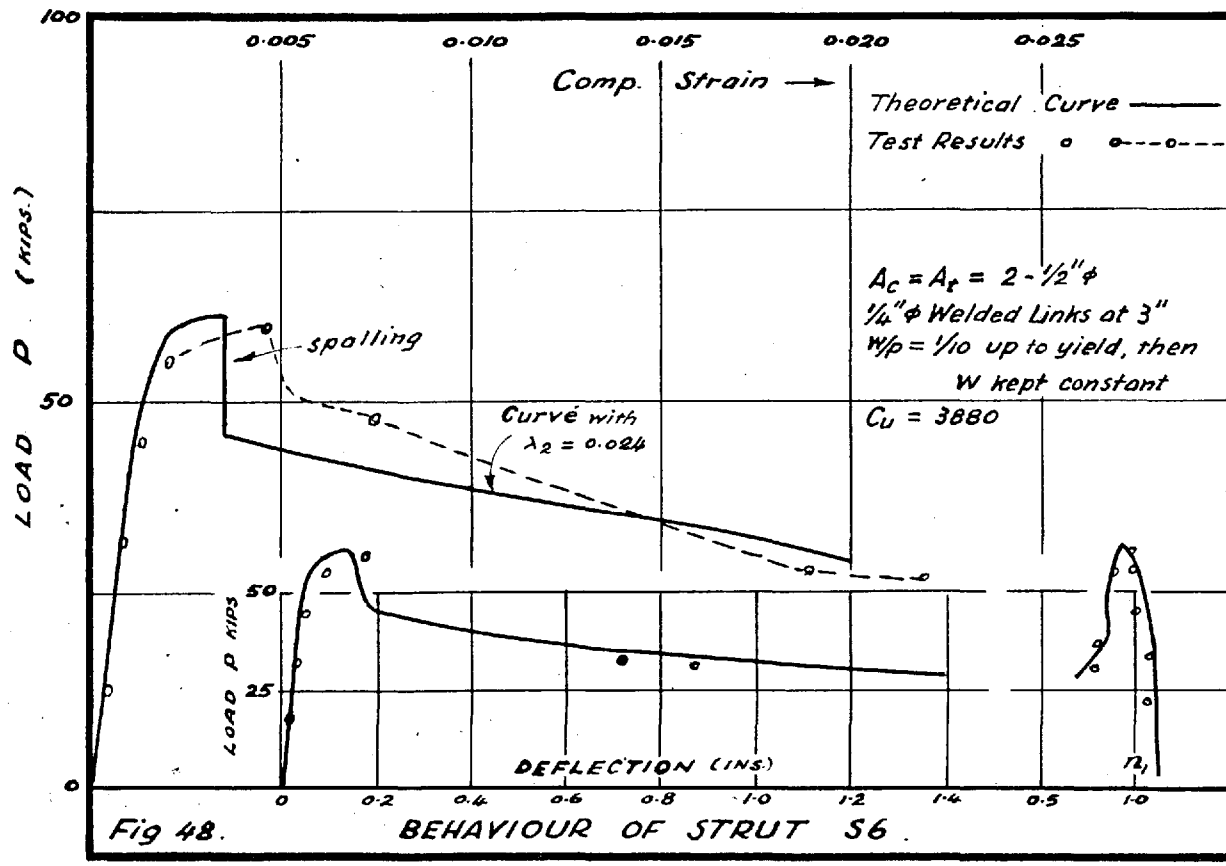


Fig 48. BEHAVIOUR OF STRUT S6.

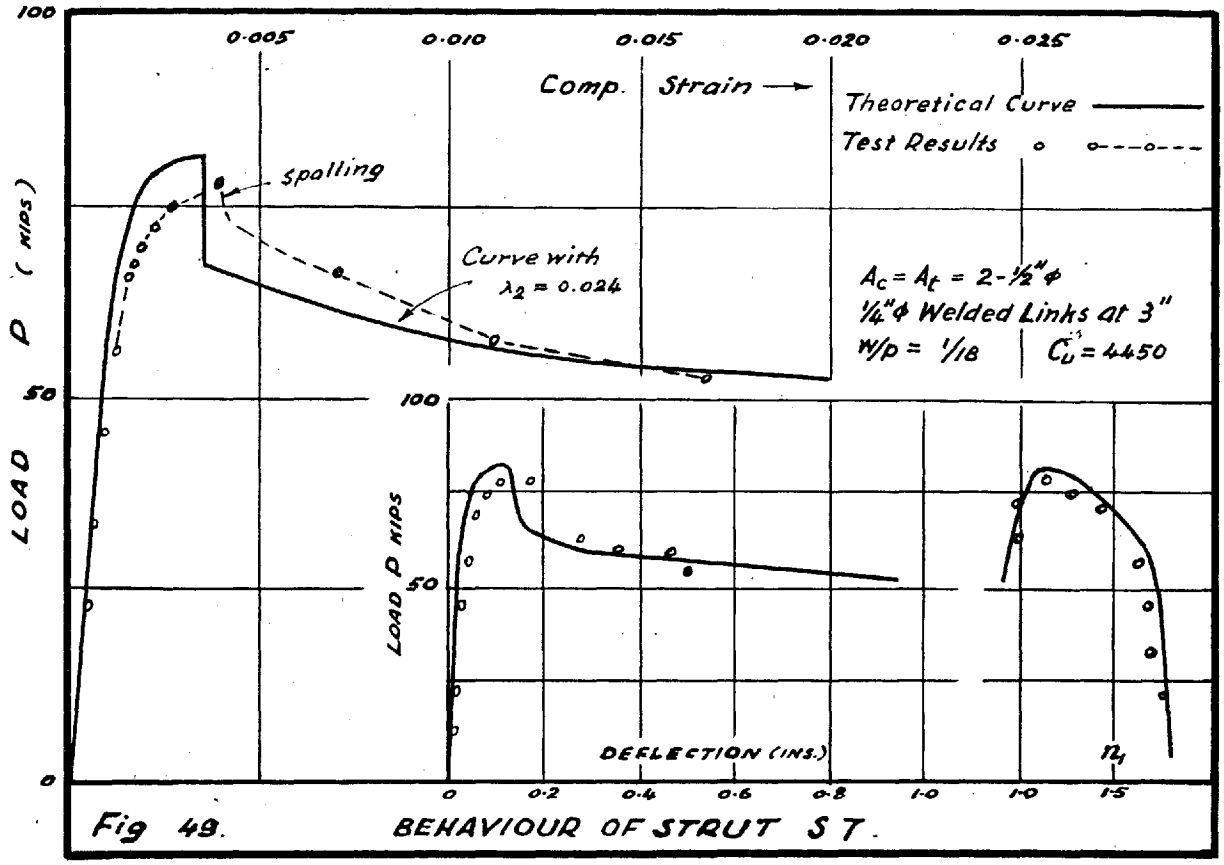


Fig 49. BEHAVIOUR OF STRUT S T.

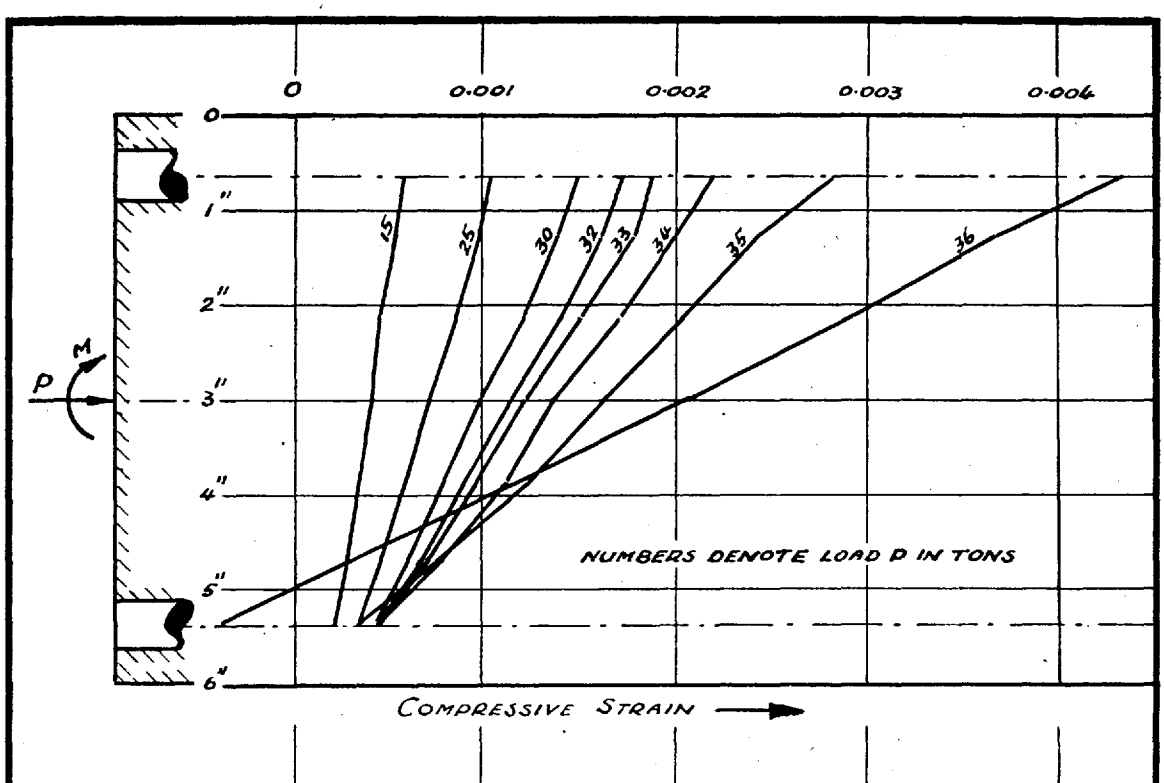


Fig 50. TYPICAL STRAIN DISTRIBUTION — NEAR CENTRE OF STRUT S T.

ELASTIC STAGE

UNBOUND PLASTIC STAGE

ULTIMATE BOUND PLASTIC STAGE.

Bending Moment KIP-INS.

100
75
50
25

P = 52000

P = 79000

P = 52700

n's

n's

n's

Max. Concrete Strain $\epsilon \times 10^{-3}$

15
10
5

Rotation $\epsilon_{n,d} = M/EI$ (rad. $\times 10^{-4}$)

30
20
10

$EI \times 10^{6}$

400
200

0 5" 10 15 20 25 Length (inches)

0 5 10 15 20 25 Length (inches)

0 5 10 15 20 25 Length (inches)

Theoretical Curve ——

Test Results o o o

Fig. 51. ELASTIC & PLASTIC BEHAVIOUR ALONG LENGTH OF STRUT S1.

ELASTIC STAGE

UNBOUND PLASTIC STAGE

ULTIMATE BOUND PLASTIC STAGE

Bending Moment kip-ins.

100
75
50
25

P = 36000

P = 61500

P = 43000

h's

17.5

Max. Concrete Strain $\varepsilon \times 10^{-3}$

15
10
5

Rotation $\theta_{md} = M/EI$ (rad. $\times 10^{-4}$)

30
20
10

$EI \times 10^6$

400
200

0 5 10 15 20 25

Length (inches)

Fig. 52. ELASTIC & PLASTIC BEHAVIOUR ALONG LENGTH OF STRUT S2

Test Results o. o o

Theoretical Curves ——

ELASTIC STAGE

UNBOUND PLASTIC STAGE

ULTIMATE BOUND PLASTIC STAGE

Bending Moment Mlb-ins.

100
75
50
25

P = 85000

P = 90000

P = 62000

h's

h's

r.s

Max. Concrete Strain $\epsilon \times 10^{-3}$

15
10
5

Rotation $\epsilon_{m.d} = M/EI$ (rad $\times 10^{-4}$)

30
20
10

$EI \times 10^6$

400
300

0 5 10 15 20 25 Length (inches)

Fig. 53. ELASTIC & PLASTIC BEHAVIOUR ALONG LENGTH OF STRUT S3.

Test Results • ○ ○

& Theoretical Curves ——

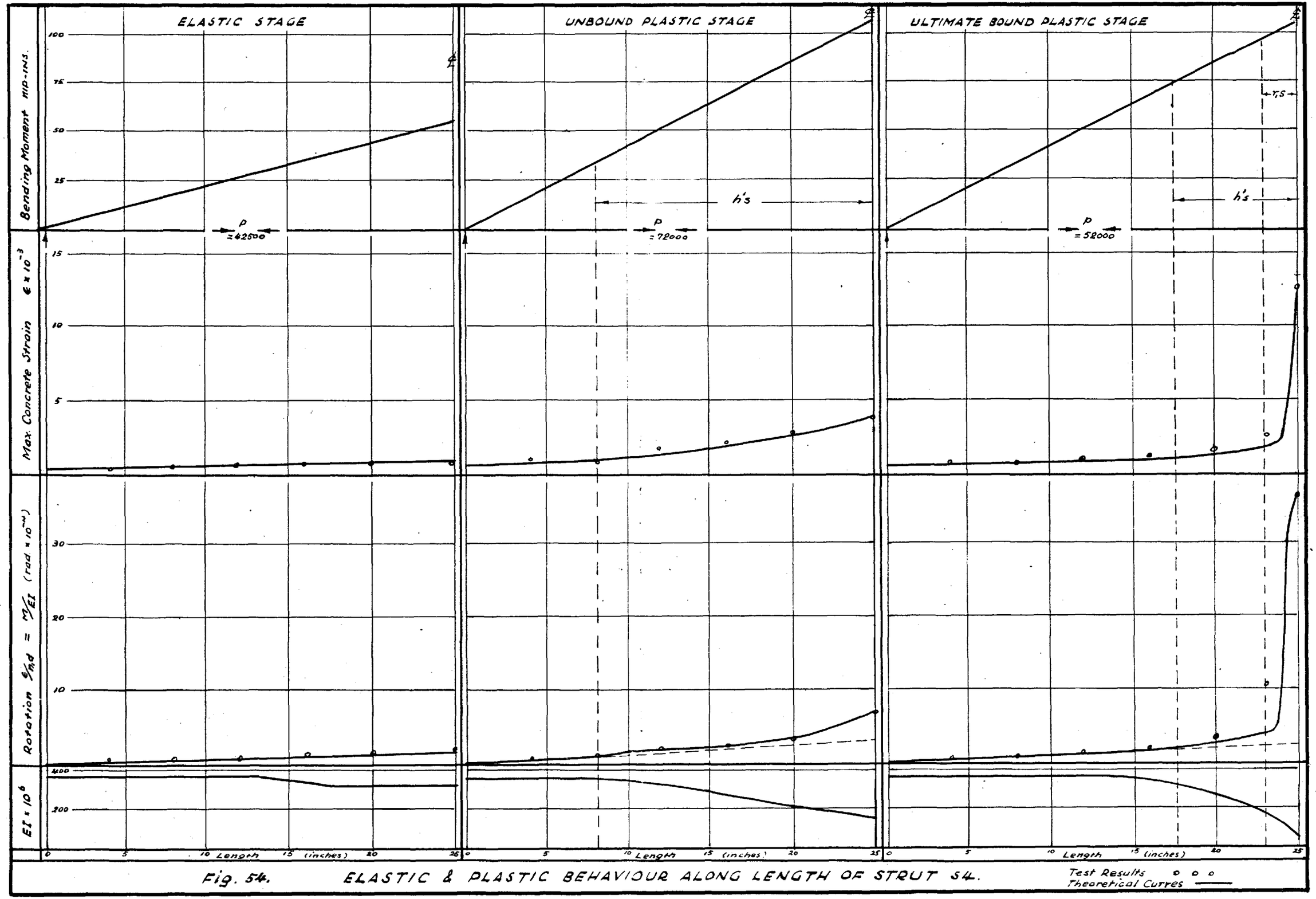


Fig. 54. ELASTIC & PLASTIC BEHAVIOUR ALONG LENGTH OF STRUT S4.

ELASTIC STAGE

UNBOUND PLASTIC STAGE

ULTIMATE BOUND PLASTIC STAGE

Bending Moment kip-ins.

100
75
50
25

P = 40000

P = 60500

h's

P = 60500

h's

Max. Concrete Strain $\epsilon \times 10^{-3}$

15
10
5

Rotation $\theta/Ad = M/EI$ (rad. $\times 10^{-4}$)

30
20
10

$EI \times 10^6$

400
200

0 5 10 15 20 25

Length (inches)

0 5 10 15 20 25

Length (inches)

0 5 10 15 20 25

Length (inches)

Fig. 55. ELASTIC & PLASTIC BEHAVIOUR ALONG LENGTH OF STRUT S5.

Test Results o o o

Theoretical Curve ——

ELASTIC STAGE

UNBOUND PLASTIC STAGE

ULTIMATE BOUND PLASTIC STAGE

Bending Moment kip-ins.

100
75
50
25

P = 35000

P = 62000

h's

P = 35000

h's

Max. Concrete Strain $\varepsilon \times 10^{-3}$

15
10
5

Rotation $\theta_{md} = M/EI$ (rad. $\times 10^{-4}$)

30
20
10

$EI \times 10^6$

400
200

0 5 10 15 20 25 Length (inches)

0 5 10 15 20 25 Length (inches)

0 5 10 15 20 25 Length (inches)

Fig. 56. ELASTIC & PLASTIC BEHAVIOUR ALONG LENGTH OF STRUT S6.

Test Results o o o
Theoretical Curves ——

ELASTIC STAGE

UNBOUND PLASTIC STAGE

ULTIMATE BOUND PLASTIC STAGE

Bending Moment Kip-ins

100
75
50
25

P = 51000

P = 79000

P = 82000

h's

1.5 h's

Max Concrete Strain $\epsilon \times 10^{-3}$

15
10
5

Rotation $\theta_{rad} = M/EI$ (rad. $\times 10^{-4}$)

30
20
10

$EI \times 10^6$

400
200

0 5 10 15 20 25 Length (inches)

Fig. 57. ELASTIC & PLASTIC BEHAVIOUR ALONG LENGTH OF STRUT S7.

Test Results o o o
Theoretical Curves ——

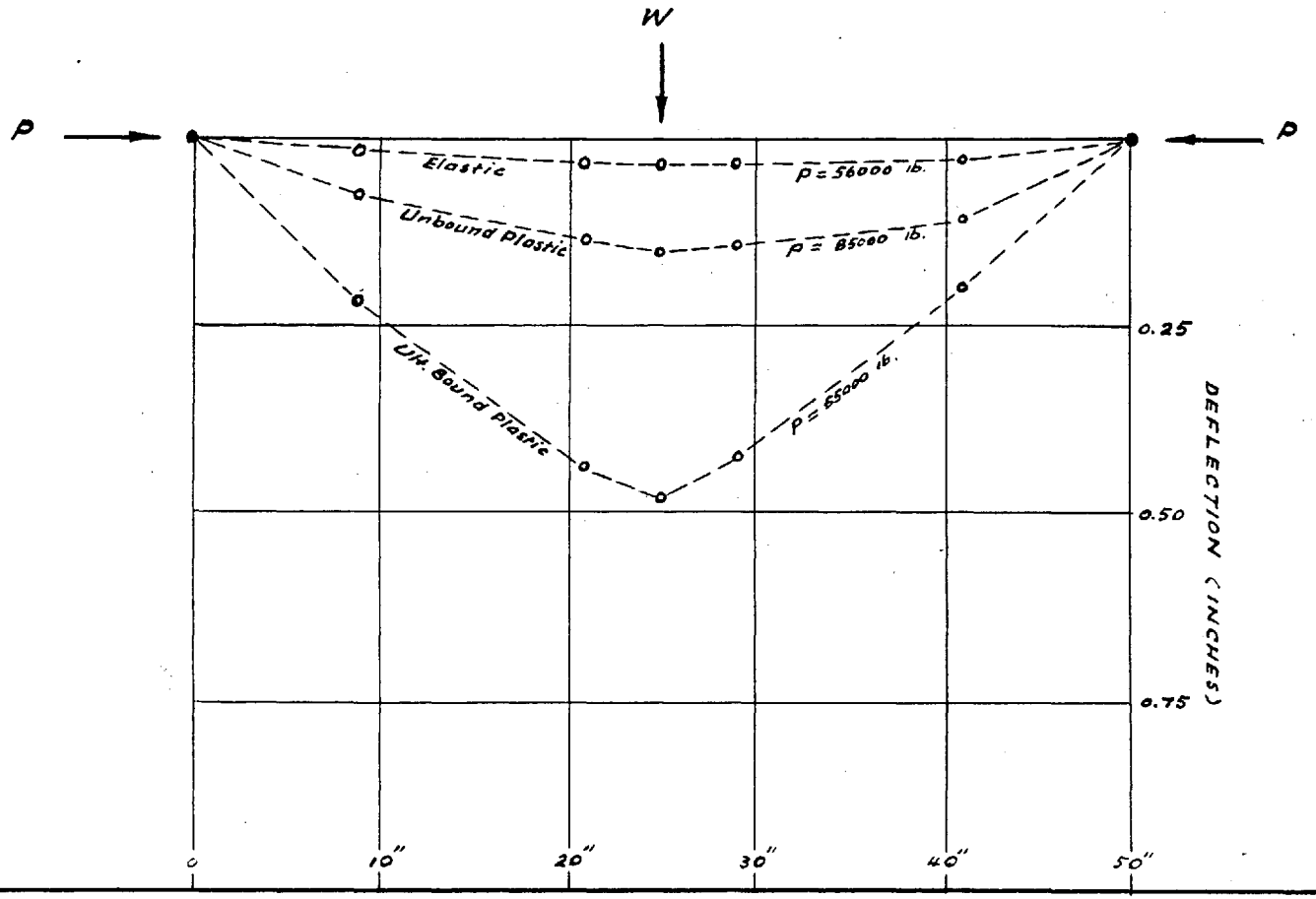


Fig. 58. STRUT S1 DEFLECTED FORM FROM SELECTED LOAD STAGES

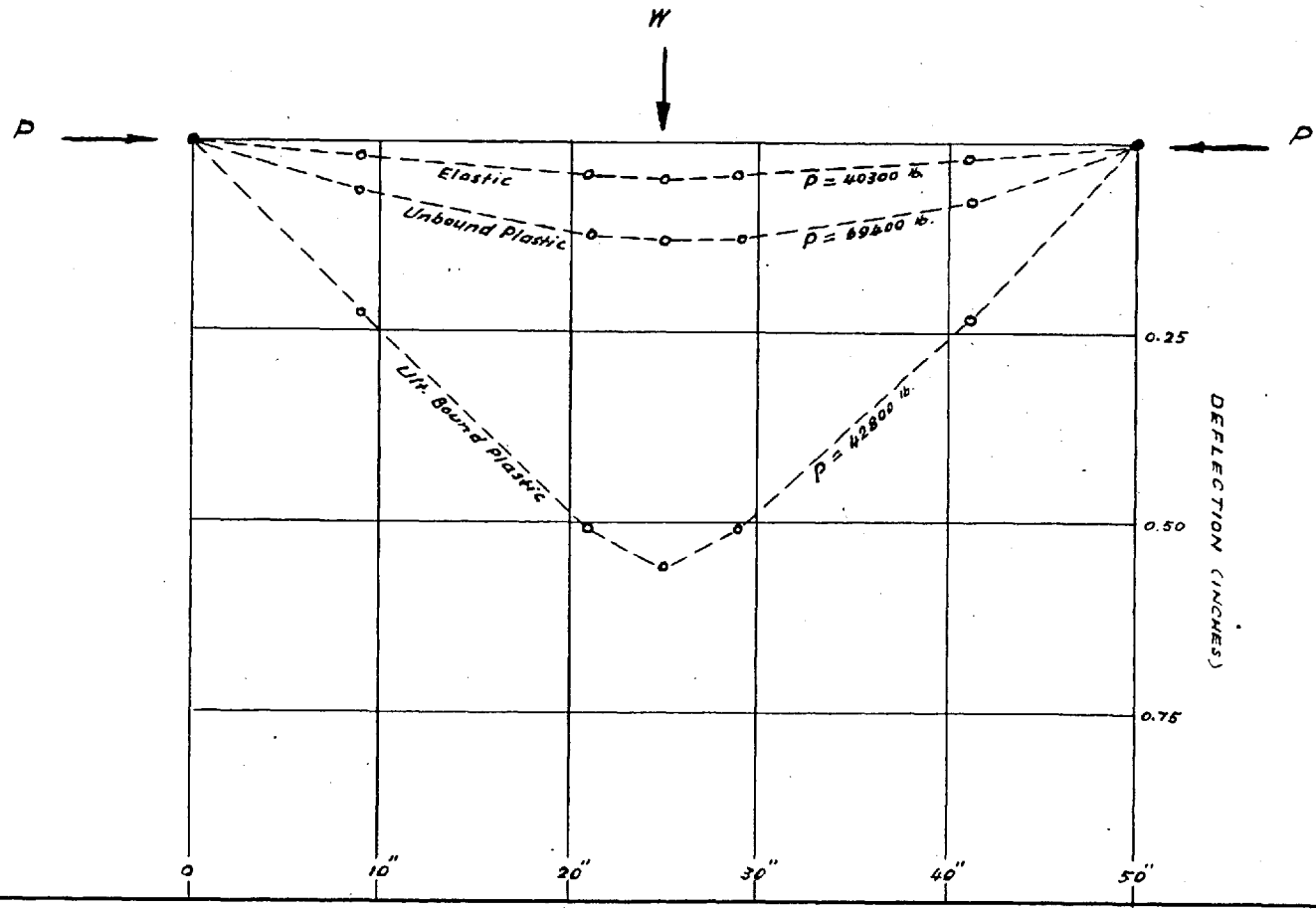


Fig. 59. STRUT S2 DEFLECTED FORM FROM SELECTED LOAD STAGES

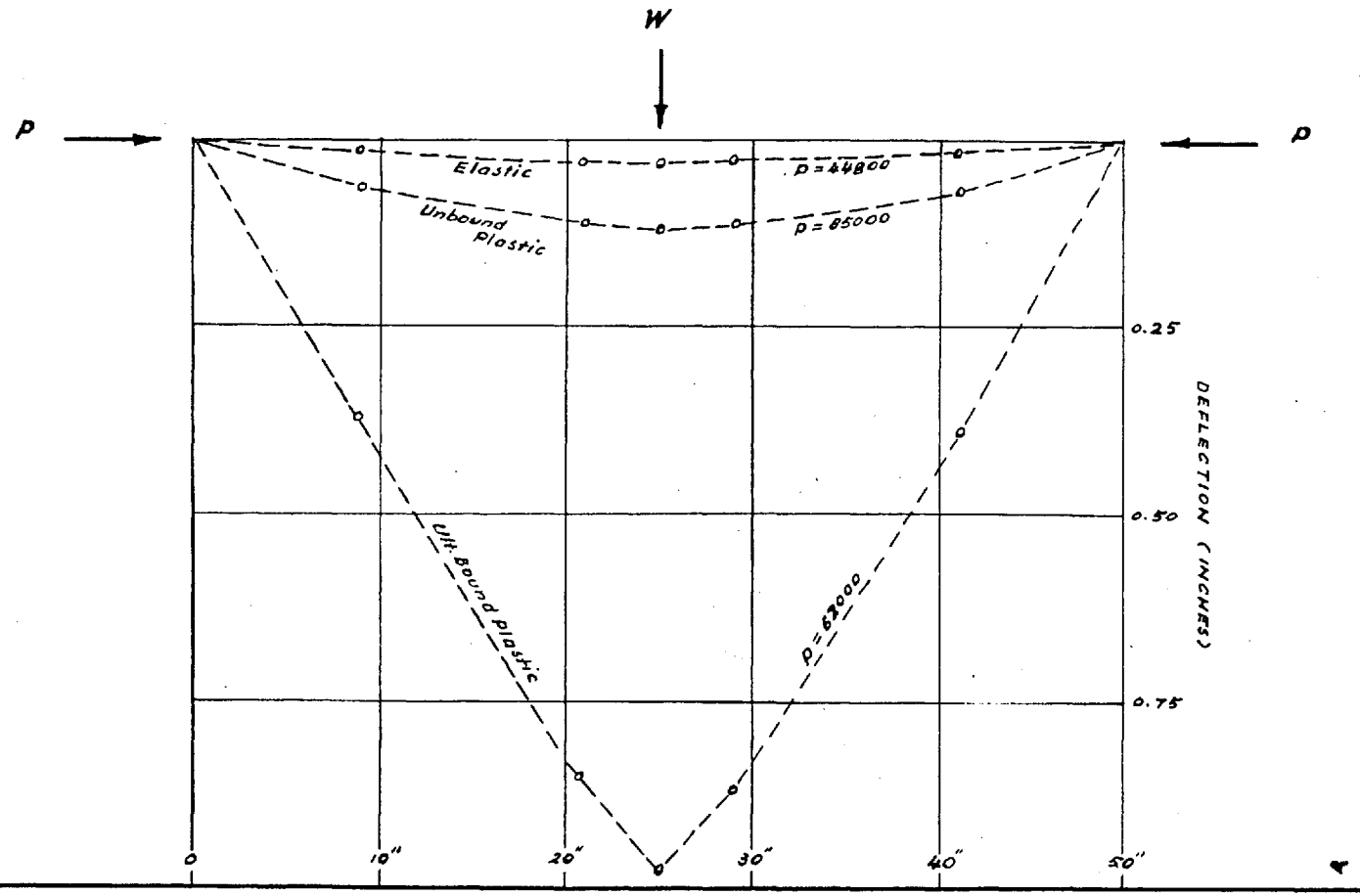


Fig. 60. STRUT S3 DEFLECTED FORM FROM SELECTED LOAD STAGES.

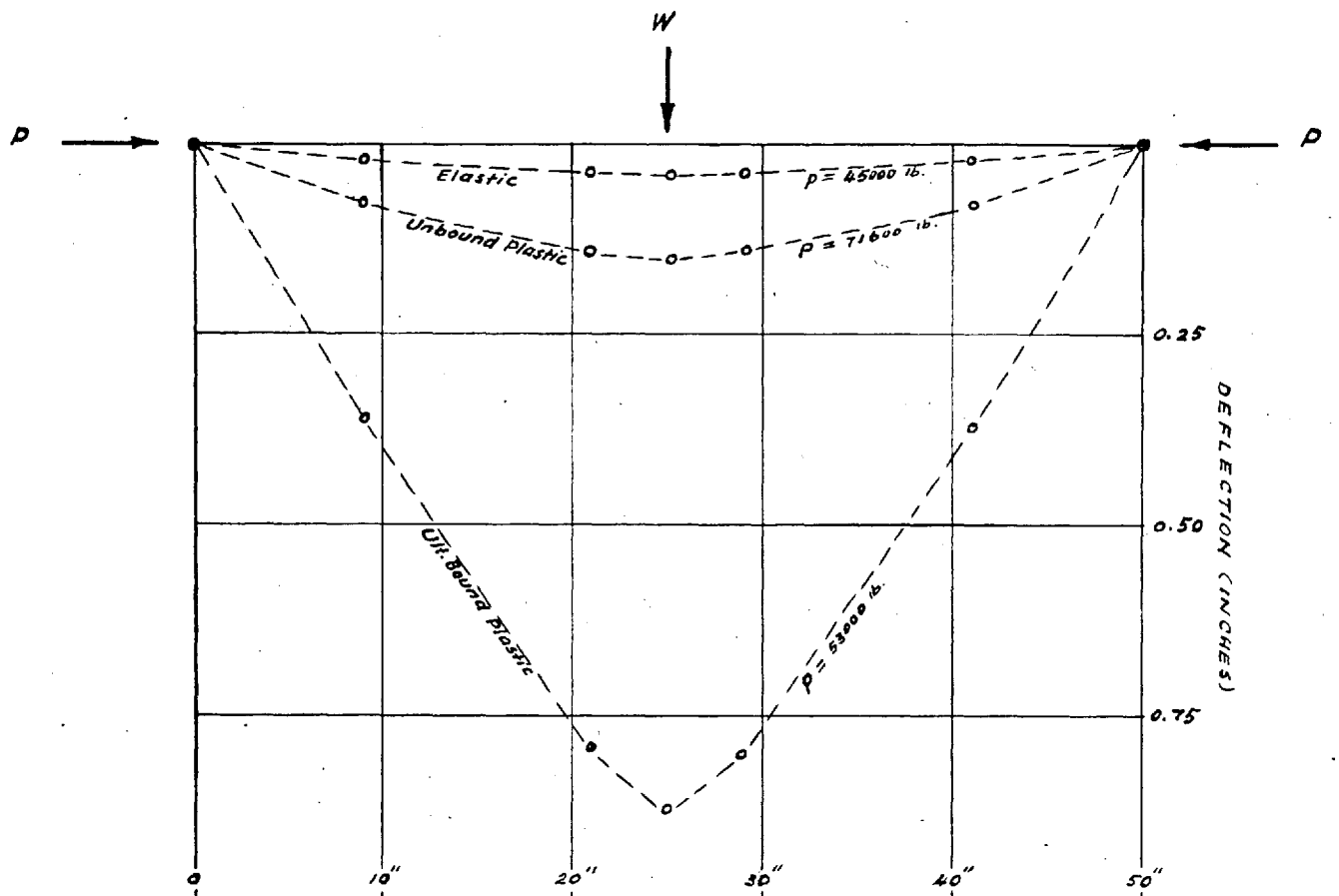


Fig. 61. STRUT S4 DEFLECTED FORM FROM SELECTED LOAD STAGES

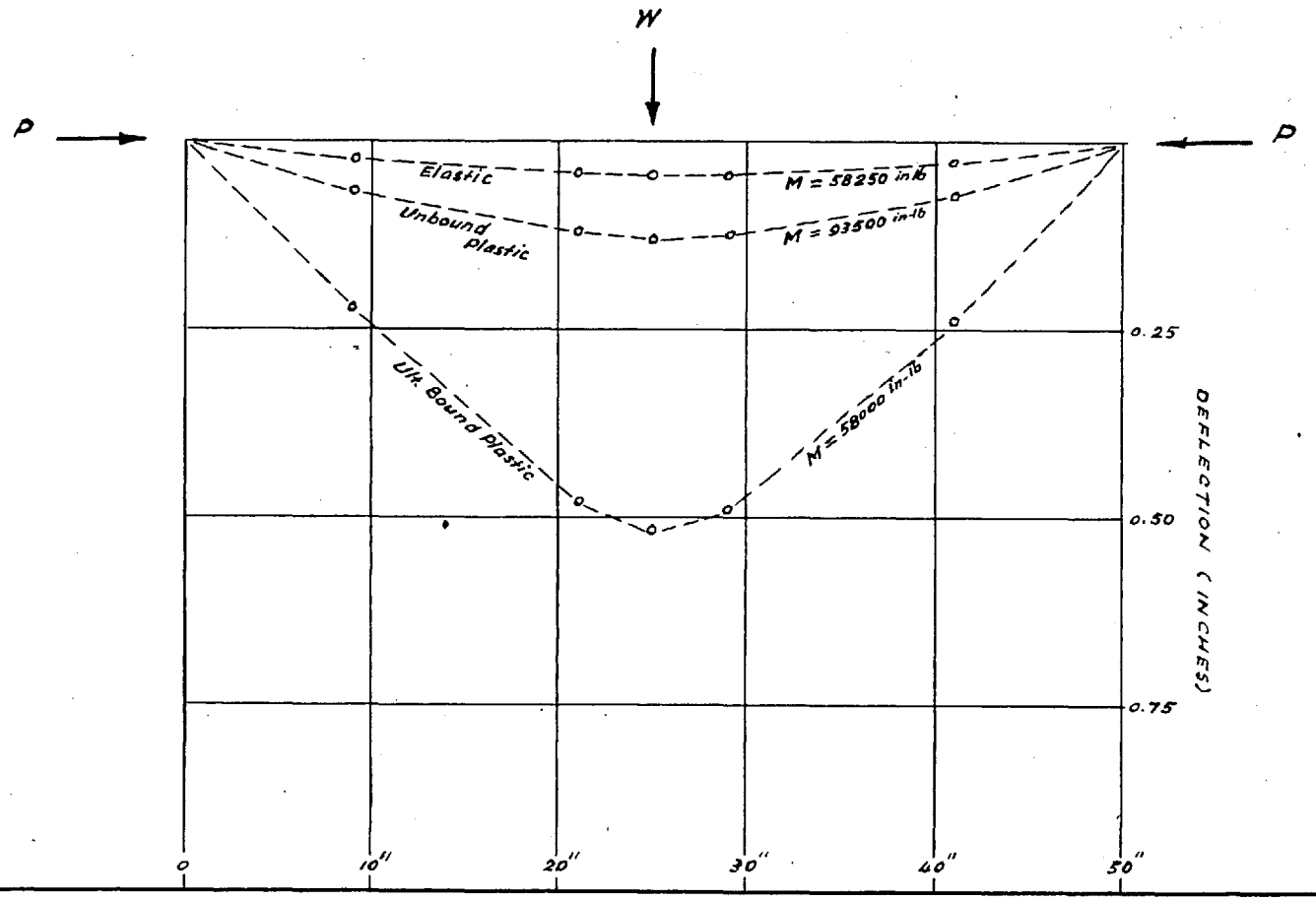


Fig. 62. STRUT S5 DEFLECTED FORM FROM SELECTED LOAD STAGES

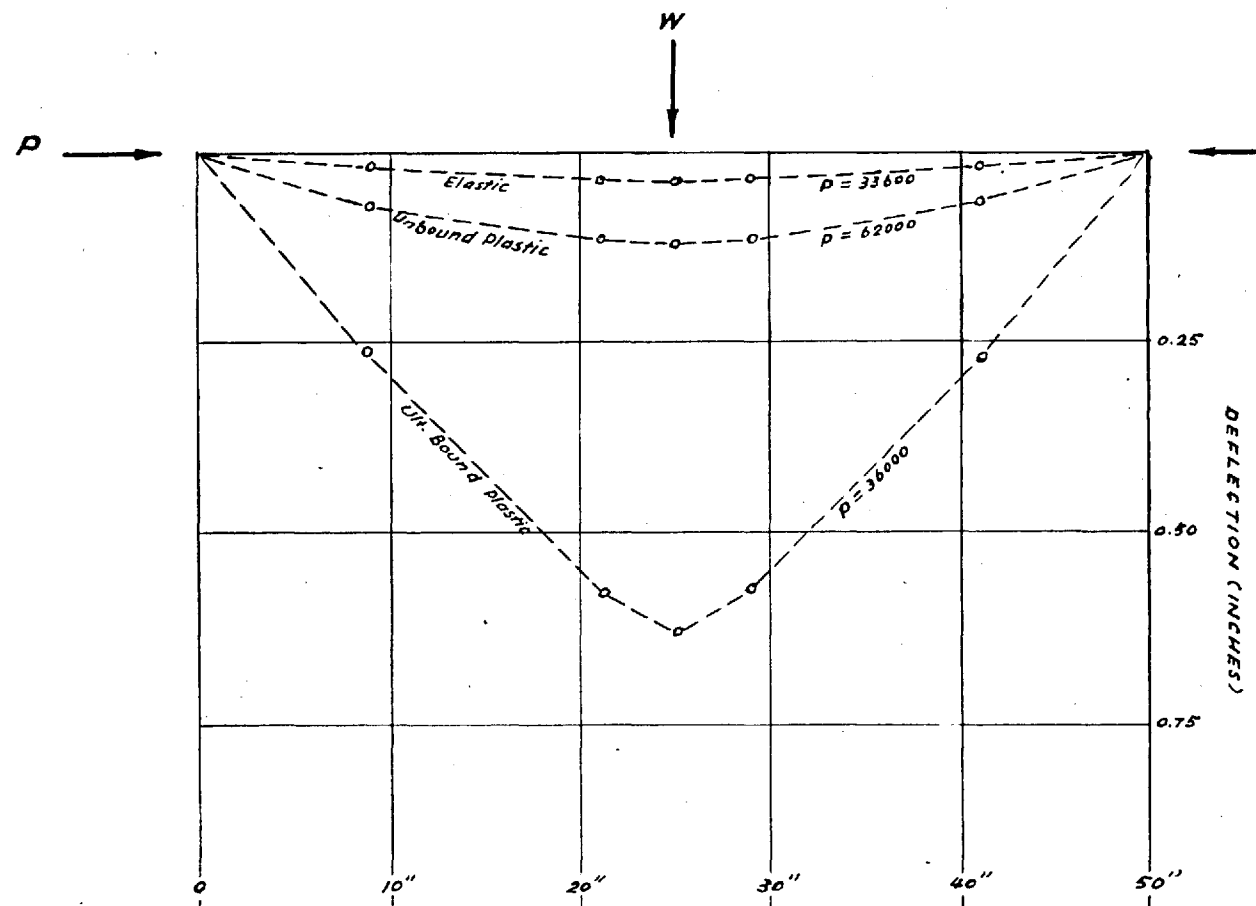


Fig. 63. STRUT S6 DEFLECTED FORM FROM SELECTED LOAD STAGES

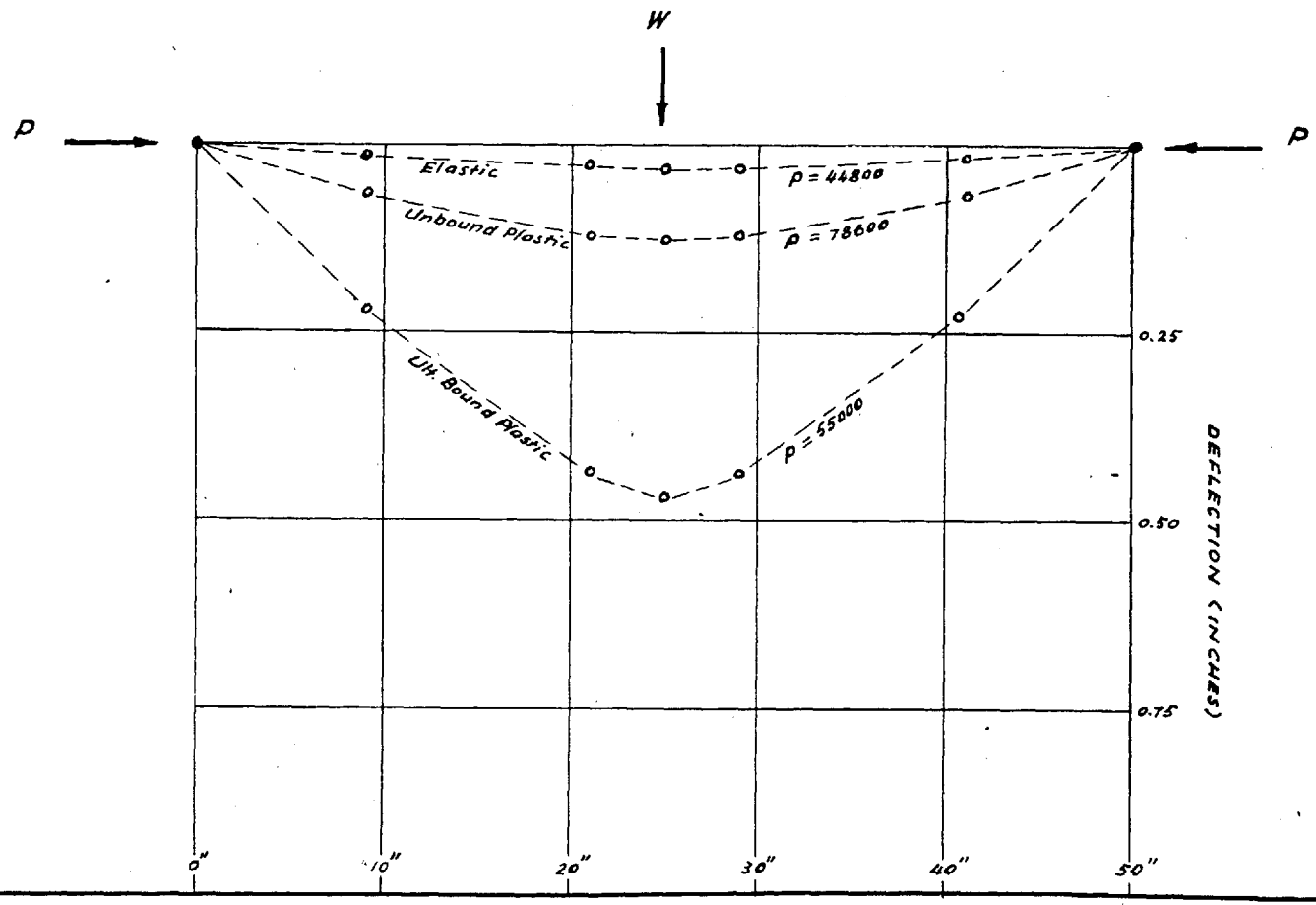


Fig. 64. STRUT S7 DEFLECTED FORM FROM SELECTED LOAD STAGES

Discussion of Experimental Results.

Presentation.

Series B & C . For each of these test specimens, the following graphs were plotted from experimental records, together with the corresponding curves calculated from the author's method of analysis:

1. The Load-Deformation relationship (P - ϵ) throughout the entire history of loading;
2. The Load-Deflection curve;
3. The curve of Load against the neutral axis factor;
4. Typical diagrams of distribution of strains across the section .

These graphs are given from Figs. 25 to 42 .

Series S . For each of these struts, similar curves to those mentioned in 1. to 4. above were also plotted for the behaviour at the centre of each strut. (Figs. 44 to 50) and in addition were plotted:

5. The distribution of concrete strains at the top edge along the length of the strut;
6. The distribution of curvature along the length;
7. The variation of the flexural rigidity EI along the length;
8. The deflected form of the strut from dial gauge readings.

These graphs (items 5 to 8) were plotted only for three significance load stages representing the elastic, unbound plastic, and bound plastic conditions.

All the graphs of this series may be found from Figs. 51 to 64 .

Comparison of Analytical and Experimental Results.

The experimental results have been plotted side by side with the theoretical curves, and excellant agreement is found in almost all the curves in the elastic and initial plastic ranges. In the plastic bound concrete range, the departure of the experimental curves from the theoretical ones is slightly more pronounced. This is understandable considering the high creep encountered in this range. The spalling load cannot always be predicted very closely during testing, since it often occurs between load-stages, with the result that no strain readings could be recorded at that load.

Thus the experimental results seem to indicate that the generalized stress-strain relationship for plain and laterally bound concrete furnishes a satisfactory basis on which the strength and deformation of plain and bound plastic hinges may be analysed.

The Ultimate Strength and Deformation of Plain and Bound Concrete.

Measurement of the ultimate loads and strains of all the test specimens having varying shapes and quantities of lateral binding, have enabled the ultimate concrete stress and strain to be related to the lateral binding ratio.

Grouping the results of the tests of series B, C and S in this way, the following relationships have plotted in Figs. 65 & 66 :

(1). The ultimate equivalent concrete stress $q_u.f_p$ (corresponding to $\alpha c'$ in Professor A.L.L. Baker's Plastic Theory) is plotted in terms of the cube strength C_u as $K_u = \frac{q_u f_p}{C_u} = \frac{\alpha c'}{C_u}$ against the lateral binder ratio p_b for circular and rectangular binders. Although no unbound specimen was tested, the point on the graph for $p_b = 0$ could be obtained by the condition of the specimens at the spalling load, since this load would have been the ultimate load of unbound concrete.

Slightly less .. External confinement reduces spalling effect!

Within the range of lateral binder ratio covered in the author's tests, namely,

$p_b = 0$ to 0.0495 for circular binders,

$= 0$ to 0.0375 for rectangular binders,

where the lateral binding ratio is defined as

$$p_b = \frac{\text{Volume of binder}}{\text{Volume of concrete}}$$

$$= \frac{\text{(Section area of binder)x(length/loop)}}{\text{(Pitch)x(net section area of bound core)}}$$

it was found that, although some irregular scatter is indicated in the experimental results plotted, the following parabolic equations appeared to express a satisfactory empirical relationship between the ultimate equivalent concrete stress and lateral binding ratio:

For circular binders, $p_b = 0.0375\ (K_u - K_o)^2$ ---(V.1)

For rectangular binders,

$$p_b = 0.1890\ (K_u - K_o)^2 \quad \text{---(V.2)}$$

as plotted in Fig.65, where K_o is the value of K when $p_b = 0$. The value of f_p is found to vary slightly for members of different size and shape when related to the standard test cube or cylinder of fixed dimensions. In the author's tests, it was found that

$f_p = 1.0\ C_u$ for the short prisms of series B,

$= 0.72\ C_u$ for the struts of series S,

$= 0.855\ C_u$ for the cylinders of series C.

This resulted in

$K_o = 0.696$ for circular binders,

$= 0.82$ for rectangular binders.

(2). The ultimate strain ϵ_u has been plotted against the lateral binding ratio for both circular and rectangular binders. The ultimate strain for unbound concrete $p_b = 0$, had the average value $\epsilon_o = 0.0035$ as observed at the spalling load.

It was again found that the experimental points could be conveniently and satisfactorily expressed by mathematical relationships. In this case, the best form of curve found by trial appeared to be the equation of a cubic parabola. Thus the best fitting curves were found to be:

For circular binders, $p_b = 4970\ (\epsilon_u - \epsilon_o)^3$ ---(V.3)

For rectangular binders, $p_b = 14600(\epsilon_u - \epsilon_o)^3$ ---(V.4)

Although the lateral binding ratios included in the tests covers the practical range that can be used, it is hoped that future experimental work will enable these curves to be extended to a yet higher range of lateral binding ratios. Also, these equations only apply to the particular type of binder steel used.

The design of bound plastic hinges is rapidly achieved with the aid of these equations.

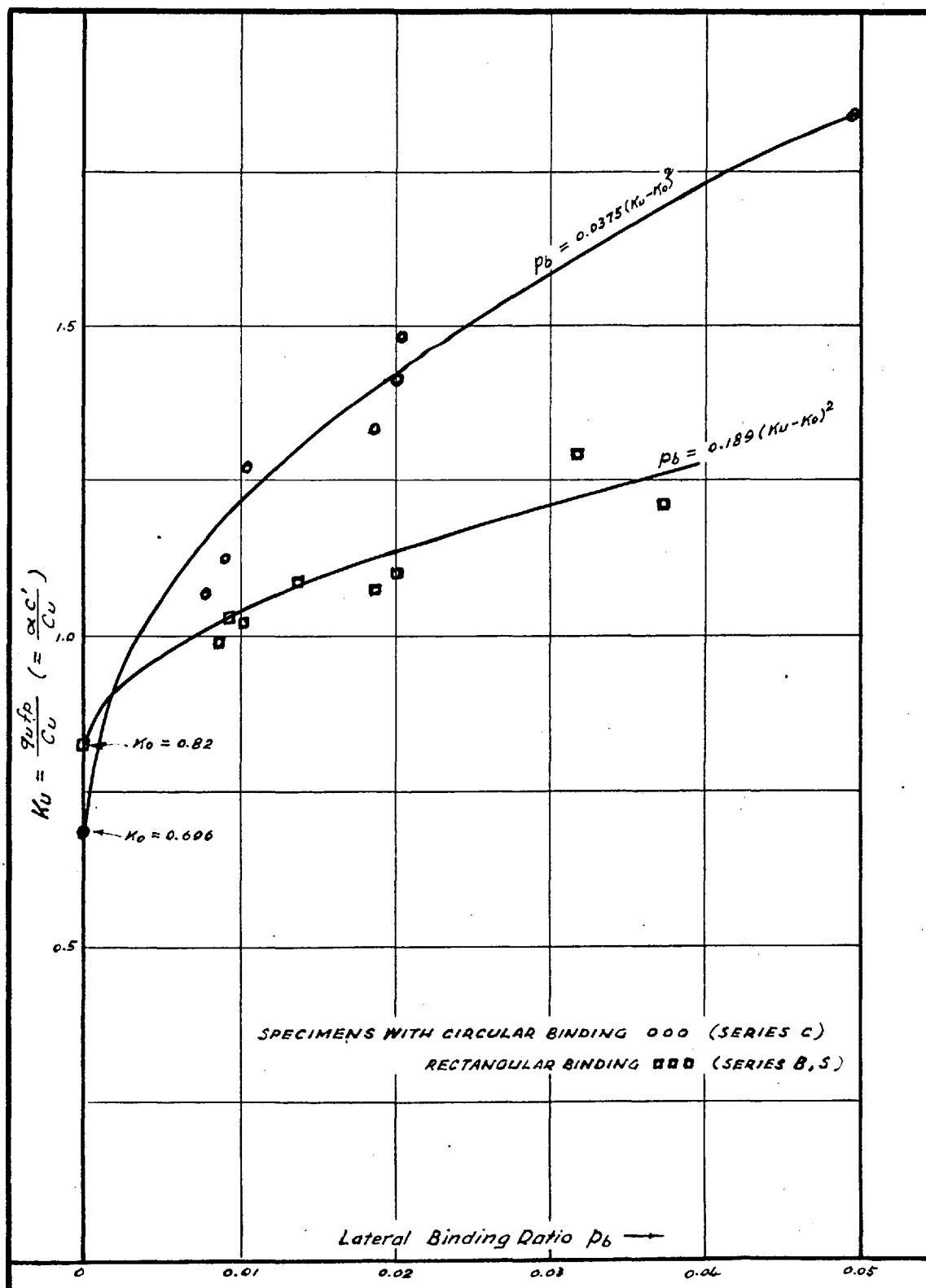


Fig. 65. RELATION BETWEEN ULTIMATE EQUIVALENT CONCRETE STRESS AND LATERAL BINDING RATIO FROM TESTS

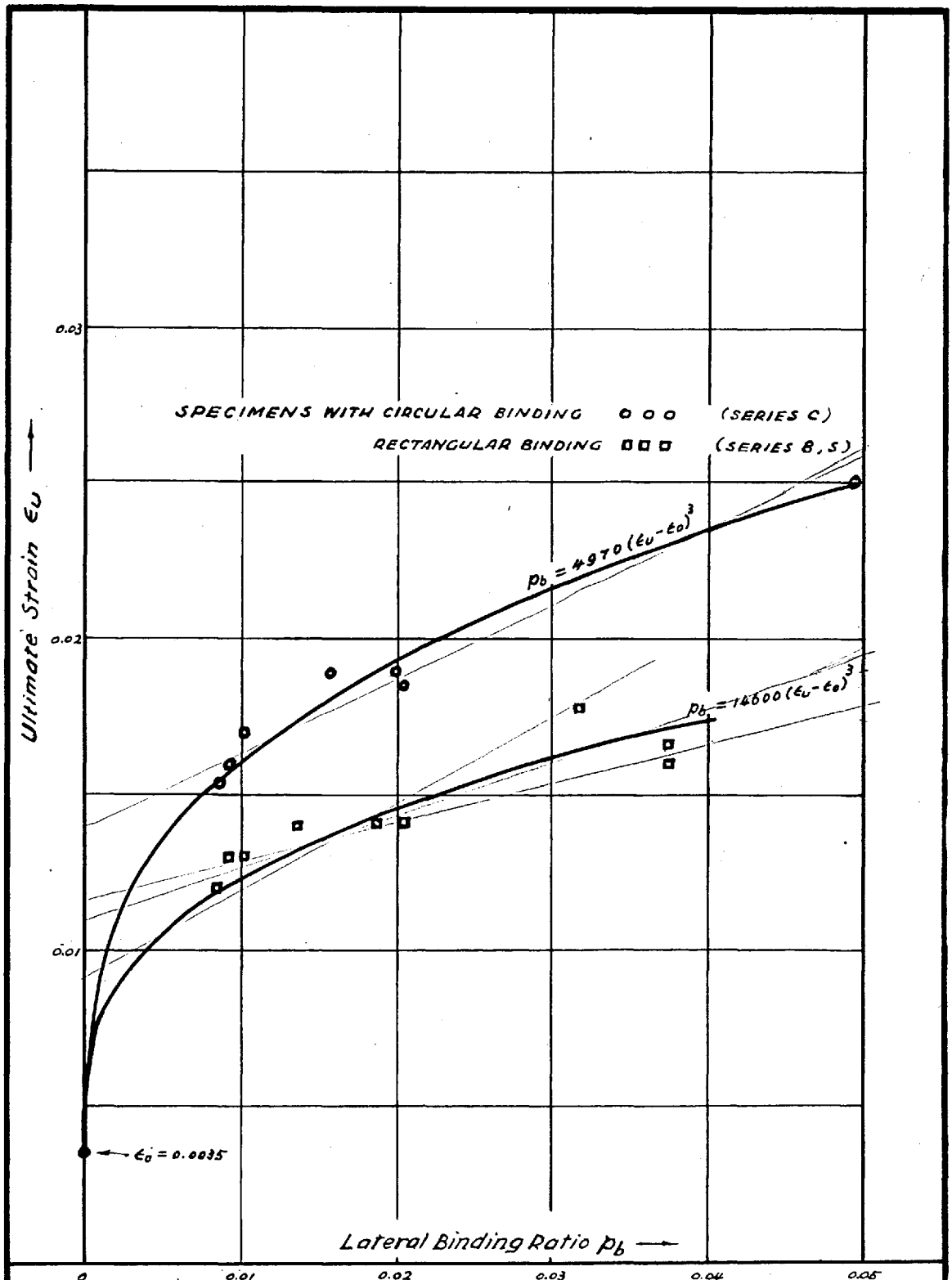


Fig. 66. RELATION BETWEEN ULTIMATE CONCRETE STRAIN AND LATERAL BINDING RATIO FROM TESTS

Distribution of Curvature and Strain along Members with Varying Bending Moment.

Sets of strain measurements across the section taken at close intervals along the lengths of the struts of series S, enabled the distribution of strain and curvature along the lengths to be studied.

Figs. 51 to 57 show graphs of maximum concrete strain ϵ, unit rotation $\epsilon/n_1 d$, and the flexural rigidity EI plotted against a symmetrical half length along the struts, at three relevant load stages, namely, elastic, unbound plastic, and ultimate bound plastic stages.

Experimental results are plotted together with the corresponding curves calculated analytically, and show that fair agreement exists between the actual and predicted behaviour.

To the author's knowledge, little information is available regarding the distribution of curvature and strain along the length of reinforced concrete members, since measurements have usually been carried out on critical sections of test members only. Some curvature-length relationships were given by El-Katib[22], calculated analytically.

Inspection of Figs. 51 to 57 shows that in the

elastic range, strain and distribution of curvature are proportional to the bending moment and no plastic rotation is developed.

In the unbound plastic stage, plasticity spreads over a considerable length of the member, being longer for a higher axial load, and the strain and curvature are no longer proportional to the bending moment, but increases at a higher rate along the plastic zone, thus giving a plastic rotation in excess of the rotation developed within the same zone if the member had remained elastic.

When spalling took place, the drop in load was accompanied by a contraction of the length of the plastic zone, and the length of spalling was observed to extend to a length of approximately 1/5 of the bending moment intercept. This resulted in a concentration of most of the plastic rotation within the length of spalling.

By graphical integration of the curvature distribution diagrams in the two plastic stages, experimental values of the curvature distribution factor β in the equation

$$\theta = \beta\, h's\, M_u \left[\frac{1}{EI_u} - \frac{1}{EI_e}\right] \text{----------(IV.5)}$$

as given in Part IV for the practical design of plastic hinges, were determined, the average values being,

β = 0.305 for unbound plastic range,

= 0.21 for bound plastic range,

for the case of linear bending moment distribution.

The Ultimate Strength and Rotation of Bound Plastic Hinges.

From the relationship between lateral binding and concrete ultimate stress and strain as determined from tests and given in Figs. 65 & 66, and from the β values obtained from the strut tests, curves have been plotted for the ultimate strength and rotation of bound plastic hinges, and are given in Figs. 67 to 74 , for both circular and rectangular binders.

In most cases, under-reinforced beams will develop sufficient hinge rotations without the aid of lateral binding. For over-reinforced beams, rotations may be insufficient and lateral binding may have to be used to provide higher rotations. However, a very high ratio of lateral binding is required to effect a small increase in rotation. This indicates that where circumstances permit, under-reinforcing in beams would be a more economical method of providing for large plastic hinge rotations.

For hinges subjected to combined bending and axial loads, Figs. 71 to 74 show that the use of lateral

binding greatly increases the available rotation, and often provides the only solution in cases where the required rotations and axial loads are both high. The interaction curves of Figs. 72 and 74 show that the most economic design for ultimate bending strengths occur at between $P/P_u = 0.25$ to 0.50, within which a near-balance failure occurs. This is in agreement with interaction curves given by Hognestad [16], who also showed that this was roughly true for other percentages of reinforcement. Lower P/P_u may be used to advantage, and high rotation values characteristic of under reinforced sections are obtained. For P/P_u values higher than say 0.60, both the ultimate strength and bending available rotations are decreased rapidly. This shows that for plastic hinges in columns, the most economical designs are achieved when P/P_u does not exceed 0.60.

Figs. 67 to 70 also show that spiral binding enables higher strengths and rotations to be developed in bound concrete hinges as compared to rectangular binders. However, rectangular binders occur more frequently in practice.

Fig. 75 gives elastic EI values for different tension steel ratios, in which the tensile strength in

concrete is neglected, i.e., assuming a cracked section. In actual fact, it is not strictly true to assume a cracked section in the elastic stage, since in this stage the ultimate tensile strain of concrete has probably not been exceeded, so that the uncracked tension zone contributes some tensile strength to the section. This causes the true elastic EI value to be higher than the assumed cracked-section value, especially in under-reinforced sections, where the tension zone is large. However, the assumption of cracked sections is simpler to apply, and errs on the safe side, since required rotations so calculated would then be higher than the exact value.

Fig. 76 gives elastic EI values plotted against the axial load ratio, and the comments regarding cracked sections also apply in this case. When the axial load is such that $n_1 \geqslant 1$, then the whole section is in compression, and no error due to the assumption of cracked sections arises.

Knowledge of elastic EI values enables the stiffnesses of framework members to be determined and applied to the trial and adjustment method of the Plastic Hinge Theory, and also enables the net plastic hinge rotations to be calculated.

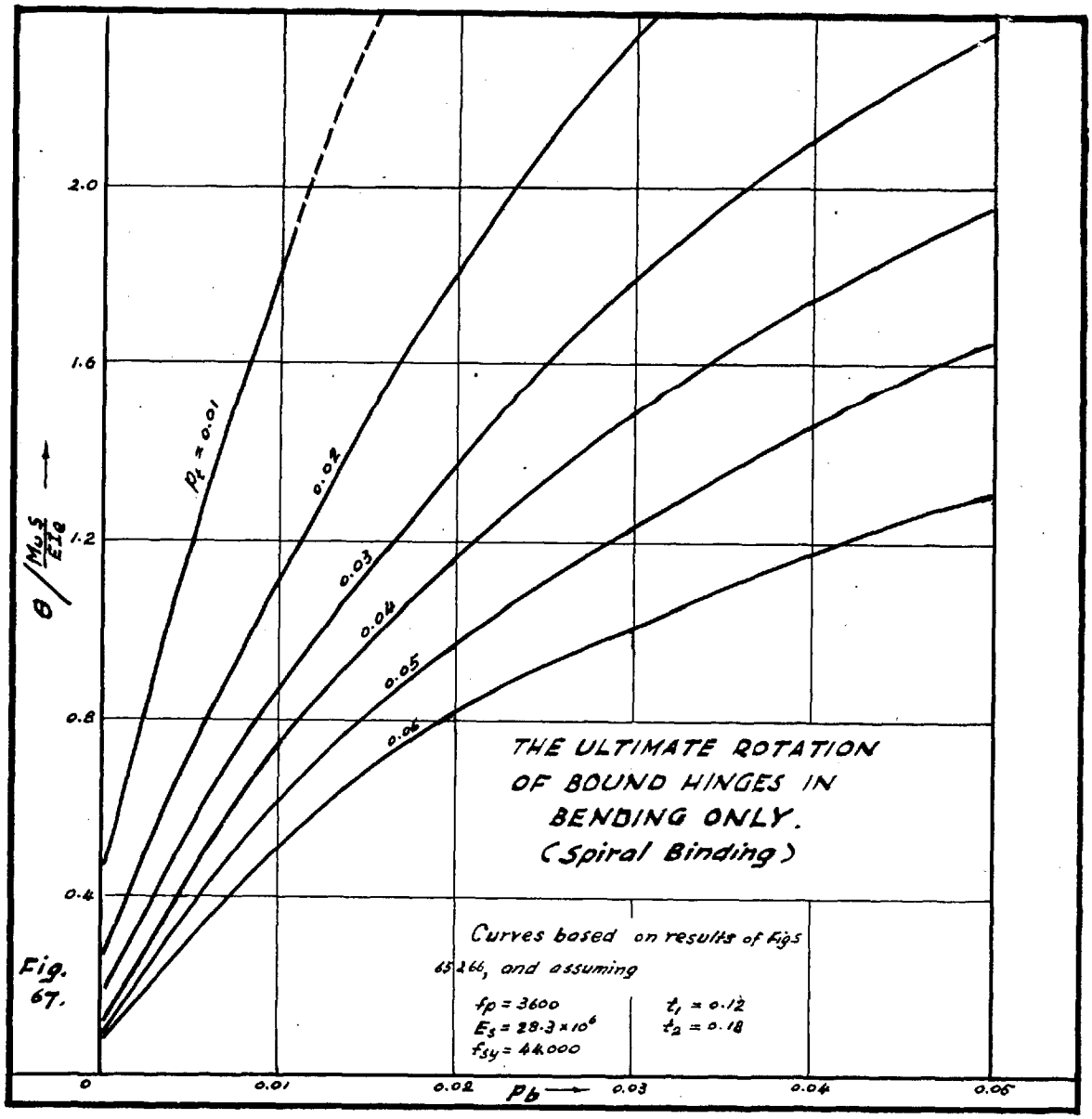

2.0
1.6
1.2
0.8
0.4
$\theta / \frac{M_u s}{E I_e}$ →
$p_t = 0.01$
0.02
0.03
0.04
0.05
0.06
THE ULTIMATE ROTATION OF BOUND HINGES IN BENDING ONLY. (Spiral Binding)
Curves based on results of Figs 65 & 66, and assuming
$f_p = 3600$
$E_s = 28.3 \times 10^6$
$f_{sy} = 44{,}000$
$t_1 = 0.12$
$t_2 = 0.18$
0
0.01
0.02
p_b →
0.03
0.04
0.05

Fig. 67.

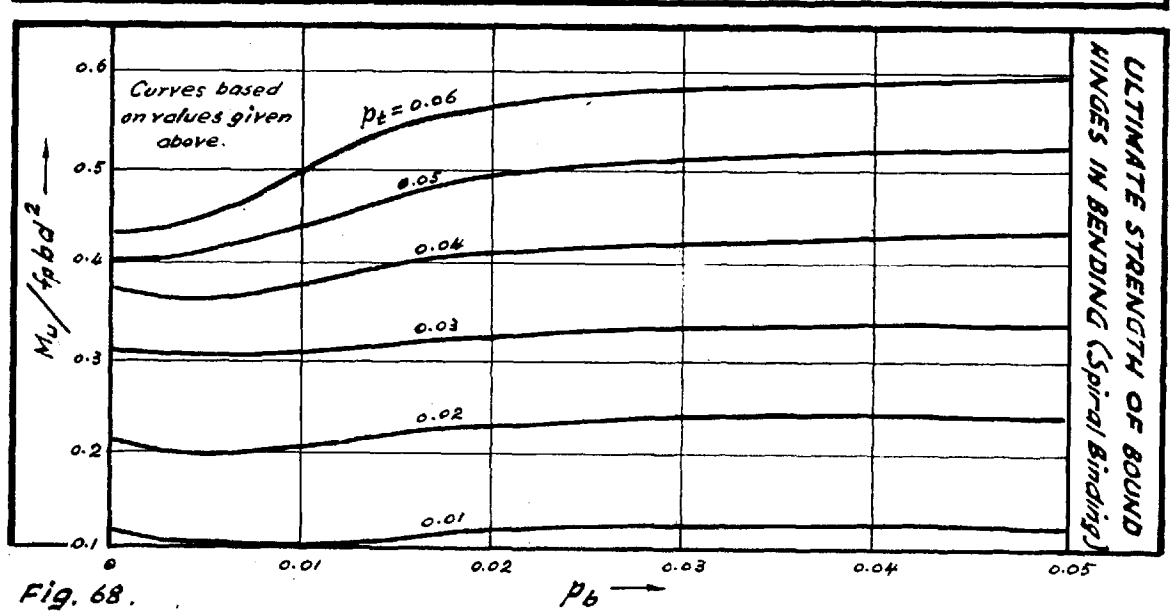

0.6
0.5
0.4
0.3
0.2
0.1
$M_u / f_p b d^2$ →
Curves based on values given above.
$p_t = 0.06$
0.05
0.04
0.03
0.02
0.01
0
0.01
0.02
0.03
0.04
0.05
p_b →
ULTIMATE STRENGTH OF BOUND HINGES IN BENDING (Spiral Binding)

Fig. 68.

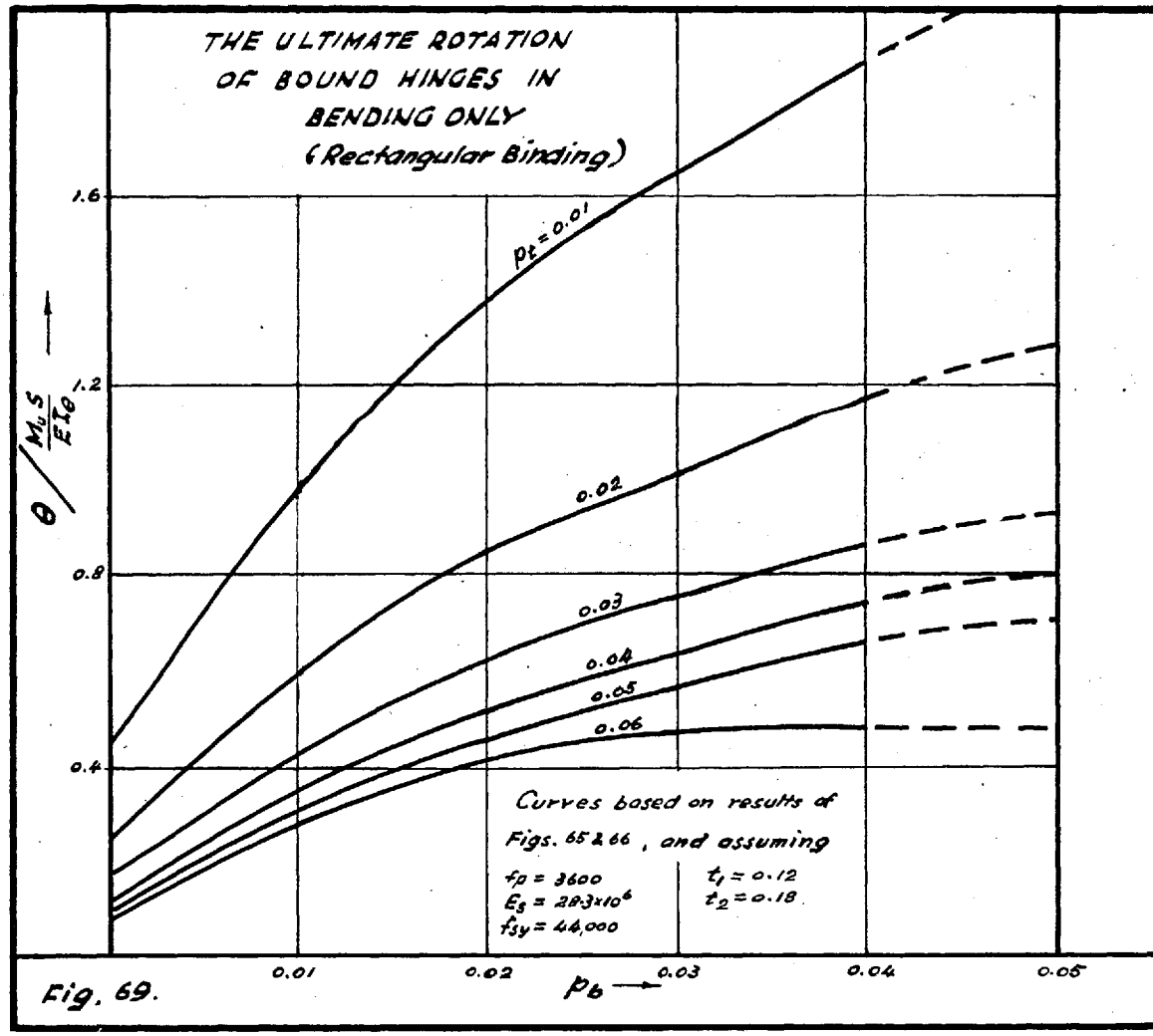

THE ULTIMATE ROTATION
OF BOUND HINGES IN
BENDING ONLY
(Rectangular Binding)
θ / M₀S / EI₀
1.6
1.2
0.8
0.4
pt = 0.01
0.02
0.03
0.04
0.05
0.06
Curves based on results of
Figs. 65 & 66, and assuming
fp = 3600
Es = 29.3x10⁶
fsy = 44,000
t1 = 0.12
t2 = 0.18
0.01
0.02
0.03
0.04
0.05
pb

Fig. 69.

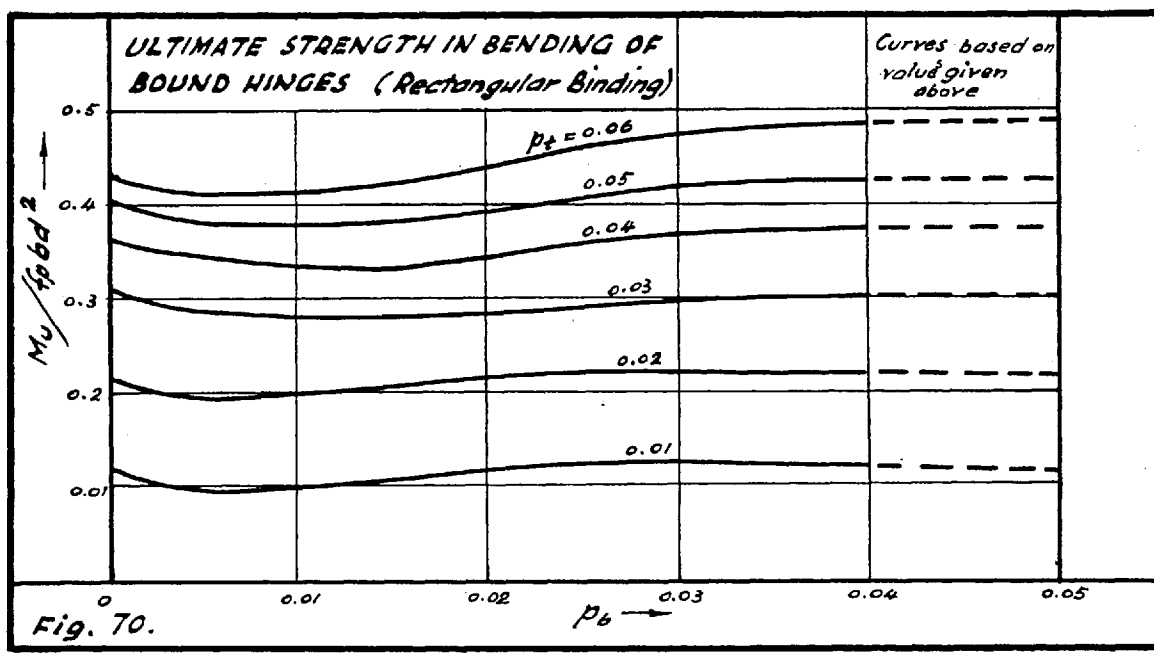

ULTIMATE STRENGTH IN BENDING OF
BOUND HINGES (Rectangular Binding)
Curves based on
values given
above
Mu / fp bd²
0.5
0.4
0.3
0.2
0.01
pt = 0.06
0.05
0.04
0.03
0.02
0.01
0
0.01
0.02
0.03
0.04
0.05
pb

Fig. 70.

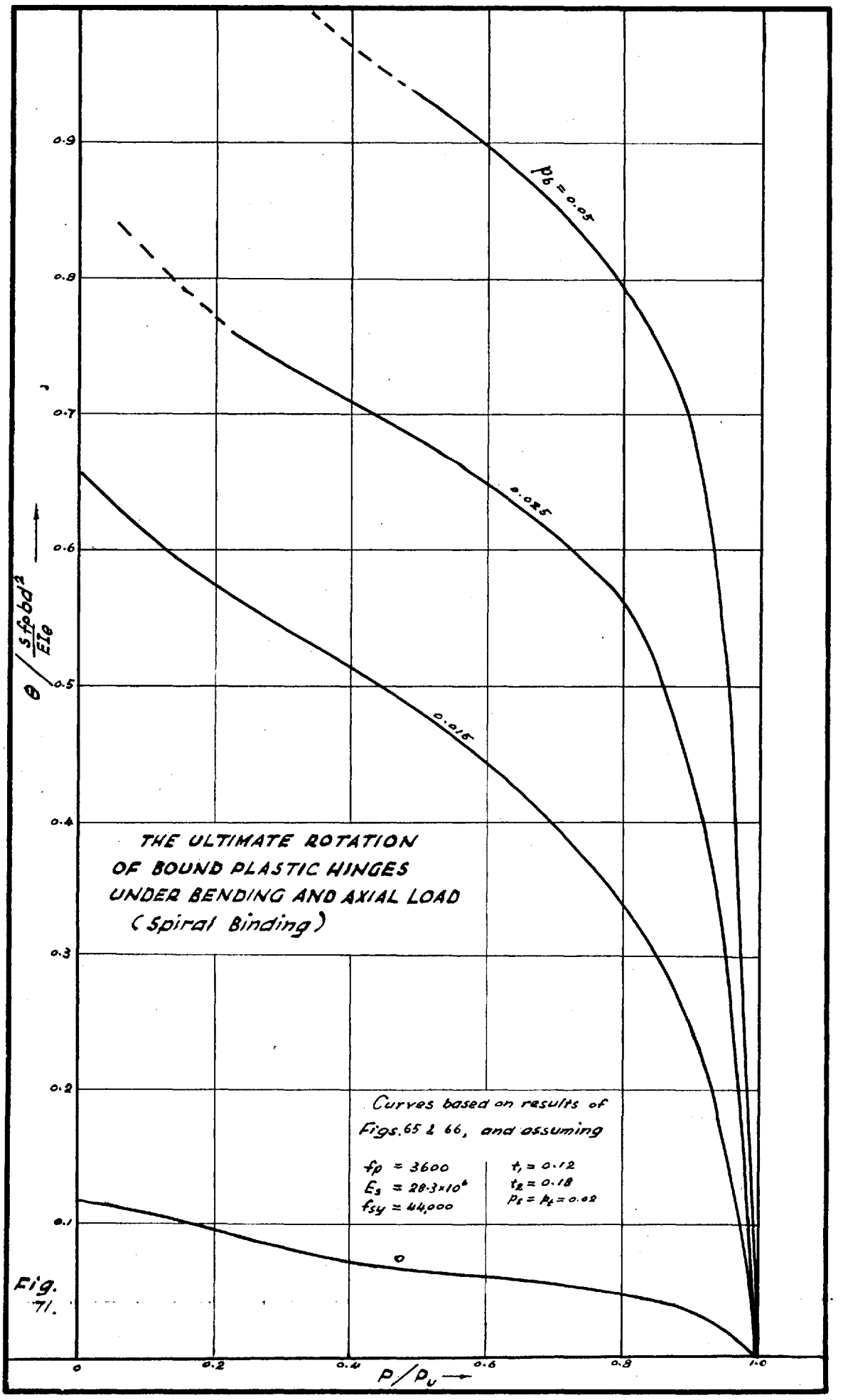

$p_b = 0.05$
0.025
0.015
0
$\theta / \frac{s f_p b d^2}{E I \theta}$
0.9
0.8
0.7
0.6
0.5
0.4
0.3
0.2
0.1
THE ULTIMATE ROTATION
OF BOUND PLASTIC HINGES
UNDER BENDING AND AXIAL LOAD
(Spiral Binding)
Curves based on results of
Figs. 65 & 66, and assuming
$f_p = 3600$
$E_s = 28.3 \times 10^6$
$f_{sy} = 44{,}000$
$t_1 = 0.12$
$t_2 = 0.18$
$p_t = p_t' = 0.02$
0
0.2
0.4
0.6
0.8
1.0
P / P_u

Fig. 71.

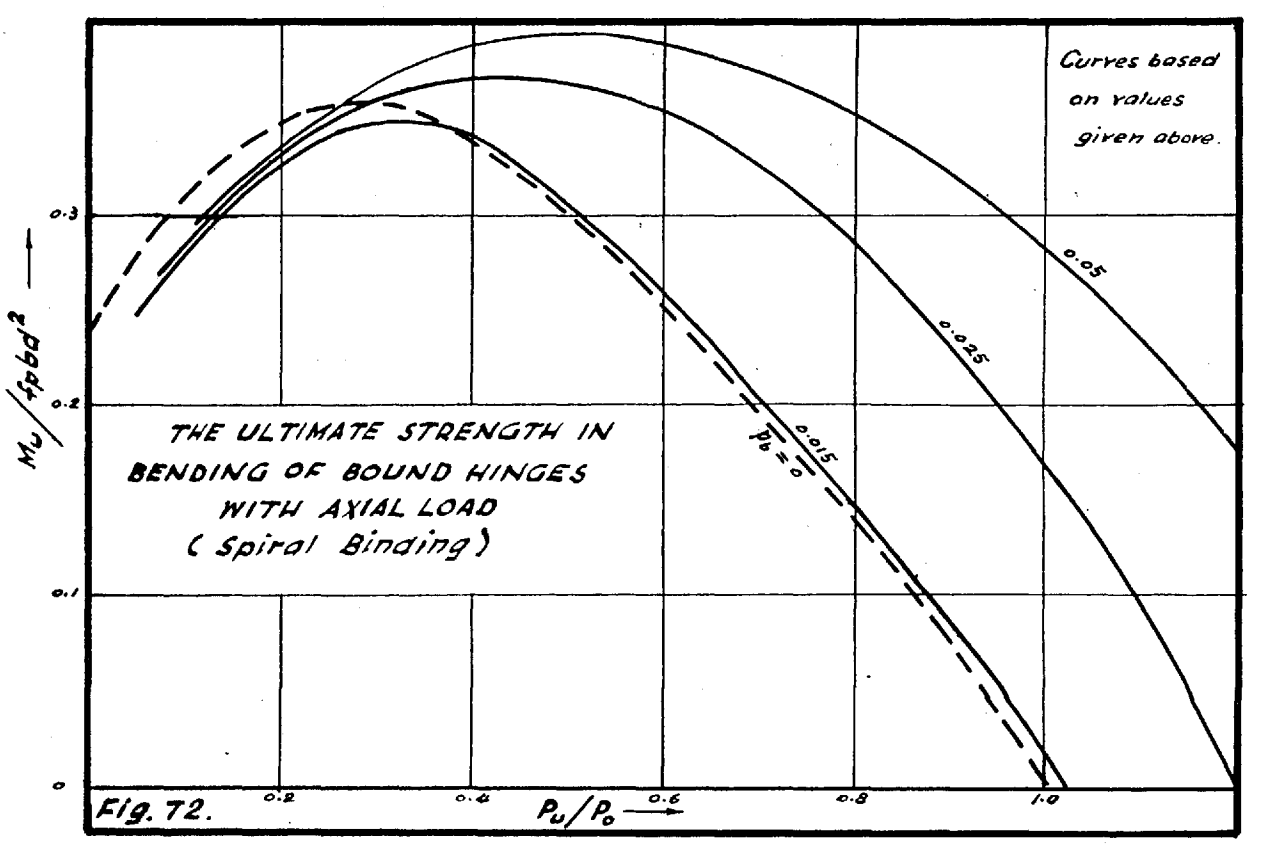

Curves based
on values
given above.
0.05
0.025
0.015
$p_b = 0$
$M_u / f_p b d^2$
0.3
0.2
0.1
0
THE ULTIMATE STRENGTH IN
BENDING OF BOUND HINGES
WITH AXIAL LOAD
(Spiral Binding)
0.2
0.4
0.6
0.8
1.0
P_u / P_o

Fig. 72.

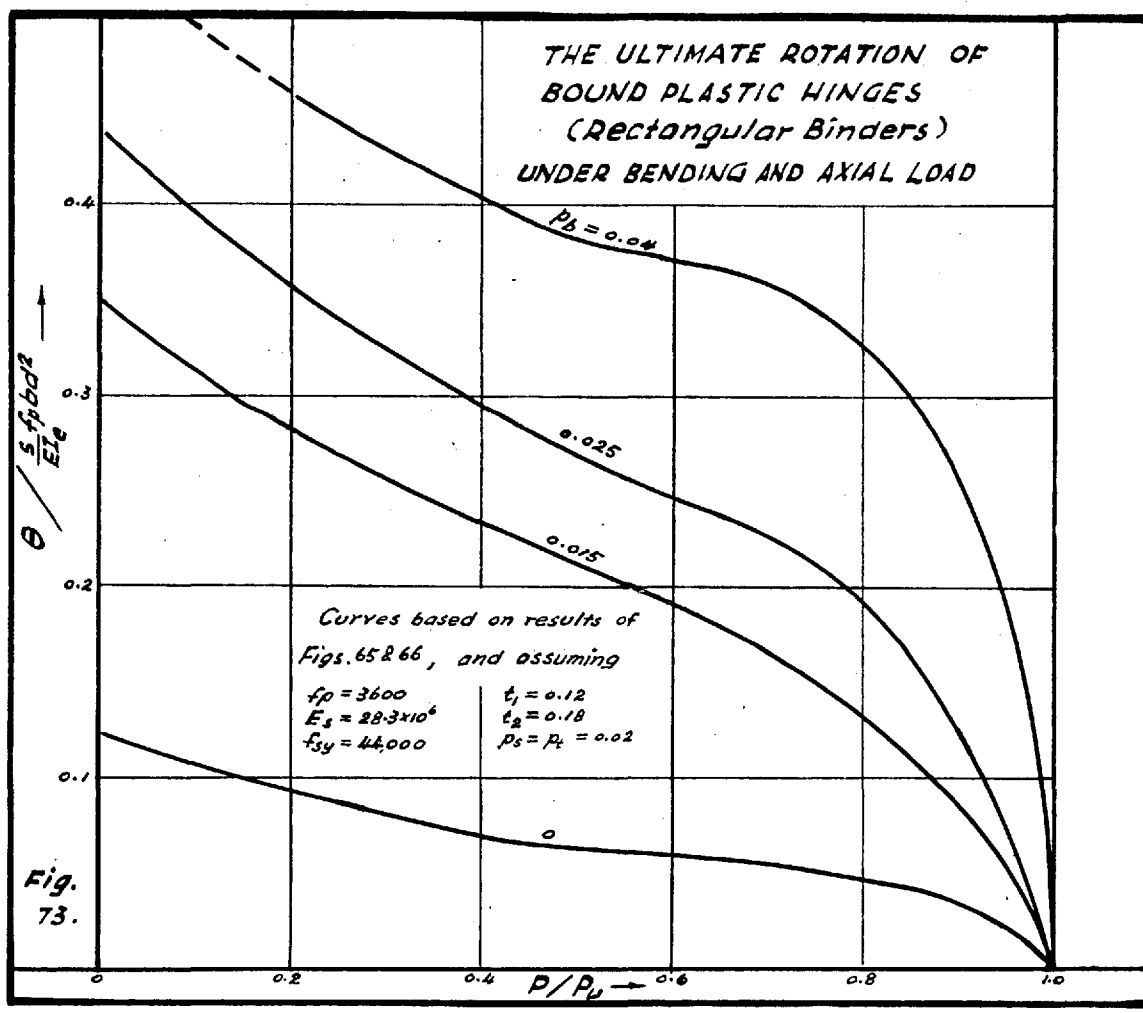
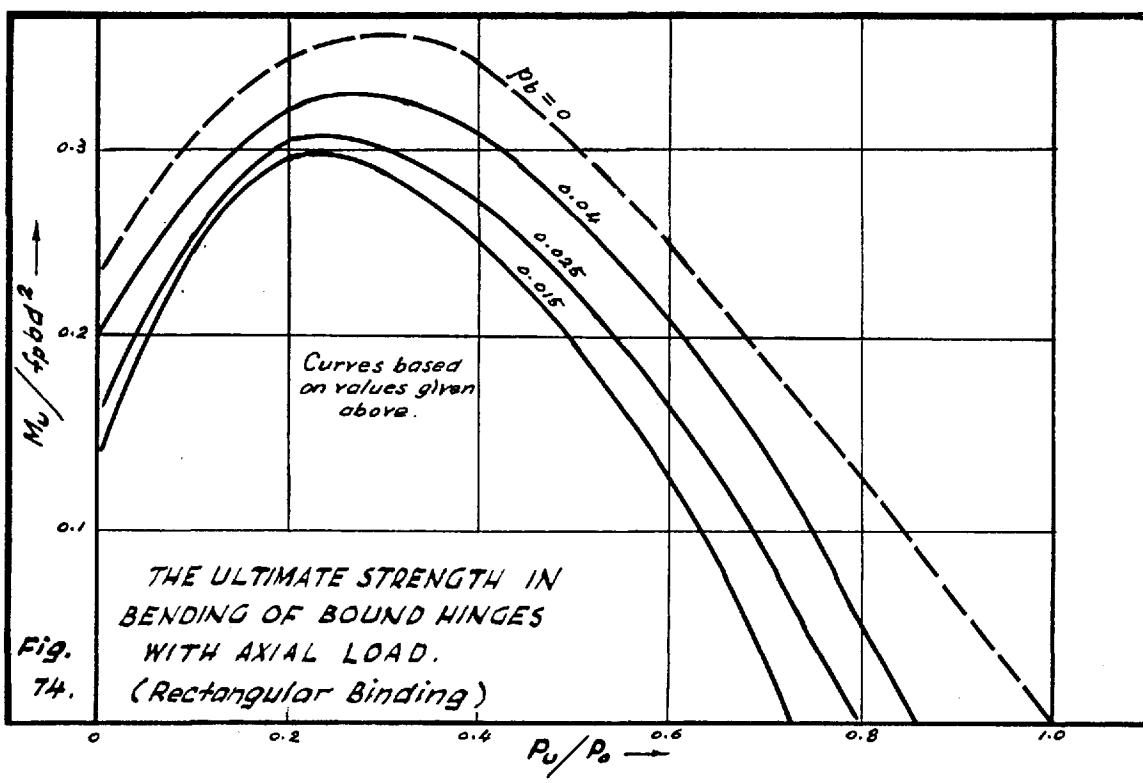


Fig. 73.



THE ULTIMATE STRENGTH IN BENDING OF BOUND HINGES WITH AXIAL LOAD. (Rectangular Binding)

Fig. 74.

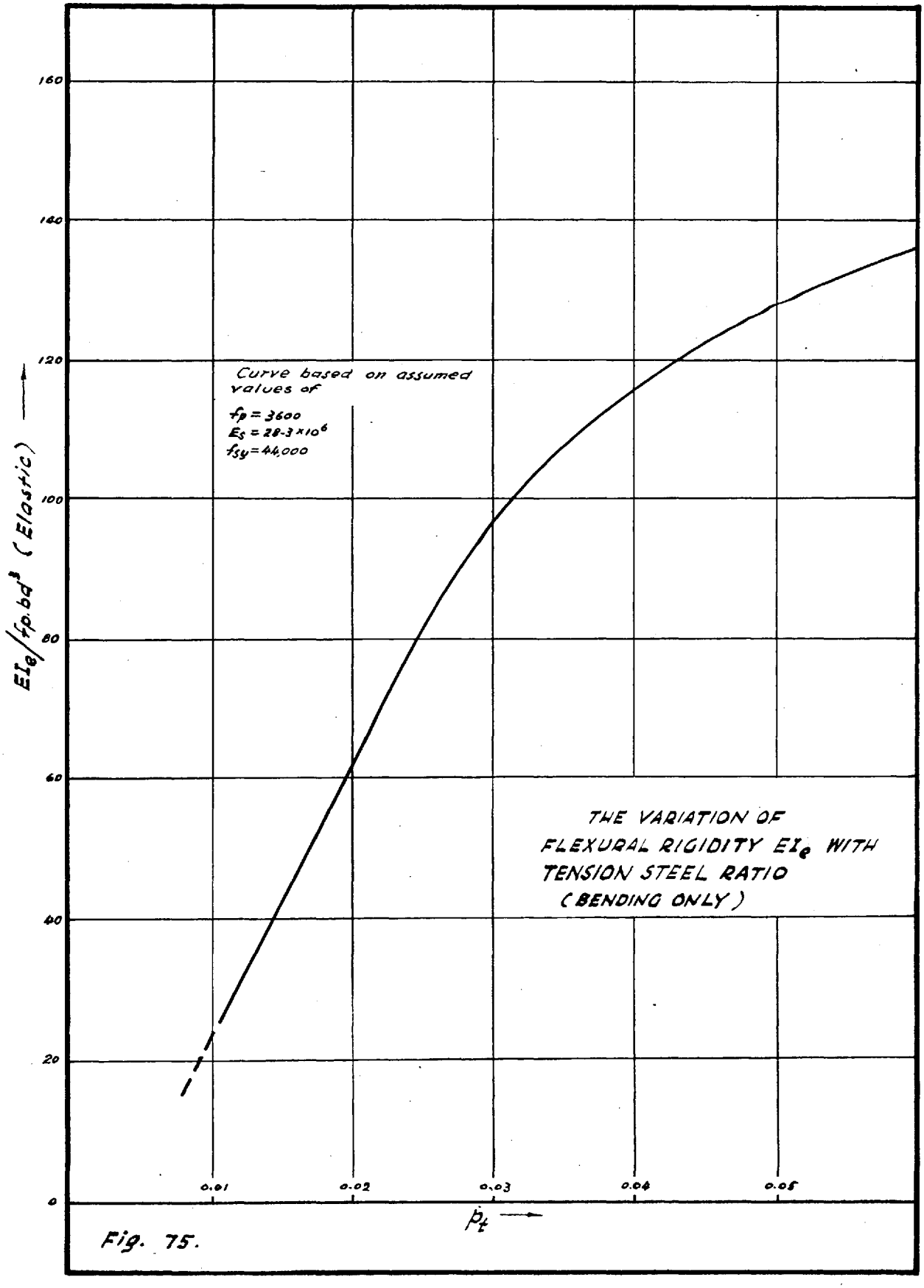

160
140
120
100
80
60
40
20
0
$E I_e / f_p . b d^3$ (Elastic) ⟶
Curve based on assumed values of
$f_p = 3600$
$E_s = 28{\cdot}3 \times 10^6$
$f_{sy} = 44{,}000$
THE VARIATION OF FLEXURAL RIGIDITY EI_e WITH TENSION STEEL RATIO (BENDING ONLY)
0.01
0.02
0.03
0.04
0.05
p_t ⟶

Fig. 75.

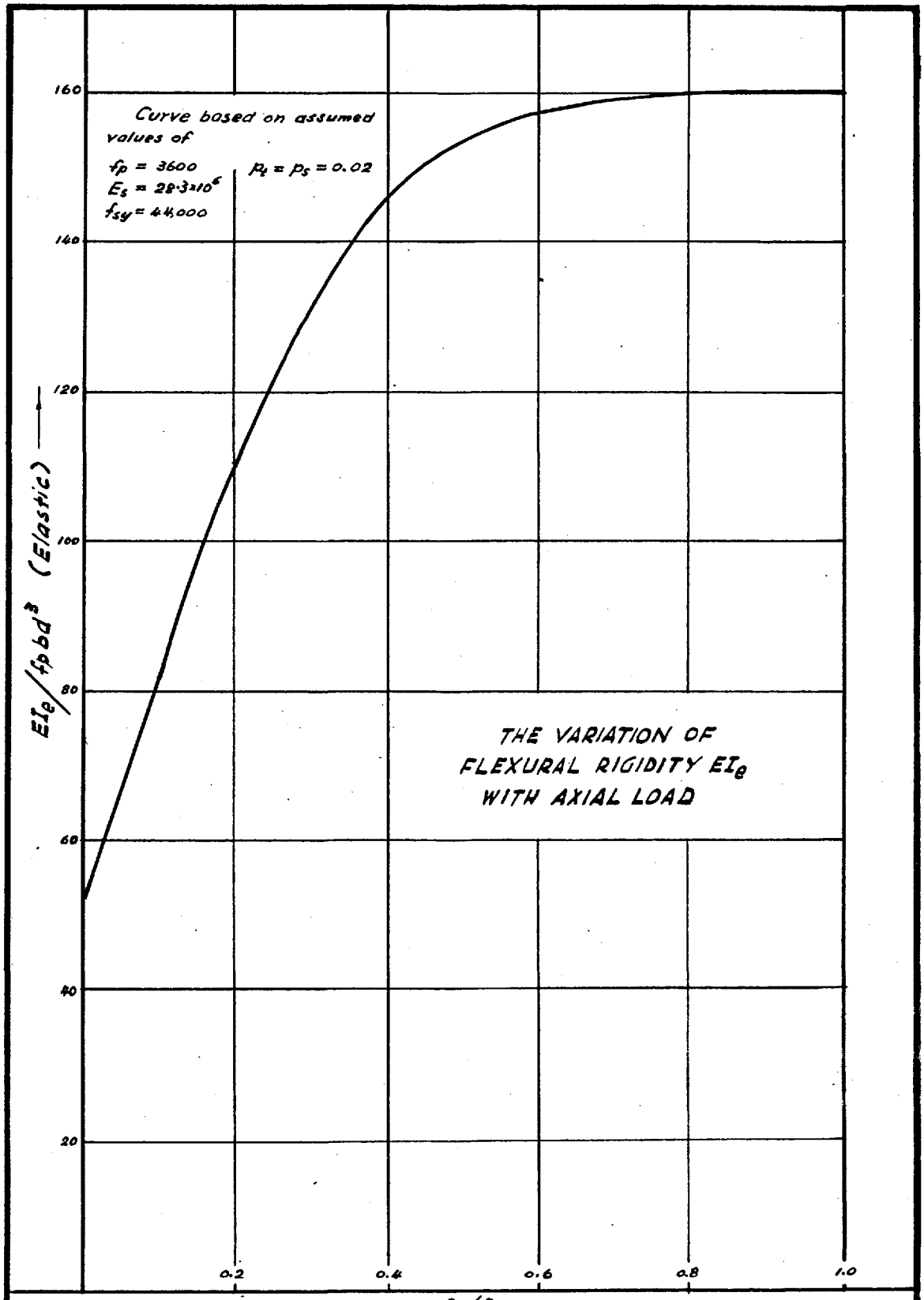
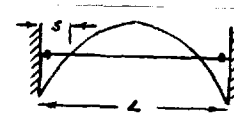
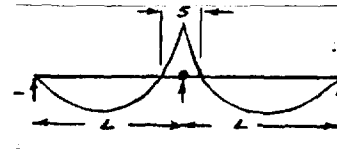
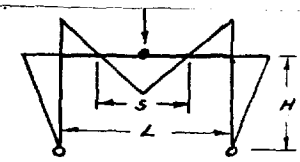
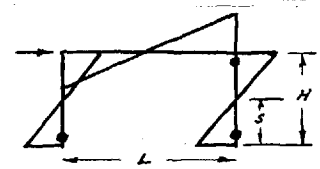

Curve based on assumed values of
$f_p = 3600$
$E_s = 28{\cdot}3 \times 10^6$
$f_{sy} = 44{,}000$
$p_t = p_s = 0.02$
THE VARIATION OF FLEXURAL RIGIDITY EI_e WITH AXIAL LOAD
$EI_e / f_p bd^3$ (Elastic)
160
140
120
100
80
60
40
20
0.2
0.4
0.6
0.8
1.0
P / P_y

Fig. 76.

Typical Required Values of Plastic Hinge Rotations.

There are a limitless number of ways in which combinations of proportioning of dimensions of structures, form, magnitude and order of loading, etc., can produce ill-conditioned cases of ultimate bending moment distribution and axial load, giving required θ values for complete moment redistribution which are too large to be safely accommodated by critical regions of a structure. There are therefore extreme cases in which the plastic theory cannot be applied with advantage to any material, be it concrete or steel. These extreme cases, however, do not occur in most practical cases.

The determination of required θ values for complex frameworks cannot be dealt with in detail in this investigation, but is being studied by Yu.[10] So many parameters govern the rotation of plastic hinges in such structures, that critical hinge rotations cannot be readily isolated for general cases. Some values of required θ for the more simple structures, calculated by equation(I.1), are given below, for the condition of full redistribution.

Structure	Required θ	Value of s	
Fixed-end beam, U.D.L.	$\frac{M_u L}{6EI_e}$	0.146 L	
2-span cont. beam, U.D.L.	$0.153\ \frac{M_u L}{EI_e}$	0.344 L	
2-pinned portal, central pt. load	$\frac{2M_u H}{3\ EJ_e}$	0.50 L	
Fixed portal, pt. sway load.	$\frac{M_u L}{6EI_e}$	0.50 H	

Since the available rotation depends also on the value of s as well, one of the critical cases from the above examples is the fixed-end beam, in which a very low value of $s = 0.146$ L occurs, so that

$$\theta \Big/ \frac{M_u \cdot s}{EI_e} = \frac{1}{6} \cdot \frac{1}{0.146}$$

$$= 1.14 .$$

Reference to Fig. 69 shows that this value cannot be accommodated by unbound hinges, even with a tension steel ratio as low as 0.01 . By using rectangular binders, say $p_b = 0.015$, and $p_t = 0.01$ gives $\theta \Big/ \frac{M_u \cdot s}{EI_e} = 1.12$, which is then satisfactory provided

the low tension steel ratio does not result in excessive weakening due to bond slip or wide cracks. If a higher value of p_t is found to be more suitable, then a higher p_b is required for a given value of θ .

The above case represents one of the most ill-conditioned structures in practice, since all the plastic rotations can only develop over a very short length of the beam. Assuming that $h' = 0.4$, then the length of the plastic zone would be only

$$0.4 \times 0.146L = 0.0584\ L$$

$$= 1/17 \text{ of the span.}$$

In a column, there is usually only one point of contraflexure along the whole length, so that the value of s is high, usually having the value of $\frac{1}{2}$ for full redistribution. Thus, although the required θ value may often appear to be high, the high value of s enables large plastic hinge rotations to be developed over a long plastic zone. The magnitude of axial load is often a parameter independent of the bending moment, so that the worst order of axial load cannot be assessed. An increase in axial load tends to decrease the value of strain available for flexural deformations, but on the other hand, tends to increase the length of the plastic zone over which considerable plastic hinge

rotations can develop. Hence when the value of P/P_u is not too excessive, the net effect of axial load is to spread the plastic zone only, while the available rotation is self-adjusting. In practice, the condition of $P/P_u \not> 0.6$ can usually be realized; lateral binding may also be used to increase the available rotation many times, so that it may be said that column hinge rotations will, if suitably designed, cover most cases of required θ values.

Thus it appears that reinforced concrete plastic hinges are capable of accommodating the required plastic hinge rotations in most practical cases. With the use of lateral binding which considerably increases the ductility of ordinary concrete, the ultimate strain of concrete may be raised to more than 2%, or 20 times its elastic strain. This figure compares well with the ductility of structural steel frameworks, and shows that, while lateral binding is neither often economical nor necessary, it can be used with advantage in critical cases, thus affording favourable support for the ultimate load method of design of reinforced concrete frameworks by the Plastic Hinge Theory.

PART VI

CONCLUSION

General Summary of Investigation.

It was the object of this investigation to study the characteristics of plastic hinges analytically and experimentally, in the light of application to the ultimate load method of design of reinforced concrete frameworks by the Plastic Hinge Theory.

An analytical study was made by comparing the Plastic Hinge Theory with exact theory, so that the idealized assumptions made, and the degree of approximation incurred in the Plastic Hinge Theory could be examined.

A generalised stress-strain relationship for plain and bound concrete was adopted, from which equations for the strength and deformation of plain and and bound reinforced concrete sections subjected to various forms of applied load, were developed. These general equations are valid throughout the entire history of loading.

The available plastic hinge rotation which can be developed in the region of plastic hinge behaviour, was discussed with reference to the length of the plastic

zone, the curvature distribution, and the influence of reinforcement, concrete strength, axial load, lateral binding, and spalling of concrete cover.

Tests were conducted on 23 reinforced concrete specimens, consisting of 9 laterally bound short prisms, 7 spirally bound short cylinders, and 7 rectangular struts.

The prisms and cylinders enabled the strength and deformation of concrete bound with different ratios of lateral binding to be studied, while the strut tests showed the distribution of curvature within the plastic zone, and the influence of varying the ratio of axial load to bending load on the plastic hinge rotation.

The analytical and experimental findings were finally correlated and discussed.

General Conclusions.

Within the scope of this work, the following conclusions appear to be justified:

1. It has been shown that although the idealized conception in the Plastic Hinge Theory does not interprete the exact structural behaviour of a statically indeterminate framework, it provides a very simple and powerful approximation method for determining the most economical bending moment distribution and required plastic hinge rotation values in structures subject to yield and economic redistribution of bending moments at ultimate load.

2. The error incurred by the Plastic Hinge Theory when compared with exact theory has been found to be ~~on the safe side and~~ generally negligible, the worst case being of the order of a few percent.

3. The local detailing and design of plastic hinge regions should be based on the actual plastic behaviour.

4. The available plastic hinge rotation as defined by the Plastic Hinge Theory is approximately the total rotation less the corresponding elastic rotation over the length of the plastic zone, and is given by

$$\theta = \int_0^{h_k} \frac{M}{EI_s} ds - \int_0^{h_k} \frac{M}{EI_e} ds \quad \text{----(I.6)}$$

5. Under short-time loading conditions, the stress-strain curve of plain and bound concrete throughout its entire history of loading may be closely approximated by 3 connected straight lines.

6. Lateral binding does not not sensibly influence the strength and deformation of concrete sections until the crushing strain of plain concrete is attained; at this stage, lateral pressure gradually builds up in the binders due to the large lateral deformations developed by the concrete, and this induced triaxial compression delays failure and extends the stress-strain range of the concrete, transforming it into a more ductile material.

7. Test results indicate that the ultimate strength and deformation of bound concrete under flexural compression may be approximately related to the lateral binding ratio p_b by the following empirical equations for the particular type of binder steel used in the author's tests:

For circular binders, within the range $p_b = 0$ to 0.0417,

$$p_b = 0.0375\ (K_u - K_o)^2 \qquad \text{----------(V.1)}$$

$$p_b = .4970\ (\epsilon_u - \epsilon_o)^3 \qquad \text{----------(V.3)}$$

For rectangular binders, range $p_b = 0$ to 0.0324.

$$p_b = 0.189\ (K_u - K_o)^2 \qquad \text{----------(V.2)}$$

$$p_b = 14600\ (\epsilon_u - \epsilon_o)^3 \qquad \text{----------(V.4)}$$

8. The concrete used in the tests commenced to spall at a strain of $\epsilon_o = 0.0035$, and propagated along the length of members with varying bending moments, until a lower limiting strain $\epsilon_r = 0.0022$ was reached. The spalled length was approximately 1/5 of the bending moment intercept, and was found to be rather insensitive to small changes in the length of the plastic zone.

9. The proposed general strength and deformation equations predict satisfactorily the behaviour of plain and bound reinforced concrete members.

10. High plastic hinge rotations can be developed in unbound under-reinforced sections, and where the bending moment intercept is long.

11. Laterally bound sections can develop very high plastic hinge rotations, and is particularly efficient for column hinges. The spalling of concrete cover in laterally bound plastic hinges causes a slight drop of load, contraction of the length of plastic zone, and the concentration of plastic hinge rotations within the spalled length.

12. A semi-empirical method for rapidly determining the available plastic hinge rotation, is given by the equation

$$\theta_k = M_u \beta h's \left[\frac{1}{EI_u} - \frac{1}{EI_e}\right] \quad \text{---(IV.5)}$$

where the curvature distribution factor β was found from the strut tests to have the values

β = 0.305 for unbound hinges,

= 0.21 for laterally bound hinges.

13. In beams, the length of the plastic zone is approximately 0.4 of the bending moment intercept. Assuming the highest value of B.M. intercept to be $\frac{1}{4}$, the length of the plastic zone is therefore not greater than 1/10 of the span.

In columns, the length of the plastic zone is increased by the presence of axial load. Although it is possible for the length of the plastic zone to reach a theoretical maximum value equal to the entire length of the bending moment intercept, in practice the value of P/P_u may be assumed to be less than 0.6, i.e., if the bending moment intercept has the value of $\frac{1}{2}$, then the plastic zone for column hinges is therefore not greater than 0.35 of the length of the column. This spread of plasticity does not affect the validity of the Plastic Hinge Theory.

14. In most structures, economic redistribution of ultimate moments can be achieved without using lateral

binding. In critical cases, laterally bound plastic hinges generally enables sufficiently high rotations to be accommodated.

15. Lateral binding gives great ductility to concrete, and ultimate strains exceeding 20 times the elastic strain are possible. Besides its use in plastic hinges, bound concrete avoids sudden brittle collapse normally associated with compression failure in reinforced concrete members, and justifies the use of a lower factor of safety..

Recommendations for Future Work.

The investigation of the characteristics of plastic hinges is obviously far from complete, and with the limitations of the author's work in view, the following recommendations are given for future work in this field.

1. More tests on laterally bound concrete should be carried out with a wider range of variables, namely, binders of various shapes and sizes, different pitches and types of steel.

2. Limitation of equipment did not permit the author's test specimens to be full-sized members. Consequently, the accuracy of strain measurements was not as high as could be desired. This is particularly marked when the neutral axis is outside the section. Testing of larger specimens should therefore give strain measurements of improved accuracy.

3. Creep tests should be carried out on laterally bound concrete. The author's tests were carried out for short-time loading conditions only, and hence little is yet known of the creep characteristics of bound concrete.

4. The flexural rigidity of bound concrete EI is very low compared to the elastic value, and where axial

load is high, lateral instability is very liable to occur. For such members, the safe allowable slenderness ratios and reduction-coefficients for bound concrete, as applied to the ultimate load design method in the Plastic Hinge Theory, should be determined by conducting tests on bound concrete members of varying slenderness ratios to investigate plastic buckling behaviour.

BIBLIOGRAPHY

1. J.F.Baker, "A Review of Recent Investigations into the Behaviour of Steel Frames in the Plastic Range." Proc. I.C.E.,Jan.,1949.

2. B.G.Neal and P.S.Symonds, "A Method for Calculating the Failure Load for a Framed Structure subjected to Fluctuating Loads." Proc. I.C.E.,Jan.,1951.

3. A.L.L.Baker, "Recent Research in Reinforced Concrete, and its Application to Design." Proc. I.C.E.,Feb. 1951.

4. A.L.L.Baker, "Further Research in Reinforced Concrete, and its Application to Ultimate Load Design." Proc. I.C.E.,Aug.,1953.

5. A.L.L.Baker, "The Design of Reinforced Concrete Frameworks by Ultimate Load Theory." Reinforced Concrete Review(to be published).

6. A.L.L.Baker, "A Plastic Theory of Design for Ordinary Reinforced and Prestressed Concrete,including Moment-Redistribution in Continuous Members." Mag. of Concrete Research No.2, June, 1949.

7. Glanville and Thomas, "Redistribution of Moments in Reinforced Concrete Beams and Frames." Proc. I.C.E., April, 1936.

8. K.A.Everard, "Moment Redistribution in Statically Indeterminate Structures due to Inelastic Effects in Steel and Concrete." Ph.D. thesis,London Univ.,1952.

9. A.L.Moss-Morris, Ph.D. thesis, London Univ., (to be submitted).

10. C.W.Yu, Ph.D. thesis, London Univ., (to be submitted).

11. J.Morley English, "Design of Frames by Relaxation of Yield-Hinges." Proc. A.S.C.E. Nov.,1953.

12. von Karman,Th., "Festigkeitsversuche unter allseitigem Druck." Mitteilungen über Forschungsarbeiten auf dem Gebiete des Ingenieurwesens, Vol.118, 1912 .

13. A.Considere, "Resistance a la Compression du Beton Arme et du Beton Frette." Genie Civil, 1903.

14. Richart, Brandtzaeg and Brown, "A Study of the Failure of Concrete under Combined Compressive Stresses." Univ. of Illinois Bull. No.185, 1928 .

15. Richart, Brandtzaeg and Brown, "The Failure of Plain and Spirally Reinforced Concrete in Compression." Univ. of Illinois Bull. No.190, 1929.

16. E.Hognestad, "A Study of Combined Bending and Axial Load in Reinforced Concrete Members." Univ. of Illinois Bull. No.399, 1951.

17. L.H.N.Lee, "Inelastic Behavior of Reinforced Concrete Members subjected to Short-time Static Loads." Proc. A.S.C.E.,Sept., 1953.

18. A.Nadai, "Theory of Flow and Fracture of Solids." McGraw-Hill Book Co.1950.

19. J.M.Prentis, "The Distribution of Concrete Stress in Reinforced and Prestressed Concrete Beams when tested to Destruction by a Pure Bending Moment." Mag. of Concrete Research No.5, Jan., 1951.

20. R.W.Smithies, "Stress Strain Relationship in Concrete by Bending Simulation." Ph.D. thesis, London Univ.,1952.

21. K.G.Bassi, "M.Sc. thesis, London Univ., (to be submitted)..

22. M.T.El-Katib, "An Analytical and Experimental Investigation of the Bending Moment Distribution in Prestressed Concrete Continuous Beams." Ph.D. thesis, London Univ., 1953.